Immunoengineering nanoparticles for mucosal drug and vaccine treatment of sexually transmitted infections

Renuka Ramanathan

A dissertation submitted in partial fulfillment
of the requirements for the degree of

Doctor of Philosophy

University of Washington
2016

Reading Committee:
Kim A. Woodrow, Chair
Daniel M. Ratner
Florian Hladik

Program Authorized to Offer Degree:
Bioengineering
Nanotechnology & Molecular Engineering

University of Washington

Abstract

Immunoengineering nanoparticles for mucosal drug and vaccine treatment of sexually transmitted infections

Renuka Ramanathan

Chair of the Thesis Committee:
Professor Kim A. Woodrow
Bioengineering

Sexually transmitted infections (STIs) are a major burden on human health worldwide, accounting for nearly 1 million infections daily. Women's sexual and reproductive health is disproportionately impacted by the most commonly transmitted pathogens, including Hepatitis B, human simplex virus (HSV), human immunodeficiency virus (HIV), and human papilloma virus (HPV). The impact of these diseases on women's health extends from higher rates of infections to the danger of mother-to-child transmission to secondary conditions such as cervical cancer. While drugs have been developed to address symptoms, the spread of these diseases will truly be curbed with development of vaccines. Astoundingly, while nearly 30 sexually transmitted pathogens have been identified, we currently have developed vaccines to address only two of these pathogens. A key observation driving research is that effective HPV vaccines stimulate the generation of neutralizing antibodies in the genital tract. This has inspired work that is focused on evaluating administration routes, which directly allow for immunization at the site of infection. Additionally, nanomaterial carriers show great promise in the delivery of vaccine antigens after mucosal immunization. These systems allow us to specifically modify carrier composition and surface properties to deliver vaccines and drive immunogenic responses in the vaginal mucosa.

In this dissertation, we leverage Bioengineering strategies to address fundamental challenges in reproductive immunology. We demonstrate that protein growth factors can be delivered vaginally to expand key immune cell populations, which play a major role in mounting protective immune responses. We build a proof-of-concept, protein-functionalized nanoparticle system to enhance transepithelial transport of nanocarriers post-vaginal delivery. Finally, we evaluate our nanoparticle systems for vaccine antigen delivery to T cells, and demonstrate the generation of functional effector T cell responses. Our research highlights the barriers to generating protective immune responses in the genital tract, and we demonstrate that biomaterials can be leveraged to address these challenges. We hope to have laid the groundwork for further investigation and validation of nanoparticle systems to engineer mucosal immune protection for application as vaccines against STIs.

Acknowledgements

This dissertation represents the contributions of many individuals who have offered scientific insights, global-minded perspectives, inspiration, and moral support.

First and foremost, I would like to acknowledge my thesis advisor Dr. Kim A. Woodrow for her unparalleled support in the pursuit of scientific knowledge. Kim has a unique talent to always engage even the toughest lines of scientific inquiry and motivate the work from two important angles: scientific discovery and contribution to human health. Her mentorship has been key in shaping my academic and professional career, and has influenced my choice to seek out diverse opportunities that allow me to develop invaluable skills essential to scientific research and development. Kim once said to me, “If you are not working on the fringes of uncertainty, then what is the point?” Her words have carried through with me to this day, and have inspired me to face and embrace even the hardest challenges head on.

I would like to thank the UW STD & AIDS Research Training Program (NIH T32 AI07140) and Program Director, Dr. Sheila A. Lukehart, for supporting this thesis with a pre-doctoral fellowship. Apart from funding support, this training program has provided me with immense opportunities to interface with scientists, clinicians, and global and public health researchers committed to improving the lives of those affected by HIV/AIDS. This program has opened my eyes to the many challenges that must be overcome to truly curb the HIV pandemic. It has shown me how cooperation and collaboration among people from diverse backgrounds is necessary to address human health challenges from the standpoints of scientific discovery, clinical validation, infrastructure management, and implementation. I hope to carry forward the collaborative spirit of the training program in all my future endeavors.

To Jim, I would like to say, thank you for always having my back. Jim has provided me with an infinite amount of support and unconditional love over the past five years. He has been my scientific peer, a steadfast friend, and my fiercest advocate. Jim motivates and inspires me to be optimistic and put my best foot forward. He has shown me how to keep my head down and work hard. And he is the person with whom I unwind and appreciate life. We have grown up together during our graduate studies, and I look forward to a lifetime of partnership and happiness.

Finally, I would like to acknowledge my parents, Ram and Uma. To my dad, I am forever indebted to you for ingraining in me that the pursuit of knowledge reaps lifelong, intangible rewards. I have met no person who better exemplifies what it means to live life at the intersection of preparedness and true curiosity. To my mom, I want to say that I am forever thankful to you for showing me what it means to seize opportunity and work hard to achieve goals. Your professional trajectory demonstrates the power of drive and determination, even in the hardest of circumstances. Thank you mom and dad for your sacrifices, and for raising me to believe that I am deserving of every opportunity.

I dedicate this dissertation in memory of C.V. Seshan and C.V. Rajamal and to P.N. Ananthan and Lakshmi Ananthan for launching my family along a path of lifelong learning and pursuit of my dreams.

Table of Contents

List of Figures

CHAPTER 2

CHAPTER 3

CHAPTER 4

CHAPTER 5

APPENDIX I

List of Tables

Chapter 1: Motivation and specific aims

1.A. RESEARCH MOTIVATION

Women are the face of the HIV/AIDS pandemic. On a global scale, HIV/AIDS infections are the leading cause of mortality among women in their reproductive years and 99% of more than half a million maternal deaths occurs in developing countries annually[1]. Currently, only palliative antiretroviral therapy is available to HIV-infected individuals to suppress viral load and prevent sexual HIV-1 transmission. The development of a vaccine, which offers protection at the site of infection in the vaginal mucosa will have an essential impact on viral transmission and has the potential to truly address the HIV pandemic.

Nearly three decades after the discovery of the human immunodeficiency virus (HIV) as the cause of acquired-immunodeficiency syndrome (AIDS), the development of a protective vaccine remains elusive. Of the 218 HIV vaccine clinical trials that have been conducted since 1988, only five reached Phase IIb/III efficacy trials (Figure 1-1)[2]. The RV144 trial in October 2009 announced 31.2% efficacy in protecting against HIV infection[3]. An analysis of the immune correlates in this trial suggested the importance of

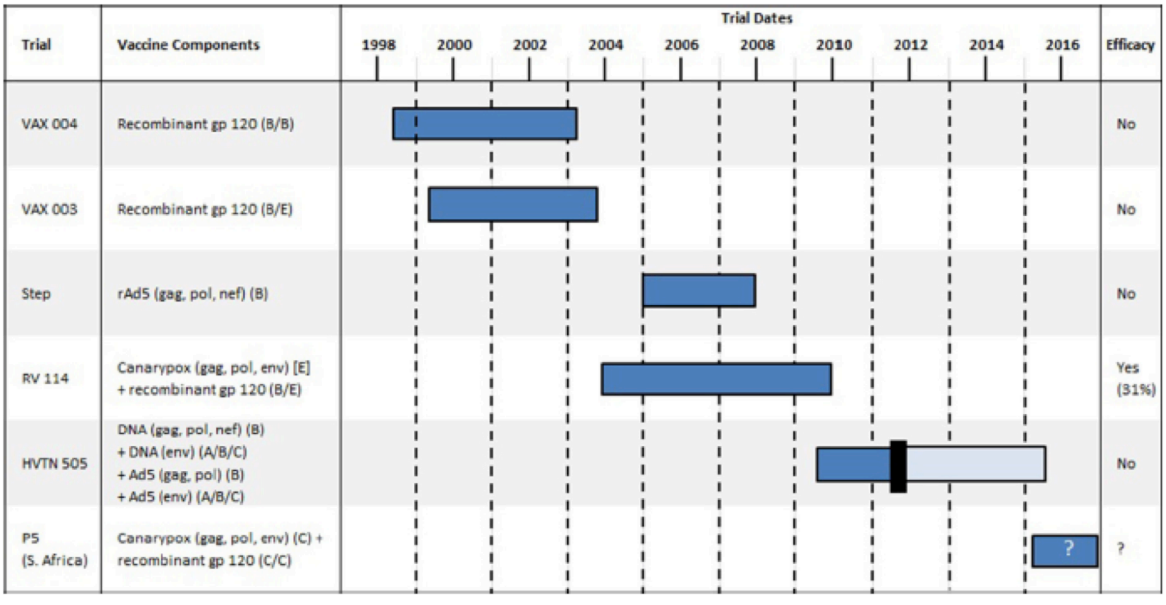

Figure 1-1 Timeline of five Phase IIb/III HIV vaccine trials. Figure credit[2]

V1V2 non-neutralizing antibodies, which may have played a role in antibody-dependent cellular cytotoxicity (ADCC) [2,4]. Regardless, research and clinical trials in pursuit of an HIV vaccine demonstrates that the immune correlates of protection encompass broadly neutralizing antibody (bNAbs) humoral responses and cytotoxic T lymphocyte (CTL) cellular responses.

A major focus of recent work has been the generation of protection at the site of HIV entry in the reproductive organs, by vaginal or rectal immunization. Several studies have evaluated vaginal immunization in women with some success[5-7]. The rationale for these studies is that vaccination strategies, which are delivered at the site of infection, may be the key to providing maximal protection against HIV-1 transmission in the genital mucosa.

While these studies have established a precedent for intravaginal vaccine delivery, several challenges prevent achievement of protective immunity. The female reproductive tract itself presents several unique challenges including an environment that restricts free migration of immune cells and lacks organized lymphoid structures[8]. Further, while the vaginal epithelium protects against foreign pathogens it also presents a physical barrier, which prevents biomaterials and biologics from gaining access to critical immune cells[9].

Nanoparticles have been an active area of research in the literature to improve the delivery of small molecules and protein biologics[10]. This research dissertation specifically focuses on bridging biomaterials engineering and applied immunology to investigate nanoparticle-based mucosal vaccines for addressing barriers to immunization against a sexually transmitted virus in the female reproductive tract. Our research focuses on assessing immune cell populations in the reproductive tract and developing strategies to modulate the antigen presenting cell populations, which are critical in mounting an immune response to a mucosal vaccine. Furthermore, we will explore the possibility of interrogating molecular targets on the vaginal epithelium, which may be leveraged to promote transcytosis of intravaginally delivered vaccine-loaded nanoparticles.

1.B. SCIENTIFIC RATIONALE

Vaccine strategies that enrich the antigen presenting cell (APC) population, particularly dendritic cells (DCs) at the site of immunization, while also promoting the active transport of biomaterials carrying antigen across the epithelium and to draining lymph nodes (DLNs) may boost the immune response to a mucosal vaccine. The goals of this dissertation are motivated by the following key observations:

First, the initial immune response to HIV-1 viral exposure in the vaginal tract is insufficient to prevent recurring, persistent infection. Enriching the local DC population in the vaginal mucosa may enhance immune responses by expanding cells required for antigen uptake, trafficking to lymph nodes, and T-cell priming.

Second, nanoparticles delivered in the vaginal tract face multiple biological barriers that limit efficient delivery to submucosal immune cells and draining lymph nodes. These challenges include being trapped in mucus, passive and poor transport across the stratified squamous epithelium, and limited access to key antigen presenting cells. Surface functionalization of nanoparticles may be a strategy to promote active transport and targeting to immune cells.

Third, while small molecules are able to reach distant organs and tissues by paracellular transport or escape through vasculature, vaccine-loaded nanoparticles are limited in their ability to cross the vaginal epithelium and access critical immune cell populations in the lamina propria or in draining lymph nodes. Functionalizing vaccine-loaded nanoparticles to bind molecular targets on the surface of the vaginal epithelium may allow for active transport from the lumen to the lamina propria, improved antigen uptake, processing, and presentation.

Based on these observations, this research is motivated by the ultimate vision of integrating into a single mucosal vaccine, the molecular signals to enrich the DC population in the vaginal tract while concomitantly promoting active transport of vaccine-loaded biomaterials across the vaginal epithelium to the APC-rich lamina propria and draining lymph nodes.

1.C. SPECIFIC AIMS

1.C.1. Investigate intravaginal expansion of antigen presenting cell populations to direct nanoparticle biodistribution

Hypothesis: Intravaginally administered DC chemokines and growth factors promote local expansion of antigen presenting cells to direct biodistribution of nanoparticle vaccines. A significant challenge in intravaginal vaccination against mucosal pathogens concerns the immune privileged environment in the genital tract, which prevents migration of immune cells in the absence of inflammation. A recent study demonstrated a new vaccine strategy for sexually transmitted diseases termed "prime and pull."[11] In the "prime and pull" paradigm, vaccines are administered parenterally to evoke a systemic immune response (prime). This is followed by topical application of chemokines CXLC9/10 to recruit and establish a local T cell population, which can provide long-term memory, curb the spread of HSV-2 to neurons, and prevent clinical manifestations of disease. Our goal is to explore a different intravaginal vaccination strategy focused on chemokine recruitment of mucosal DCs – the major antigen-presenting cell to T cells in lymph nodes. To improve DC recruitment to the genital tract, our strategy is focused on topical administration of peptide and protein DC chemokines or growth factors. In our research, we have examined a known DC chemokine (MIP-3α) and a known DC growth factor (GM-CSF) and their ability to expand the APC population in the vaginal mucosa compared to CpG.

1.C.2. Evaluate antibody-modified nanoparticle carriers (nanoparticle immune complexes, NP-ICs) for transepithelial transport and uptake by vaginal immune cells

Hypothesis: IgG protein-modified fluorescent nanoparticles will efficiently transcytose across the vaginal epithelium, associate with immune cells in the lamina propria, and drain to lymph nodes. Nanoparticles are a promising platform for optimized dosing of biologics by increasing cellular uptake and delivering biologics to intracellular sites of action, and improving overall bioavailability by preventing protein and peptide cargo from enzymatic degradation. However, one of the challenges of nanoparticle delivery in the vaginal tract is the inability to access immune cells in the lamina propria compartment due to tight junctions in the vaginal epithelium, which

restrict nanoparticle transport. This results in retention in the vaginal lumen, and eventual discharge due to constant mucus turnover and vaginal secretions. Our lab is currently investigating existing Fc receptor pathways present on epithelial surfaces and on immune cells, which bind the Fc domain of IgG and have been implicated in transcytosis, increased uptake, and promoting cross-presentation of antigen[12-14]. By modifying nanoparticle surfaces with IgG, we may leverage these Fc receptors to promote luminal to basal transcytosis of intravaginally delivered biomaterials across the epithelium. Once nanoparticles have reached the lamina propria, they may freely traffic to draining lymph nodes or associate with vaginal antigen presenting cells. This functionality has the potential to have a significant impact on mucosally administered nanoparticle vaccines, which must reach draining lymph nodes to potentiate a protective immune response.

1.C.3. Synthesize ovalbumin loaded, antibody-nanoparticles immune complexes for intravaginal immunization (OVA-NP-ICs)

Hypothesis: Intravaginal immunization of IgG-modified polymer nanoparticles loaded with ovalbumin will elicit antigen-specific T-cell proliferation in local and systemic lymphoid tissues. Poly(lactic-co-glycolic acid) nanoparticles have recently been used as carriers for protein biologics and can be functionalized with IgG. To test whether a mucosal vaccine comprised of antigen-loaded, IgG-modified polymer nanoparticles has the ability to elicit antigen-specific immune responses, we will evaluate intravaginal immunization with the model antigen ovalbumin (OVA) encapsulated in IgG-coated nanoparticles (OVA nanoparticle immune complexes, OVA-NP-ICs). Standard *ex vivo* T-cell assays will be employed to evaluate antigen-specific T-cell proliferation and cytokine secretion *ex vivo* and *in vivo*.

1.D. SUMMARY

In conclusion, my dissertation research proposal bridges biomaterials engineering and applied immunology to evaluate if the combination of molecular cues and targeted nanoparticles can be used to produce an efficacious mucosal vaccine. Most importantly, we hope to bridge the gap between materials that promote delivery and also shape the activation state and immune responses elicited by innate immune cells. We expect that

our contributions in the field of vaginal mucosal vaccine delivery will highlight key challenges in the field of mucosal nanoparticle application and propose innovative ways of approaching the design of functional biomaterials that will boost immune responses to intravaginal immunization.

1.E. REFERENCES

1. World Health Organization. Women's health, Fact sheet No. 334, November 2009. (2013).
2. Esparza, J. A brief history of the global effort to develop a preventive HIV vaccine. *Vaccine* **31,** 3502–3518 (2013).
3. Rerks-Ngarm, S. *et al.* Vaccination with ALVAC and AIDSVAX to prevent HIV-1 infection in Thailand. *New England Journal of Medicine* **361,** 2209–2220 (2009).
4. Haynes, B. F. *et al.* Immune-correlates analysis of an HIV-1 vaccine efficacy trial. *New England Journal of Medicine* **366,** 1275–1286 (2012).
5. Lewis, D. J. *et al.* Phase I randomised clinical trial of an HIV-1 (CN54), clade C, trimeric envelope vaccine candidate delivered vaginally. *PloS one* **6,** e25165 (2011).
6. Kozlowski, P. A. *et al.* Differential induction of mucosal and systemic antibody responses in women after nasal, rectal, or vaginal immunization: influence of the menstrual cycle. *The Journal of Immunology* **169,** 566–574 (2002).
7. Johansson, E.-L., Wassén, L., Holmgren, J., Jertborn, M. & Rudin, A. Nasal and vaginal vaccinations have differential effects on antibody responses in vaginal and cervical secretions in humans. *Infection and immunity* **69,** 7481–7486 (2001).
8. Naz, R. K. Female genital tract immunity: distinct immunological challenges for vaccine development. *Journal of reproductive immunology* **93,** 1–8 (2012).
9. Hickey, D. K., Patel, M. V., Fahey, J. V. & Wira, C. R. Innate and adaptive immunity at mucosal surfaces of the female reproductive tract: stratification and integration of immune protection against the transmission of sexually transmitted infections. *Journal of reproductive immunology* **88,** 185–194 (2011).
10. Zhang, L. *et al.* Nanoparticles in medicine: therapeutic applications and developments. *Clinical pharmacology & therapeutics* **83,** 761–769 (2008).
11. Shin, H. & Iwasaki, A. A vaccine strategy that protects against genital herpes by establishing local memory T cells. *Nature* **491,** 463–467 (2012).
12. Li, Z. *et al.* Transfer of IgG in the female genital tract by MHC class I-related neonatal Fc receptor (FcRn) confers protective immunity to vaginal infection. *Proceedings of the National Academy of Sciences* **108,** 4388–4393 (2011).
13. Ye, L., Zeng, R., Bai, Y., Roopenian, D. C. & Zhu, X. Efficient mucosal vaccination mediated by the neonatal Fc receptor. *Nature biotechnology* **29,** 158–163 (2011).
14. Rafiq, K., Bergtold, A. & Clynes, R. Immune complex-mediated antigen presentation induces tumor immunity. *Journal of Clinical Investigation* **110,** 71–80 (2002).

Chapter 2: Introduction

2.A. Defenses of the reproductive tract

Sexually transmitted infections (STIs) are a significant cause of morbidity and mortality globally, where over a million new infections are acquired daily and lead to other adverse health consequences including increased risk for HIV acquisition[1-6]. In the United States, there is a high incidence of STIs amongst youth ages 15-24 and the economic burden to the healthcare system is estimated to be $16 billion annually[7,8]. Safe and effective vaccines have the greatest potential to reduce the worldwide health burden of STIs including HIV. In particular, women and adolescent girls, who are disproportionately impacted by STIs, would benefit considerably from the availability of vaccines[9]. Topical delivery of drugs and vaccines may expand the toolbox of prevention strategies to protect the site of infection. However, vaccines are available for only two of the over 30 different pathogens that are transmitted sexually. A critical barrier to the development of effective STI vaccines is the lack of immunological correlates associated with protection against the many diverse mucosally transmitted pathogens. In addition, the unique immunological environment of the female genital tract mucosa imposes challenging constraints for vaccine design. Here we discuss barriers and opportunities for developing vaccines to protect against mucosal pathogens that are transmitted sexually. In this review, we focus specifically on the challenges in eliciting protective immune responses from topical administration of vaccines to the vaginal mucosa and discuss bioengineering strategies to elicit protective immunity to STIs.

2.A.1. The role of reproductive tract anatomy in the defense against pathogens

The vast majority of infectious pathogens invade through mucosal surfaces lining the nasal and oral cavities, the gut, and the genitourinary tract. In immunocompetent individuals, a range of innate and adaptive immune defenses recognizes and responds to these foreign pathogens[10]. In the female reproductive system, these defenses are uniquely organized to protect the host against infectious bacteria, fungi, and viruses, while maintaining tolerance towards spermatozoa and a semiallogeneic fetus. The organization of the reproductive tract, including its anatomy, hormonal control over the

tissue environment, presence of antimicrobials and mucus, lymphatics, dominant antibody types, and cellular composition collectively defend the reproductive tract against sexually transmitted pathogens. Compartmentalization within the mucosal immune system also suggests that immune responses are likely to be strongest at and proximal to the site of mucosal immunization. For example, a human clinical trial identified that vaginal immunization leads to greater and more robust local mucosal IgG and IgA antigen-specific antibody responses than parental immunization or immunization at a distal mucosal site such as intranasally[1,3,5]. This result provides strong rationale that eliciting local protective mucosal cellular and antibody responses may require immunization in the target mucosa. An understanding of the key features of the female reproductive system will inform development of biomaterials for intravaginal drug and vaccine delivery, which may have the potential to modulate mucosal immunity.

The female reproductive anatomy can be subdivided into two distinct compartments, which differ in function (Figure 2-1). An anatomical appreciation of both the upper and lower female reproductive tracts is critical to understanding mechanisms of pathogen infection, and informing the design of novel biomaterials that can access the necessary immunological tissues and cells. The upper genital tract is classified as a type I mucosal surface and shares features common to the gut, small intestine, colon, and lungs[11-14]. The upper female reproductive organs include the endocervix, uterus, oviducts, and ovaries. As a type I mucosal surface, the upper genital tract is comprised of one layer of columnar epithelial cells, which are joined by tight junctions[11,13,15]. The lower genital tract is classified as a type II mucosal surface and shares features common to the cornea, oral cavity, and esophagus[13,14]. The lower female reproductive organs include the ectocervix and the vagina. The lower genital tract is comprised of multiple layers of non-keratinized and squamous epithelial cells, which cover a basement membrane. As squamous epithelial cells are turned over, they are renewed from basal epithelial cells in the basement membrane[13,16]. One of the many functions of this multi-layered squamous epithelium is to protect the underlying tissue from disruption during intercourse [10,11]. The anatomical features of murine reproductive tracts

differ from humans in one notable aspect in that the upper female murine reproductive organs include the endocervix and uterine horns[11-13,17].

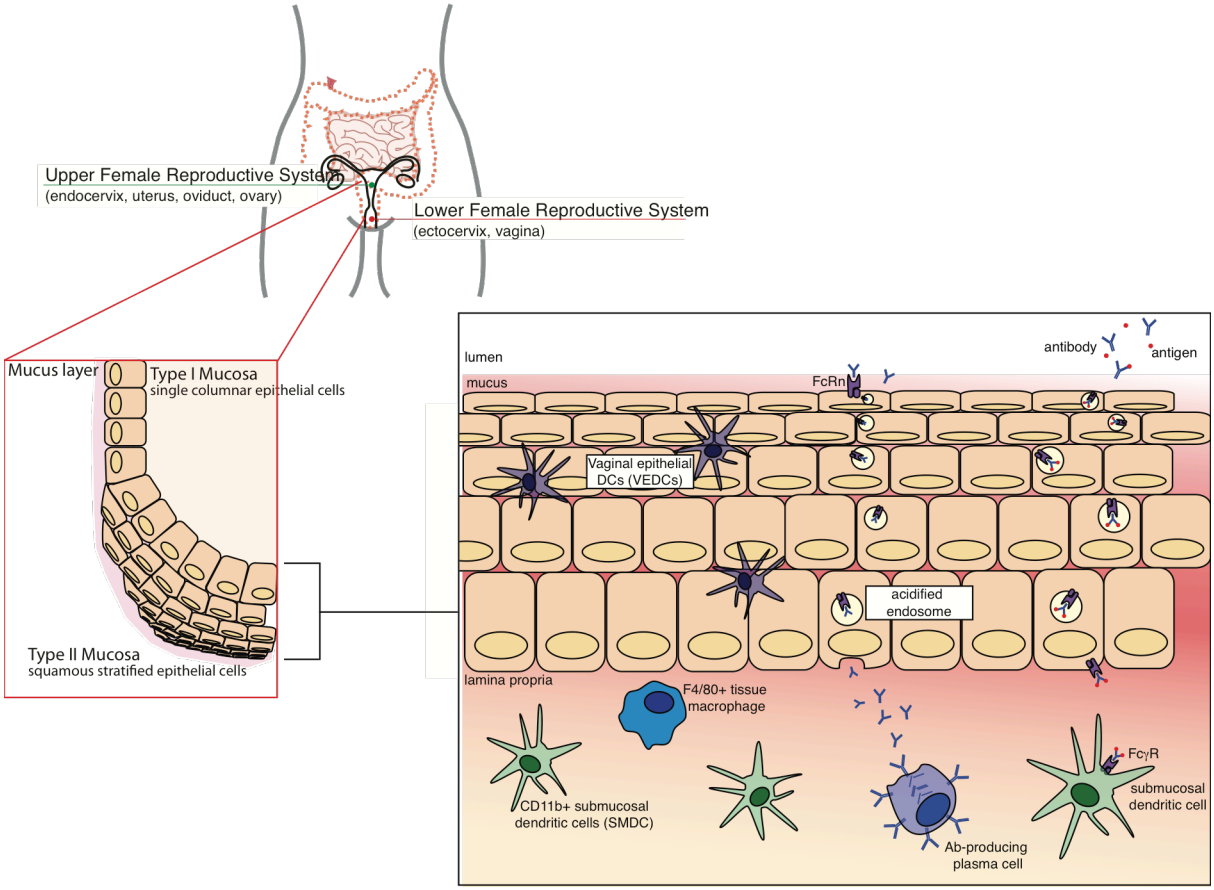

Figure 2-1 Unique features of the reproductive tissues include type I and II mucosal epithelium in the upper and lower genital tract, respectively. Type I mucosal tissues include a single layer of columnar epithelial cells while type II mucosal tissues consist of multiple layers of stratified squamous epithelial cells. The luminal side of the genital tract is coated in a layer of mucus, which is constitutively produced in the reproductive tissues. Various immune cells populate the vaginal epithelium and the submucosal tissues including vaginal epithelial dendritic cells (VEDCs), macrophages, and submucosal dendritic cells (SMDCs). The reproductive tissues has mechanisms for bidirectional transcytosis of IgG across the vaginal epithelium by the neonatal Fc receptor (FcRn).

A critical region of the genital tract is the “transitional zone” between the upper and lower genital tract marked by the change from columnar to squamous epithelial cells near the cervix[11-14]. It is thought that the “transitional zone” is the most immunologically active region of the entire female reproductive system. Unlike the close association of the upper tract columnar epithelial cells, tight junctions do not join the squamous epithelial cells. This subtle variation in epithelial tissue allows for the escape

of small molecules from the lumen into the tissue. While recent research has shown that HIV virions are able to transcytose through the vaginal epithelium to access target tissues, some groups postulate that the lack of tight junctions between the squamous epithelial cells enable HIV virions to pass between cells and access Langerhans cells (LCs) and CD4+ T cells in the lamina propria[11,12,18,19]. Alternatively, secretion of inflammatory cytokines during infection, such as TNF-a, has been implicated in loosening epithelial cell junctions and facilitating easier transepithelial pathogen transport[11,15].

2.A.2. Dendritic cell subsets of the reproductive tract

While epithelial cells themselves play an important role in mucosal immunity in the reproductive tract[13,16,20-22], the major mediators of inflammation and immunity in the vaginal tract are the professional antigen presenting cells, most notably dendritic cells (DCs)[23]. DCs are thought to be the most efficient of the professional antigen presenting cells. Unlike macrophages, only DCs possess the unique capacity to migrate to draining lymph nodes after antigen uptake to prime B and T cells. A summary of subsets in different regions of the body is presented in Figure 2-2. At steady-state, DC precursors exit the bone marrow and enter circulation, eventually entering lymph nodes and differentiating into various DC subsets. DCs can be subdivided into two categories – tissue DCs, which reside in the mucosa, skin, and internal organs; and blood DCs, which are found in blood and lymphoid tissues. Mucosal DCs have been studied and phenotypically described well in murine models, which will be the focus of this review. It is important to note that there are key differences in receptors and cell surface markers between human and mouse mucosal DCs.

In the murine reproductive mucosa, tissue DCs are subdivided into vaginal epithelial dendritic cells (VEDCs) and submucosal dendritic cells (SMDCs). VEDCs sit in the vaginal epithelium and play a key role in antigen sampling from the lumen (Figure 2-1). VEDCs share similarities to Langerhans cells found in the skin, but are distinct in a few key ways[24]. First, VEDCs express much lower levels of Langerin than Langerhans cells found in skin epithelium[24,25]. Second, while both cell types show morphology consistent with round, cytoplasmic granules, Langerhans cells contain distinct Birbeck

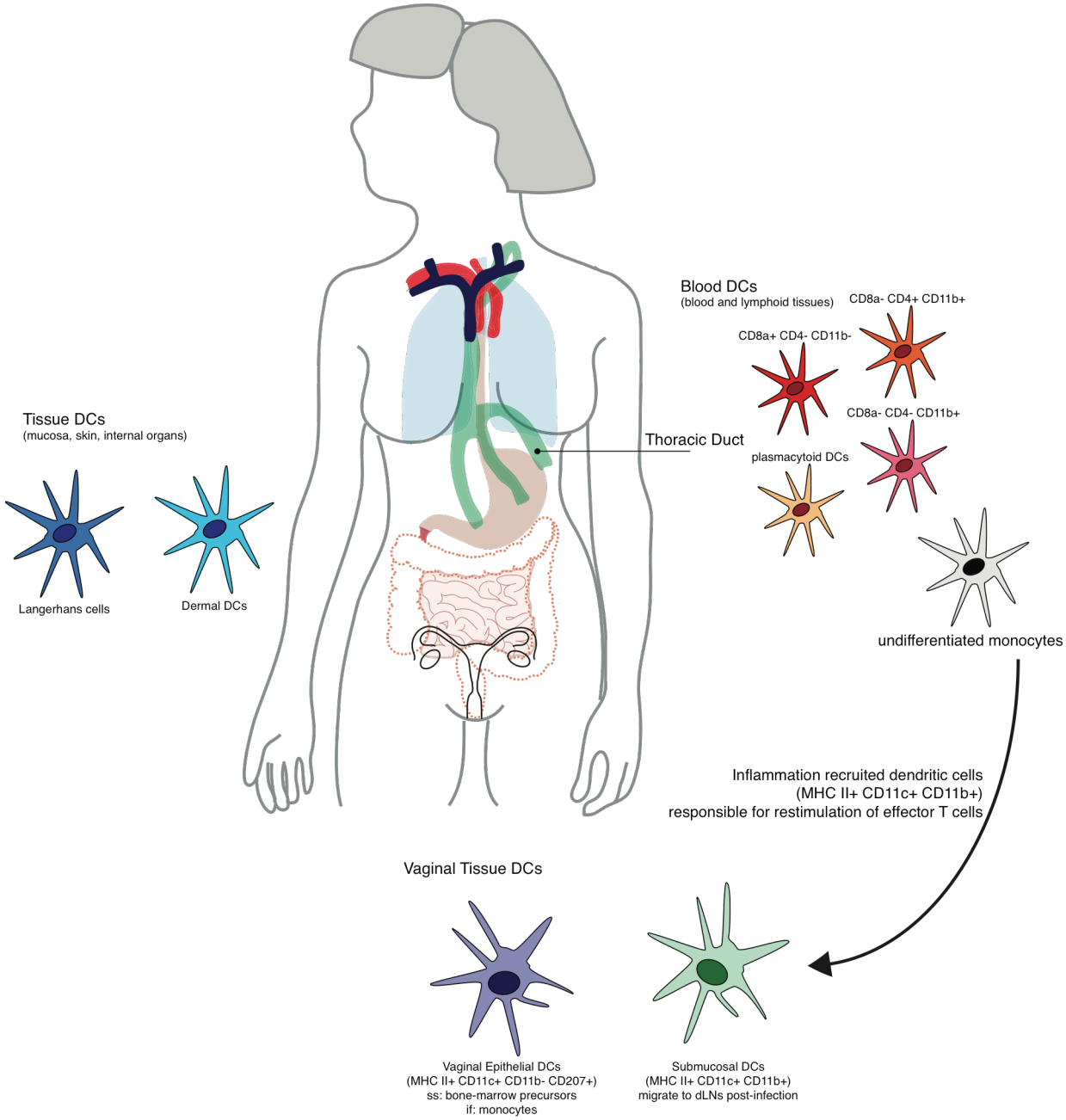

Figure 2-2 Dendritic cells subsets include blood DCs, tissue DCs, and specialized mucosal DCs in the vaginal tract. VEDCs in the reproductive mucosa are identified by cell surface markers MHC II, CD11c, and CD207. Submucosal DCs (MHC II+ CD11c+ CD11b+) play a key role defending against primary infections by sampling antigen and trafficking to draining lymph nodes. During inflammation, circulating undifferentiated monocytes are rapidly recruited into the reproductive tissues to provide response to secondary infection and restimulation of effector T lymphocytes.

granules that are rod-shaped, and contain striations[25]. Third, while most DC precursors are monocytes, in non-inflammatory conditions VEDCs are renewed from non-monocyte

bone-marrow derived precursors. Under inflammatory conditions such as during HSV-2 infection, VEDCs, like skin Langerhans cells, differentiate from monocytes. Finally, VEDCs express low levels of CD207 and have a generally more activated phenotype than skin Langerhans[23-25].

MHC class II+ CD11b+ DCs found within the submucosal lamina propria of the mouse vaginal mucosa are referred to as submucosal dendritic cells (SMDCs)[23]. SMDCs share similarities to dermal DCs found in skin and are characterized by surface expression of MHC class II, CD11c, and DC-SIGN in humans, CD123 in rhesus macaques, and CD11b in murine models[20,23]. In an elegant experiment by Zhao *et al.* (2003), it was demonstrated that after genital HSV-2 infection, MHC class II+/CD11c+/CD11b+ submucosal DCs migrated to draining lymph nodes where they primed CD4+ T cells and initiated a Th1 response[26]. While a thorough rationale for why DC precursors migrate to tissues and then differentiate into DCs is not completely elucidated, it is hypothesized that in the absence of inflammatory stimuli and constitutive expression of chemokines regulate the steady-state recruitment of DCs into tissues[23]. It is thought that cytokine-induced recruitment of monocyte-derived DCs during inflammation increases the local population up to 100-fold. One important distinction between local SMDCs and recruited monocyte-derived DCs is that the latter is recruited to sites of inflammation in a CCR2 dependent manner and in response to type I interferon[27]. Furthermore, rather than stimulation of naive T lymphocytes, these recruited DCs are responsible for restimulation of Th1 effector and memory T cells.

In general, cell recruitment to infected tissues is a multi-step process. During tissue inflammation, the chemokine CCL20 is produced and induces the recruitment of monocyte-derived DCs[28]. Monocytes or monocyte-derived DCs travel through blood vessels towards CCL20 via the CCR6 receptor. Monocytes bind selectin on endothelial cells via adhesion molecules and extravasate across the endothelium[10]. After recognizing and phagocytosing antigens, DCs downregulate CCR6 and upregulate expression of CCR7, which allows them to home to lymph nodes. These mature DCs further present antigen on MHC class II molecules and co-stimulatory molecules on their surface to engage TCRs and provide priming and co-stimulation of T cells.

2.A.3. Differences in the lymphatic structures that guard mucosal surfaces

A major component of immune responses to vaccination at mucosal surfaces is the architecture of lymphatic vessels that drain the tissue. One of the most marked differences between the vaginal mucosal environment and other mucosal compartments is the composition of organized lymphoid structures, including secondary lymphoid organs. The nasopharynx and bronchial passage and the gastrointestinal tract contain organized lymphatic structures, which are termed the bronchial-associated lymphoid tissues (BALT) and the gut-associated lymphoid tissues (GALT), respectively[29]. In addition to an extensive network of lymphatic vessels, which drain the mucosal tissues, these mucosal sites have large lymphoid aggregate structures similar in tissue organization and function to lymph nodes. For example, in the gut Peyer's patches are lymphoid aggregate structures, which contain in their epithelium special cells that are highly efficient in antigen uptake[30]. These highly specialized cells, known as M cells, are able to phagocytose antigen from the lumen of the bronchial and gastrointestinal tract and deliver antigen to DCs in secondary lymphoid structures. Peyer's patches in the gut and lymphoid aggregates in the subepithelial space of the nasal and bronchial tract are able to efficiently scrub lymph drained from these tissue for antigens, and subsequently promote drainage to systemic lymph nodes.

In contrast to the BALT and the GALT, the reproductive tract does not have associated lymphoid tissues or specialized M cells. Two major sets of lymph nodes drain the reproductive tract tissues. The iliac lymph nodes, comprised of the caudal, sacral, and lymph lymph nodes, drain the upper two-thirds of the reproductive tract. The inguinal lymph nodes are responsible for draining the lower third of the vagina[23]. It has been reported that the uterus contains a lymphoid structure containing B and T cells, but the exact role and function is unclear. During post primary infection with virus, foci of T and B lymphocytes and DCs have been observed to organize near the epithelium, providing rapid response to secondary infection[13]. The lack of organized lymphoid structure in the reproductive tract limits the migration of leukocytes and lymphocytes in and out of the tissue. Therefore, the role of professional antigen presenting cells in

aiding with efficient immune responses to pathogens and vaccines in this compartment is undeniable: DCs are responsible for vaccine uptake, processing, and presentation. However, in the absence of inflammation, the insufficient numbers of steady-state professional antigen presenting cells in reproductive tissues is a major challenge facing immunization in the vaginal tract.

2.A.4. Role of mucus and maintenance of vaginal pH

In addition to reduced lymphatic drainage of intravaginally delivered vaccine antigens, poor mucus penetration traps vaccines, which can be subsequently degraded by enzymes. Reproductive tissues, like other mucosal surfaces, are constantly producing mucus to promote ciliary clearance as well as to perform other immune defense mechanisms. In contrast to type I mucosal surfaces where mucus is produced by Goblet cells, in the reproductive system mucus is secreted from epithelial cells in the vagina and from cervical crypts, which extend down into the lower genital tract during the ovulatory phase of the menstrual cycle[11,13]. Mucus secretions are composed of a number of different mucin proteins, which are encoded for by the MUC1 gene[31].

A straightforward mechanism of defense in the genital tract is the restricted diffusivity of opsonized pathogens in cervicovaginal mucus[32]. Mucin proteins are heavily glycosylated and high in molecular mass[13]. These large, complex proteins allow for entanglement and entrapment of pathogens in the lumen that may be retained until they are eventually secreted. Similar to antimicrobial and chemokine production, mucus production is also influenced by different stages of the menstrual cycle. For example, mucus viscosity is lower prior to and during ovulation[11], which is important for sperm motility and movement up the lower vaginal tract. The cervical mucus plug plays an important role acting as a physical barrier to lower the incidence of pathogen transmission to the upper female reproductive tract where pregnancy can be compromised[33].

The presence of mucus also has a significant impact on the local pH of the vaginal environment, which is generally maintained by commensal host bacteria[11]. The predominant bacterium in the reproductive tract is *Lactobacillus*, which is responsible for lactic acid production that maintains the low acidic pH in the vagina. Normal pH in the

female reproductive tract is maintained in the range of 4-5 and can vary between different ethnicities. It murine models, the vaginal pH is slightly higher, between 6.2-6.5[34]. Infection by bacteria has been shown to alter the local pH. An important aspect of the local acidic pH is charge shielding of HIV virions, which posses an overall negative surface charge[35]. Charge shielding by mucin proteins slows HIV diffusion through mucus. Interestingly, the presence of semen buffers the vaginal pH to alkaline conditions (pH 8-9). As such, HIV virions that are present in semen are likely in an environment more conducive to transmission.

Variability in mucus and vaginal pH can arise from a number of factors, including hormonal regulation during the lifecycle[36]. While the normal pH of the vaginal environment is acidic, it has been noted that the local pH transiently becomes more alkaline during ovulation, in the presence of semen post-coition, and during certain infections such as bacterial vaginosis [37,38]. The impact of vaginal pH and mucus on virus-like particle diffusion has been well characterized in *ex vivo* models. Shukair *et al.* reported that while HIV-1 particles exhibited reduced diffusion in cervicovaginal mucus (CVM) as compared to a saline solution, this phenomenon was not dependent on the presence of HIV envelope glycoproteins[39]. Moreover, they found that virion diffusion directly correlated to pH. Separate studies confirmed that HIV-1 and HSV-1 virions were immobilized in low pH CVM, characterized by a lactic-acid rich environment[35]. However, virions freely diffused in mucus near neutral pH. Further studies revealed that IgG freely diffused through vaginal mucus only transiently and weakly interacting with mucin proteins. However, the presence of IgG (even non-neutralizing IgG) within mucus was essential in trapping and immobilizing virions[40]. Leukocyte motility in cervical mucus and their ability to penetrate the mucus layer has also been documented [41]. For example, the measured motility coefficient of neutrophils in human midcervical mucus is $\sim 10^{-8}$ $cm^2 \cdot s^{-1}$ and increases up to 4-fold in the presence of a formylated tripeptide chemokine. Leukocytes were also observed to completely penetrate across a mucus layer of 500 μm thickness but not larger. These data support the effective migration of leukocytes in mucus, which may play an important role in immunity and infection.

2.A.5. Antibody production

Antibody production at mucosal surfaces varies in different mucosal tissues. In many type I mucosal surfaces, such as the gut mucosa, IgA is the predominant antibody subtype. IgA produced in the subepithelial space is transcytosed as dimeric IgA by the poly Ig receptor (pIgR) across the gut epithelium[42]. In contrast, the predominant antibody type produced in reproductive tract tissues is IgG. Control of IgG presence in the vaginal lumen is not fully understood. However, it has been shown that IgG can be paracellularly transported from the subepithelial space to the surface of the mucosa. It has also been shown that IgG can be transcytosed bidirectionally across the vaginal epithelium by receptors expressed on vaginal epithelial cells [43] (Figure 2-1). It is possible that both mechanisms of IgG transport act together to provide protective concentrations of neutralizing antibodies in the lumen and to transport opsonized pathogens back into the lamina propria where they may be taken up by professional antigen presenting cells via the Fcg receptor[44].

2.B. Bioengineering intravaginal vaccines for sexually transmitted infections

Several strategies have been employed to improve or promote the specific effector mechanisms required for protective immunity in the genital mucosa. One strategy is focused on local enrichment of effector immune cells. A recent study by Shin et al. demonstrated a new vaccine strategy for sexually transmitted diseases termed “prime and pull”[45]. In the “prime and pull” paradigm, vaccines are subcutaneously injected to evoke a systemic immune response (“prime”). This is followed by topical application of chemokines CXLC9/10 to recruit (“pull”) and establish a local T cell population, which can provide long-term memory and curb the spread of HSV-2 to neurons and prevent clinical manifestations of disease. This strategy allows for systemic “priming” and active “pulling” of effector T lymphocytes to the genital mucosa in order to respond efficiently during viral infection. However, this strategy requires pairing mucosal delivery of agents with a subcutaneous immunization, rather than local delivery of the immunization itself within the reproductive tissues.

A separate strategy focuses on the administration of protein or peptide biologics to recruit leukocytes (specifically antigen presenting cells) into tissues to promote

vaccine uptake, processing, and presentation. The observation that strong adjuvants are required to potentiate mucosal immune responses to non-replicating subunit vaccines administered to the vaginal mucosa suggests a critical role for mucosal DCs in shaping the immune response in the genital tract. In the context of vaccines, research has shown that antigen delivery at the site of infection may be important in imprinting T cells during priming with the ability to home back to the site of pathogen encounter[46,47]. The specific recruitment of immature or not fully differentiated antigen presenting cells minimizes non-specific inflammation, which may be a result of upregulated inflammatory cytokine and chemokine secretion. One approach has been to administer chemokines, which promote chemotaxis of APCs from distal sites to sites of immunization. For example, CCL20 is commonly used as a chemoattractant for CCR-6 bearing DCs and macrophages[48,4953,54]. CCL20 is a chemokine ligand endogenously produced at basal levels in the body by a variety of cell types. It has been demonstrated that CCL20 production can be upregulated in the presence of other pro-inflammatory signals such as TNF-a[50,51]. *In vitro*, CCR6 agonists such as macrophage inflammatory protein (MIP)-3a have been shown to promote chemotaxis of CCR6 bearing cells[28,52-55]. Research groups have shown that particles, which slowly release CCL20 over time are able to recruit monocytes and immature DCs, as well as bone marrow-derived dendritic cells[56]. Furthermore, studies have shown the ability to recruit DCs and macrophages to sites of immunization *in vivo* with CCL20[28,57]. Aside from CCL20, studies have also evaluated the potential for antimicrobial b-defensins to act as DC chemoattractants[50,58,59]. Although b-defensins are constitutively expressed as antimicrobial agents by mucosal epithelial cells[60] and are also CCR6 agonists[61], their affinity for CCR6 is much lower than CCL20[62].

The use of molecular adjuvants to boost the immune response by stimulating upregulation of co-stimulatory molecules is common and well studied[63-66]. CpG, a TLR9 agonist, is a commonly used vaccine adjuvant via systemic and mucosal routes of administration. Many lines of evidence suggests that mucosal vaccines delivered in the presence of strong adjuvants such as CpG, which stimulates epithelial cells via the TLR9 receptor, induce cytokine secretion and increased infiltration of activated CD8+ T-

cells[67,68]. Furthermore, intravaginally delivered CpG has been shown to recruit DCs[69]. However, molecular adjuvants non-specifically stimulate the immune system by a number of mechanisms of action by recruiting and activating a broad range of cell types. This non-specific mechanism of cell activation, and its application for vaccine delivery strategies, is controversial due to potential tissue toxicity[70,71]. Other general mucosal adjuvants apart from CpG have also been used to enhance co-stimulation of lymphocytes including cholera toxin and monophosphoryl lipid A (MPLA), a TLR4 agonist[2,72]. More recently, polycationic polymers such polyethylenimine (PEI) have been employed as potent mucosal adjuvants[73]. A major component of selecting adjuvants for intravaginal vaccination is their mechanism of action, and whether the molecular targets engaged by general mucosal adjuvants are distributed on vaginal epithelial cells.

Recently, research has focused on leveraging molecular targets presented on vaginal epithelial cells as potential targets for adjuvanting function. Lipopeptides are self-adjuvanting vaccines synthesized by conjugating synthetic peptide immunogens with lipid agonists for Toll-like receptor 2 (TLR-2), a pattern recognition receptor highly expressed by vaginal epithelial cells[70,71,74]. Di- and tri-acylated peptides have shown enhanced affinity for TLR-2, and the hydrophobic lipid tails allow for enhanced cell penetration and uptake. Furthermore, intravaginally delivered HSV-2 lipopeptides show enhanced immune responses, including improved priming of functional T-lymphocytes.

2.B.1. Nanoparticles for mucosal vaccine delivery

Intravaginal drug and vaccine delivery has been a major focus of addressing sexually transmitted pathogens[75-78]. In the context of microbicides, topical administration of antiretrovirals may allow for delivery of agents directly at the site of infection. While several intravaginally delivered vaccines have shown the ability to elicit immune responses in murine models, these systems still face many challenges including poor vaginal retention, limited access to critical immune cells, and degradation by proteases. A major focus of improving delivery both systemically and mucosally has been on the development of nanoparticle systems formulated to deliver drugs or antigens. Here we review the key properties of nanoparticles that may be advantageous in vaccine delivery by intravaginal administration, and examine the development of vaccine-loaded

nanoparticles designed to overcome challenges related to mucosal delivery. Nanocarriers loaded with drug, protein, and adjuvants have been synthesized in variety of sizes and materials including liposomes, nanolipogels, polymeric nanoparticles, and micelles (Figure 2-3). These nanocarrier systems can be largely categorized as polymeric and liposome carriers, which have been used in a range of mucosal delivery applications.

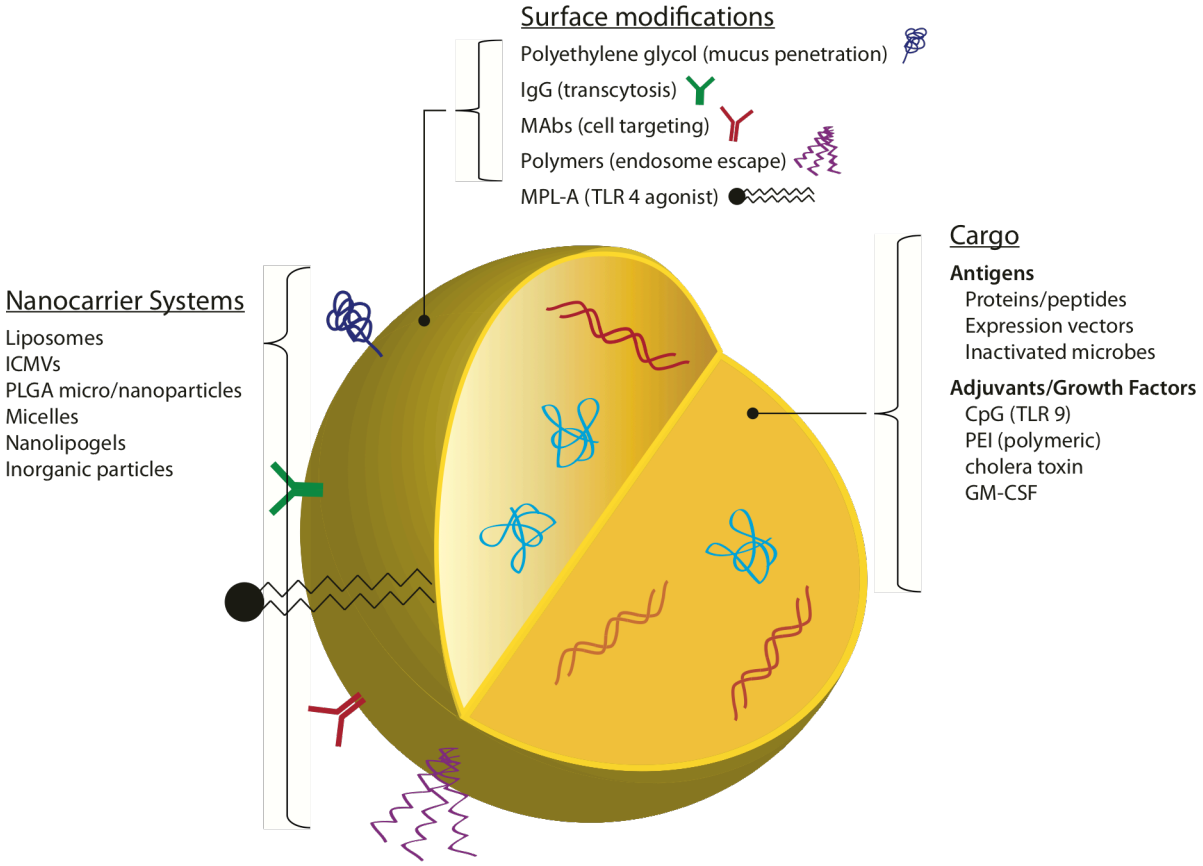

Figure 2-3 Nanocarrier platforms have been synthesized for efficient encapsulation of various cargo including protein and peptide antigens, vectors and inactivated microbes, as well as a variety of adjuvants for co-stimulation of T lymphocytes. These systems can be synthesized from lipids or polymers and range in size to include micelles, nanoparticles, and microparticles. Finally, several of these systems can be surface functionalized with a range of ligands to provide mucus penetration, cell targeting, or endosomal escape.

2.B.2. Nanoparticle platforms for delivery of mucosal antigens and adjuvants

Liposomes have prolific use as vaccines, and a specific category of liposomes known as virosomes, which are vesicle composed of natural phospholipids and fused with specific viral coat proteins, have been employed to create a clinically approved influenza vaccine and a Hepatitis A vaccine[79]. In these applications, virosome technology imitates natural virus membrane structure without delivering genetic material that would cause infection[80]. The ability to incorporate hydrophilic agents into the aqueous core and hydrophobic agents into the lipid bilayer, makes liposomes attractive for delivering a range of physicochemically diverse compounds relevant for vaccines[81,82]. In addition, the diversity of modified lipids that can be incorporated into liposomes allows them to be easily surface conjugated to targeting moieties or antigens, as well as exhibit fusogenic or pH-dependent functionality[83,84]. Furthermore, liposomes are prepared under aqueous and mild conditions that help to preserve the integrity of labile vaccine antigens that may be sensitive to denaturation or degradation. While liposomes possess many advantages they show limited serum stability *in vivo*, resulting in their inability to provide long-term sustained release[85]. Recently, interbilayer crosslinked multilamellar vehicles (ICMVs) were developed to address these challenges observed with simple liposomes[86]. ICMVs consist of multiple lipid bilayers that are chemically crosslinked to create rigid membranes encapsulating an aqueous core. Compared to simple liposomes, ICMVs demonstrate greater loading capacity of protein antigens such as ovalbumin (OVA). ICMVs also demonstrate greater serum-stability and sustained OVA release *in vitro* out to 30 d, which may predict their potential for long-term release of protein cargo *in vivo*. A robust immune response was mounted in mice administered ICMVs loaded with OVA and containing the potent adjuvant monophosphoroyl lipid A (MPLA) anchored into the lipid bilayer. In a separate study, mucosal administration of ICMVs carrying OVA in combination with two TLR-based adjuvants, improved antigen delivery from the lung to draining lymph nodes and stimulated >10-fold greater CD8+ T cell responses in draining lymph nodes than soluble protein[87]. Using an adoptive transfer model of OT-1-luc cells, researchers found that this approach to vaccination also elicited heightened expression of a4b7 mucosal homing integrin and immune responses in distal mucosal sites,

including the vagina. These results suggest that mucosal delivery of antigen in highly stable liposomes can drive cross-presentation. Furthermore, it provides evidence supporting the existence of a common mucosal immune system, which allows for vaccination at one mucosal site to impart specific immunity at other mucosal sites.

As an alternative to liposomal delivery systems, polymer-based nanoparticles also have a number of attributes that are relevant for mucosal vaccine delivery. In particular, several nanoparticle systems have been used for delivering drugs and biologics topically to the vaginal mucosa with excellent efficacy and low cytotoxicity. In the acidic conditions of the vagina, one strategy that may be useful for antigen delivery is encapsulation within a pH-triggered material that releases vaccine cargo. For example, Eudragit® polymers, composed of methacrylic acid and methyl methacrylate, showed the ability to load model hydrophilic and hydrophobic dyes in a pH dependent manner[88]. Both dyes showed enhanced release in the acidic conditions of the vaginal pH. The range of polymers available for incorporation in nanoparticles also allows for the selection of materials with surface biofunctionality that is amenable to antigen release within intracellular compartments. For example, polypropylene sulfide (PPS) nanoparticles conjugated to OVA induced cytotoxic T lymphocyte responses in the lung and spleen after intranasal delivery[89]. Moreover, conjugation of a TLR5 ligand as an adjuvant showed enhanced immune responses in distant mucosal compartments including the vagina and rectum. In this formulation, OVA antigen was conjugated to the surface of PPS nanoparticles via a disulfide bond, which is readily reduced in the intracellular environment. Finally, calcium phosphate nanoparticles that are self-adjuvanting and loaded with a HSV-2 glycoprotein-derived antigen elicited a protective systemic and mucosal immune response following viral challenge *in vivo*[90]. A major consideration in the selection of polymer materials for vaginal delivery is whether the systems promote maximal distribution along the length of the reproductive organs and sustained release, increasing the opportunity for encapsulated cargo to be delivered to target cells. In a gene therapy application, PLGA nanoparticles loaded with high levels of siRNA exhibited highly efficient gene silencing after intravaginal delivery in a murine model. PLGA-siRNA vehicles knocked down the expression of MAPK1 along the entire

length of the vaginal lumen and up into the uterine horns[91]. Moreover it was reported that PLGA nanoparticles were able to successfully penetrate into the epithelial tissue. In another example, Ham et al. showed that PLGA nanoparticles loaded with RANTES sustained release and exhibited anti-HIV activity. *Ex vivo* tissue models showed that RANTES-loaded PLGA nanoparticles exhibited a significant improvement in tissue uptake and permeation, as well as efficient migration to the basement epithelium, when compared to soluble RANTES[92].

2.B.3. Leveraging surface chemistries to overcome the mucus barrier

Mucus production and turnover at mucosal sites is imperative to rapid clearance of foreign bacterial and viral pathogens. As previously discussed, charge shielding by mucin proteins, viscosity, and low-affinity interactions with IgG all play a role in trapping or slowing diffusion of virions such as HIV, which are on the same order of magnitude in size as many vaginal nanoparticle platforms. As such, identifying the key characteristics that allow nanoparticles to overcome the mucus barrier is imperative for vaginal immunization. To date, the field remains controversial as to which physical and chemical material properties are most important. Mucoadhesion was initially considered to be an important characteristic enabling prolonged retention of nanocarriers[93-96]. However, since mucus turnover in the vaginal tract is rapid, mucoadhesive particles may actually promote entrapment by mucin proteins and eventual expulsion of particles from the reproductive tract, rather than prolonged retention or penetration of the vaginal epithelium. Recently, mucus-penetrating particles (MPPs) have been engineered to overcome deliver in the vaginal tract by employing strategies to surface functionalize nanoparticle with moieties that promote high diffusivity in mucus and improved association with the vaginal epithelium[97,98]. MPPs are composed of polymeric nanoparticles that are surface functionalized with a low molecular weight PEG, a hydrophilic polymer. Surface modification of nanoparticles with PEG can employ covalent conjugation strategies or methods that promote phase-separation and partitioning of the hydrophilic PEG polymer to the surface of hydrophobic polymer nanoparticles. The work by Hanes and others have demonstrated that low molecular weight PEG promote mucus penetration whereas high molecular weight PEG may lead

to chain entanglement with mucin proteins and result in mucoadhesion[99,100]. Cu et al. demonstrated in an *in vivo* side-by-side comparison of intravaginal nanoparticle delivery that PEG-modified PLGA nanoparticles showed increased association with the vagina while avidin-modified PLGA nanoparticles and unmodified PLGA nanoparticles were recovered predominantly in cervicovaginal lavages[97]. Intravaginal delivery of fluorescent MPPs demonstrated enhanced ability to penetrate mucus and access the deep folds in the rugae of the vagina compared to conventional polymeric nanoparticles[98]. In the same study, acyclovir-loaded MPPs resulted in a three-fold increase in protection against HSV-2 viral challenge in the murine genital tract than delivery of soluble drug.

While these studies suggest the use of a strategy to overcome the mucus barrier, the application of MPPs for vaginal delivery of vaccines remains to be realized. Furthermore, while MPPs have been shown to improve association with the vaginal epithelium, they are still faced with a secondary barrier of a complex, stratified, squamous epithelium across which to transport antigen. PEGylation of nanoparticles is commonly used to prolong circulation in blood by reducing opsonization, and reducing monocyte and macrophage uptake[101,102]. MPPs, with PEGylated surfaces, may in fact reduce cellular uptake – ultimately reducing the delivery of antigen to target cells. Future studies of vaginal MPP delivery should focus on comparing MPP uptake by local cells to conventional NPs, cell-free and cell-mediated trafficking of particulates to lymph nodes, and the impact of antigen delivery to vaginal APCs after formulation in MPPs.

2.B.4. Exploiting receptor-mediated delivery across a complex mucosal epithelium

While the Type I and Type II epithelia of the female reproductive tract is imperative in defending against foreign pathogens, it also serves as a barrier to vaginally delivered vaccines. A major focus in mucosal drug delivery design is to engineer systems that transport cargo across the epithelium without relying on the use of mucosal adjuvants, which may enhance delivery by compromising the integrity of the epithelium. Recently, several studies have evaluated mechanisms of transcytosis that utilize recycling receptors expressed by cells at mucosal sites. These recycling receptors are targeted to promote transepithelial transport from the apical to basal

membrane, where they may access organized lymphoid structures or antigen presenting cells in the lamina propria.

A recent study evaluated the delivery of gp140 across the nasal epithelium by conjugating the protein to transferrin[103]. Transferrin conjugated gp140 engaged the transferrin receptor (CD71), expressed on the nasal mucosal epithelium, promoting active delivery of cargo across the epithelium and ultimately improving systemic and vaginal immune responses to intranasal vaccination. Several other groups have exploited this same receptor by functionalizing nanoparticles with transferrin for the application of drug delivery to the brain[104,105]. Active transcytosis of nanoparticles after oral delivery has also been shown to improve delivery across the Type I intestinal epithelium[106]. In this study, PLA-PEG-based nanoparticles were modified with Fc protein, which binds the neonatal Fc receptor (FcRn). The authors found that Fc-modified nanoparticles successfully crossed the intestinal epithelium and entered the lamina propria after oral delivery, and were able to reach systemic circulation. FcRn is expressed by several organs[107], including the reproductive tract where bidirectional transcytosis of IgG has been shown in a murine model[34]. Importantly, the Fc-FcRn interaction is strongest at an acidic pH and it is hypothesized that the encounter occurs in acidified endosomes, rescuing IgG from lysosomal degradation. However, given the acidic pH of the human vagina, it is likely that Fc-FcRn interactions may also occur at the surface of the vaginal epithelium. Surface protein modification of nanoparticles to engage receptors to promote active delivery across a complex epithelium has been shown to be successful at other mucosal surfaces, and may be a strategy to enhance delivery to the lamina propria for vaginally delivered vaccines. Future studies may also aim to elucidate the specific synergy between active transcytosis and nanoparticle formulation of antigens. For example, a head-to-head comparison of intravaginal delivery of soluble antigen and nanoparticle-formulated antigen, both modified to target a recycling receptor, would inform the relative contribution and importance of nanocarriers versus transeptihelial transport.

2.B.5. Dendritic cell targeted nanoparticles for mucosal vaccination

In order to mount an effective immune response to vaginal vaccination, antigens must be taken up by relevant APCs, specifically DCs located in the lamina propria. The advantages of formulating antigen in nanoparticles include optimizing antigen in carriers that are preferentially taken up by target DCs due to size, surface charge, or morphology[108,109]. A number of studies have evaluated the impact of size on cellular uptake, and it is generally observed that nanoparticles <500 nm are preferentially taken up by DCs[110]. Specifically, after subcutaneous administration, it was observed that DEC205+ DCs preferentially internalize 20 nm and 40 nm diameter nanoparticles in draining lymph nodes. In contrast, 1 μm particles showed heightened uptake in F4/80+ macrophages. A follow up study by the same group evaluated uptake of 50 nm and 500 nm nanoparticles after intratracheal instillation in pulmonary APC subsets[111]. The results showed that 50 nm diameter nanoparticles were more significantly taken up by lung APCs, and specifically by DCs in draining lymph nodes. Both studies evaluated the use of these nanoparticles in immunotherapeutic strategies, and demonstrated that smaller sized nanoparticles resulted in more favorable immune responses. Consideration of nanoparticle size can have a major impact on intravaginal mucosal vaccines. Apart from potentially improving passive targeting of vaginal DC subsets, engineering smaller sized nanoparticles also increases the surface area to volume ratio – allowing immobilization of a higher density of antigens or targeting ligands. Further, *in vitro* studies have also suggested that engineering positively charged surfaces might be a strategy for improving nanoparticle uptake for larger sized particulates[112,113], which may have the capacity to more strongly induce DC maturation. However, exclusively engineering nanoparticles with a positive surface charge may lead to improved uptake in all cells due to their interaction with the negatively charged cell membrane, and may not skew towards DC targeting.

While consideration of nanoparticle size and surface charge allows for passive targeting of APCs, it has also been demonstrated that nanoparticle systems can be surface functionalized with moieties that target their cargo to receptors uniquely expressed by APCs. For example, a recent study evaluated the delivery of plasmid DNA

loaded chitosan nanoparticles after intranasal administration against nucleocapsid protein and found that by immobilizing a fusion protein specific for the DEC-205 receptor allowed for enhancing targeting specificity to DCs after nasal immunization[114]. Several other studies show the ability to employ nanoparticle surface functionalization to target to various DC receptors relevant in humans, *in vitro* and *in vivo*, including DC-SIGN and Fcg[115,116]. While active targeting of DCs has been shown to be successful in these studies, it remains to be realized if similar approaches can be used in vaginal nanoparticle delivery of antigens. This is largely due to the fact that while various vaginal DC subsets have been explored, there still remains a great deal of uncertainty as to which subsets promote tolerance versus immunity. Furthermore, the specific and unique expression of potential target receptors on vaginal DCs still remains to be thoroughly characterized.

2.C. Summary and future outlooks

Formulation of antigens in nanocarriers for immune stimulation has been widely explored. However, the adaptation of these strategies in the context of the specific delivery challenges in the vaginal mucosal environment may require finding synergies between multiple approaches to address efficient mucus penetration, epithelium transcytosis, and dendritic cell uptake. Nanocarrier systems provide an innovative approach for developing pathogen-mimicking materials for engineering mucosal immunity. The diversity of materials used to synthesize carrier system in addition to formulation of biologics and signaling molecules enable the ability to target mucosal DCs and potentially modulate their function towards a specific immune response. Many co-stimulatory molecules being evaluated as mucosal adjuvant candidates present significant delivery challenges that include stability and solubility, local toxicity, and requirement for targeting of specific tissues and cells while limiting systemic absorption. In addition, there is strong rationale to deliver a combination of maturation stimuli to mimic natural pathogens and realize potential adjuvant synergy. Nanocarrier delivery systems have the capacity to address challenges of co-delivering antigens with adjuvant combinations, and modulating their presentation kinetics and compartmentalization in specific mucosal DC subsets. Elucidating the mechanisms in which the interpretation of

antigen and adjuvant agents in the mucosa causes immunity or tolerance will broaden our understanding of mucosal biology and the engineering of effective mucosal vaccines.

2.D. References

1. Kozlowski, P. A., Cu-Uvin, S., Neutra, M. R. & Flanigan, T. P. Comparison of the oral, rectal, and vaginal immunization routes for induction of antibodies in rectal and genital tract secretions of women. 65, 1387–1394 (1997).
2. Park, J.-S., Oh, Y.-K., Kang, M.-J. & Kim, C.-K. Enhanced mucosal and systemic immune responses following intravaginal immunization with human papillomavirus 16 L1 virus-like particle vaccine in thermosensitive mucoadhesive delivery systems. *J. Med. Virol.* 70, 633–641 (2003).
3. Kozlowski, P. A. *et al.* Differential Induction of Mucosal and Systemic Antibody Responses in Women After Nasal, Rectal, or Vaginal Immunization: Influence of the Menstrual Cycle. *The Journal of …* (2002).
4. World Health Organization. Global strategy for the prevention and control of sexually transmitted infections: 2006-2015: breaking the chain of transmission. (2007).
5. Kozlowski, P. A., Cu-Uvin, S., Neutra, M. R. & Flanigan, T. P. Mucosal vaccination strategies for women. 179 Suppl 3, S493–8 (1999).
6. Lewis, D. A., Latif, A. S. & Ndowa, F. WHO global strategy for the prevention and control of sexually transmitted infections: time for action. *Sex Transm Infect* 83, 508–509 (2007).
7. Weinstock, H., Berman, S. & Cates, W. Sexually transmitted diseases among American youth: incidence and prevalence estimates, 2000. 36, 6–10 (2004).
8. Chesson, H. W., Blandford, J. M., Gift, T. L., Tao, G. & Irwin, K. L. The estimated direct medical cost of sexually transmitted diseases among American youth, 2000. 36, 11–19 (2004).
9. Quinn, T. C. & Overbaugh, J. HIV/AIDS in women: an expanding epidemic. *Science* 308, 1582–1583 (2005).
10. Charles A Janeway, J., Travers, P., Walport, M. & Shlomchik, M. J. Immunobiology. (2001).
11. Hickey, D. K., Patel, M. V., Fahey, J. V. & Wira, C. R. Innate and adaptive immunity at mucosal surfaces of the female reproductive tract: stratification and integration of immune protection against the transmission of sexually transmitted infections. *J Reprod Immunol* 88, 185–194 (2011).
12. Hladik, F. & McElrath, M. J. Setting the stage: host invasion by HIV. *Nat Rev Immunol* 8, 447–457 (2008).
13. Iwasaki, A. Antiviral immune responses in the genital tract: clues for vaccines. *Nat Rev Immunol* 10, 699–711 (2010).
14. Naz, R. K. Female genital tract immunity: distinct immunological challenges for vaccine development. *J Reprod Immunol* (2011). doi:10.1016/j.jri.2011.09.005
15. Ochiel, D. O., Fahey, J. V., Ghosh, M., Haddad, S. N. & Wira, C. R. Innate Immunity in the Female Reproductive Tract: Role of Sex Hormones in Regulating Uterine Epithelial Cell Protection Against Pathogens. *Curr Womens*

Health Rev 4, 102–117 (2008).
16. Kim, M., Ogawa, M., Mimuro, H. & Sasakawa, C. Reinforcement of epithelial cell adhesion to basement membrane by a bacterial pathogen as a new infectious stratagem. *Virulence* 1, 52–55 (2010).
17. LAMB, J. C., Newbold, R. R., STUMPF, W. E. & McLACHLAN, J. A. Transitional Changes in the Surface Epithelium of the Cycling Mouse Vagina, Cervix and Uterus: Scanning Electron Microscopic Studies. (1978).
18. Bobardt, M. D. *et al.* Cell-Free Human Immunodeficiency Virus Type 1 Transcytosis through Primary Genital Epithelial Cells. *J Virol* 81, 395–405 (2006).
19. Hladik, F. *et al.* Initial Events in Establishing Vaginal Entry and Infection by Human Immunodeficiency Virus Type-1. *Immunity* 26, 257–270 (2007).
20. Iijima, N., Thompson, J. M. & Iwasaki, A. Dendritic cells and macrophages in the genitourinary tract. *Mucosal Immunol* 1, 451–459 (2008).
21. Wira, C. & Tschudy, K. G. Epithelial cells in the female reproductive tract: a central role as sentinels of immune protection. *… of Reproductive …* (2005).
22. Shaykhiev, R. & Bals, R. Interactions between epithelial cells and leukocytes in immunity and tissue homeostasis. *J. Leukoc. Biol.* 82, 1–15 (2007).
23. Iwasaki, A. Mucosal dendritic cells. *Annu. Rev. Immunol.* (2007).
24. Iijima, N., Linehan, M. M., Saeland, S. & Iwasaki, A. Vaginal epithelial dendritic cells renew from bone marrow precursors. *Proc Natl Acad Sci USA* 104, 19061–19066 (2007).
25. Merad, M., Ginhoux, F. & Collin, M. Origin, homeostasis and function of Langerhans cells and other langerin-expressing dendritic cells. *Nat Rev Immunol* 8, 935–947 (2008).
26. Zhao, X. *et al.* Vaginal Submucosal Dendritic Cells, but Not Langerhans Cells, Induce Protective Th1 Responses to Herpes Simplex Virus-2. (2003).
27. Iijima, N., Mattei, L. M. & Iwasaki, A. Recruited inflammatory monocytes stimulate antiviral Th1 immunity in infected tissue. *Proc Natl Acad Sci USA* 108, 284–289 (2011).
28. Le Borgne, M. *et al.* Dendritic cells rapidly recruited into epithelial tissues via CCR6/CCL20 are responsible for CD8+ T cell crosspriming in vivo. *Immunity* 24, 191–201 (2006).
29. Ogra, P. L. Mucosal immunity: some historical perspective on host-pathogen interactions and implications for mucosal vaccines. *Immunol. Cell Biol.* 81, 23–33 (2003).
30. Neutra, M. R., Mantis, N. J. & Kraehenbuhl, J.-P. Collaboration of epithelial cells with organized mucosal lymphoid tissues - Nature Immunology. *Nat. Immunol.* 2, 1004–1009 (2001).
31. Gipson, I. K. *et al.* Mucin genes expressed by human female reproductive tract epithelia. (1997).
32. Olmsted, S. S. *et al.* Diffusion of macromolecules and virus-like particles in human cervical mucus. *Biophys J* 81, 1930–1937 (2001).
33. Wira, C. R., Patel, M. V., Ghosh, M., Mukura, L. & Fahey, J. V. Innate immunity

in the human female reproductive tract: endocrine regulation of endogenous antimicrobial protection against HIV and other sexually transmitted infections. *Am J Reprod Immunol* 65, 196–211 (2011).
34. Li, Z. *et al.* Transfer of IgG in the female genital tract by MHC class I-related neonatal Fc receptor (FcRn) confers protective immunity to vaginal infection. *Proc Natl Acad Sci USA* 108, 4388–4393 (2011).
35. Lai, S. K. *et al.* Human Immunodeficiency Virus Type 1 Is Trapped by Acidic but Not by Neutralized Human Cervicovaginal Mucus. *J Virol* 83, 11196–11200 (2009).
36. Bouvet, J.-P., Grésenguet, G. & Bélec, L. Vaginal pH neutralization by semen as a cofactor of HIV transmission. *Clin. Microbiol. Infect.* 3, 19–23 (1997).
37. Brabin, L. *et al.* Factors affecting vaginal pH levels among female adolescents attending genitourinary medicine clinics. *Sex Transm Infect* 81, 483–487 (2005).
38. Macdonald, R. R. & Lumley, I. B. Endocervical pH measured in vivo through the normal menstrual cycle. *Obstet Gynecol* 35, 202–206 (1970).
39. Shukair, S. A. *et al.* Human cervicovaginal mucus contains an activity that hinders HIV-1 movement. *Mucosal Immunol* 6, 427–434 (2013).
40. Wang, Y. Y. *et al.* IgG in cervicovaginal mucus traps HSV and prevents vaginal herpes infections. *Mucosal Immunol* 7, 1036–1044 (2014).
41. Parkhurst, M. R. & Saltzman, W. M. Leukocytes migrate through three-dimensional gels of midcycle cervical mucus. *Cellular immunology* 156, 77–94 (1994).
42. Woof, J. M. & Mestecky, J. Mucosal immunoglobulins. *Immunol Rev* 206, 64–82 (2005).
43. Kumamoto, Y. & Iwasaki, A. Unique features of antiviral immune system of the vaginal mucosa. *Current opinion in immunology* 24, 411–416 (2012).
44. Kelsall, B. L. & Rescigno, M. Mucosal dendritic cells in immunity and inflammation. *Nat. Immunol.* (2004).
45. Shin, H. & Iwasaki, A. A vaccine strategy that protects against genital herpes by establishing local memory T cells. *Nature* 491, 463–467 (2012).
46. Mikhak, Z., Strassner, J. P. & Luster, A. D. Lung dendritic cells imprint T cell lung homing and promote lung immunity through the chemokine receptor CCR4. *Journal of Experimental Medicine* 210, 1855–1869 (2013).
47. Mora, J. R. *et al.* Selective imprinting of gut-homing T cells by Peyer's patch dendritic cells. *Nature* 424, 88–93 (2003).
48. Schutyser, E., Struyf, S. & Van Damme, J. The CC chemokine CCL20 and its receptor CCR6. *Cytokine & Growth Factor Reviews* 14, 409–426 (2003).
49. Mackay, C. R. Chemokines: immunology's high impact factors. *Nat. Immunol.* 2, 95–101 (2001).
50. Ito, T., Carson, W. F., IV, Cavassani, K. A., Connett, J. M. & Kunkel, S. L. CCR6 as a mediator of immunity in the lung and gut. *Experimental Cell Research* 317, 613–619 (2011).
51. Iwasaki, A. & Kelsall, B. L. Localization of distinct Peyer's patch dendritic cell subsets and their recruitment by chemokines macrophage inflammatory protein

(MIP)-3alpha, MIP-3beta, and secondary lymphoid organ chemokine. *J. Exp. Med.* 191, 1381–1394 (2000).
52. Dieu-Nosjean, M. C., Vicari, A., Lebecque, S. & Caux, C. Regulation of dendritic cell trafficking: a process that involves the participation of selective chemokines. *J. Leukoc. Biol.* 66, 252–262 (1999).
53. Hedrick, M. N., Lonsdorf, A. S., Hwang, S. T. & Farber, J. M. CCR6 as a possible therapeutic target in psoriasis. *Expert Opin. Ther. Targets* 14, 911–922 (2010).
54. Dieu-Nosjean, M. C. *et al.* Macrophage inflammatory protein 3alpha is expressed at inflamed epithelial surfaces and is the most potent chemokine known in attracting Langerhans cell precursors. *J. Exp. Med.* 192, 705–718 (2000).
55. Dieu, M. C. *et al.* Selective recruitment of immature and mature dendritic cells by distinct chemokines expressed in different anatomic sites. *J. Exp. Med.* 188, 373–386 (1998).
56. Zhao, X., Jain, S., Larman, H. B., Gonzalez, S. & Irvine, D. J. Directed cell migration via chemoattractants released from degradable microspheres. *Biomaterials* 26, 5048–5063 (2005).
57. Song, R., Liu, S. & Leong, K. W. Effects of MIP-1α, MIP-3α, and MIP-3β on the Induction of HIV Gag-specific Immune Response with DNA Vaccines. *Mol Ther* 15, 1007–1015 (2007).
58. Oppenheim, J. J., Biragyn, A., Kwak, L. W. & Yang, D. Roles of antimicrobial peptides such as defensins in innate and adaptive immunity -- Oppenheim et al. 62 (suppl 2): ii17 -- Annals of the Rheumatic Diseases. (2003).
59. Dürr, M. & Peschel, A. Chemokines Meet Defensins: the Merging Concepts of Chemoattractants and Antimicrobial Peptides in Host Defense. *Infection and Immunity* 70, 6515–6517 (2002).
60. Sinha, S., Cheshenko, N., Lehrer, R. I. & Herold, B. C. NP-1, a rabbit alpha-defensin, prevents the entry and intercellular spread of herpes simplex virus type 2. *Antimicrob. Agents Chemother.* 47, 494–500 (2003).
61. Biragyn, A. *et al.* Mediators of innate immunity that target immature, but not mature, dendritic cells induce antitumor immunity when genetically fused with nonimmunogenic tumor antigens. *J. Immunol.* 167, 6644–6653 (2001).
62. Yang, D. *et al.* Beta-defensins: linking innate and adaptive immunity through dendritic and T cell CCR6. *Science* 286, 525–528 (1999).
63. Krieg, A. M. Antiinfective applications of toll-like receptor 9 agonists. *Proc Am Thorac Soc* 4, 289–294 (2007).
64. Vollmer, J. & Krieg, A. M. Immunotherapeutic applications of CpG oligodeoxynucleotide TLR9 agonists. *Adv. Drug Deliv. Rev.* 61, 195–204 (2009).
65. McCluskie, M. J. & Davis, H. L. CpG DNA as mucosal adjuvant. *Vaccine* 18, 231–237 (1999).
66. Bode, C., Zhao, G., Steinhagen, F., Kinjo, T. & Klinman, D. M. CpG DNA as a vaccine adjuvant. *Expert Rev Vaccines* 10, 499–511 (2011).
67. Jiang, J. Q., Patrick, A., Moss, R. B. & Rosenthal, K. L. CD8+ T-cell-mediated

cross-clade protection in the genital tract following intranasal immunization with inactivated human immunodeficiency virus antigen plus CpG oligodeoxynucleotides. *J Virol* 79, 393–400 (2005).
68. Pettini, E. *et al.* Vaginal immunization to elicit primary T-cell activation and dissemination. *PLoS ONE* 8, e80545 (2013).
69. Sajic, D., Patrick, A. J. & Rosenthal, K. L. Mucosal delivery of CpG oligodeoxynucleotides expands functional dendritic cells and macrophages in the vagina. *Immunology* 114, 213–224 (2005).
70. BenMohamed, L., Wechsler, S. L. & Nesburn, A. B. Lipopeptide vaccines--yesterday, today, and tomorrow. *Lancet Infect Dis* 2, 425–431 (2002).
71. Zhang, X. *et al.* Th-cytotoxic T-lymphocyte chimeric epitopes extended by Nepsilon-palmitoyl lysines induce herpes simplex virus type 1-specific effector CD8+ Tc1 responses and protect against ocular infection. *J Virol* 79, 15289–15301 (2005).
72. Vajdy, M. *et al.* Mucosal adjuvants and delivery systems for protein-, DNA- and RNA-based vaccines. *Immunol. Cell Biol.* 82, 617–627 (2004).
73. Wegmann, F. *et al.* Polyethyleneimine is a potent mucosal adjuvant for viral glycoprotein antigens. *Nat Biotechnol* 30, 883–888 (2012).
74. BenMohamed, L. *et al.* Lipopeptide immunization without adjuvant induces potent and long-lasting B, T helper, and cytotoxic T lymphocyte responses against a malaria liver stage antigen in mice and chimpanzees. *Eur J Immunol* 27, 1242–1253 (1997).
75. Rohan, L. C. & Sassi, A. B. Vaginal Drug Delivery Systems for HIV Prevention. *AAPS J* 11, 78–87 (2009).
76. Vermani, K. & Garg, S. The scope and potential of vaginal drug delivery. *Pharm. Sci. Technol. Today* 3, 359–364 (2000).
77. Lu, L. *et al.* A neonatal Fc receptor-targeted mucosal vaccine strategy effectively induces HIV-1 antigen-specific immunity to genital infection. *J Virol* 85, 10542–10553 (2011).
78. Cuburu, N. & Chackerian, B. Genital delivery of virus-like particle and pseudovirus-based vaccines. *Expert Rev Vaccines* 10, 1245–1248 (2011).
79. Schwendener, R. A. Liposomes as vaccine delivery systems: a review of the recent advances. *Therapeutic advances in vaccines* 2, 159–182 (2014).
80. Chang, H.-I. & Yeh, M.-K. Clinical development of liposome-based drugs: formulation, characterization, and therapeutic efficacy. *International Journal of Nanomedicine* 7, 49 (2012).
81. Rosen, H. & Abribat, T. Timeline: The rise and rise of drug delivery. *Nat Rev Drug Discov* 4, 381–385 (2005).
82. Zhang, L. *et al.* Nanoparticles in Medicine: Therapeutic Applications and Developments. *Clin Pharmacol Ther* 83, 761–769 (2007).
83. Csiszár, A. *et al.* Novel fusogenic liposomes for fluorescent cell labeling and membrane modification. *Bioconjugate chemistry* 21, 537–543 (2010).
84. Kunisawa, J., Nakagawa, S. & Mayumi, T. Pharmacotherapy by intracellular delivery of drugs using fusogenic liposomes: application to vaccine

development. *Adv. Drug Deliv. Rev.* 52, 177–186 (2001).
85. Kamaly, N., Xiao, Z., Valencia, P. M., Radovic-Moreno, A. F. & Farokhzad, O. C. Targeted polymeric therapeutic nanoparticles: design, development and clinical translation. *Chem. Soc. Rev.* 41, 2971–3010 (2012).
86. Moon, J. J. *et al.* Interbilayer-crosslinked multilamellar vesicles as synthetic vaccines for potent humoral and cellular immune responses. *Nat Mater* 10, 243–251 (2011).
87. Li, A. V. *et al.* Generation of effector memory T cell-based mucosal and systemic immunity with pulmonary nanoparticle vaccination. *Science Translational Medicine* 5, 204ra130 (2013).
88. Yoo, J.-W., Giri, N. & Lee, C. H. pH-sensitive Eudragit nanoparticles for mucosal drug delivery. *International Journal of Pharmaceutics* 403, 262–267 (2011).
89. Stano, A. *et al.* PPS nanoparticles as versatile delivery system to induce systemic and broad mucosal immunity after intranasal administration. *Vaccine* 29, 804–812 (2011).
90. He, Q., Mitchell, A., Morcol, T. & Bell, S. J. D. Calcium phosphate nanoparticles induce mucosal immunity and protection against herpes simplex virus type 2. *Clin. Diagn. Lab. Immunol.* 9, 1021–1024 (2002).
91. Woodrow, K. A. *et al.* Intravaginal gene silencing using biodegradable polymer nanoparticles densely loaded with small-interfering RNA. *Nat Mater* 8, 526–533 (2009).
92. Ham, A. S., Cost, M. R., Sassi, A. B., Dezzutti, C. S. & Rohan, L. C. Targeted delivery of PSC-RANTES for HIV-1 prevention using biodegradable nanoparticles. *Pharm. Res.* 26, 502–511 (2009).
93. Takeuchi, H., Yamamoto, H. & Kawashima, Y. Mucoadhesive nanoparticulate systems for peptide drug delivery. *Adv. Drug Deliv. Rev.* 47, 39–54 (2001).
94. Bernkop-Schnürch, A. Mucoadhesive systems in oral drug delivery. *Drug Discovery Today: Technologies* 2, 83–87 (2005).
95. Meng, J., Sturgis, T. F. & Youan, B.-B. C. Engineering tenofovir loaded chitosan nanoparticles to maximize microbicide mucoadhesion. *European Journal of Pharmaceutical Sciences* 44, 57–67 (2011).
96. Dünnhaupt, S. *et al.* Distribution of thiolated mucoadhesive nanoparticles on intestinal mucosa. *International Journal of Pharmaceutics* 408, 191–199 (2011).
97. Cu, Y., Booth, C. J. & Saltzman, W. M. In vivo distribution of surface-modified PLGA nanoparticles following intravaginal delivery. *J Control Release* 156, 258–264 (2011).
98. Ensign, L. M. *et al.* Mucus-Penetrating Nanoparticles for Vaginal Drug Delivery Protect Against Herpes Simplex Virus. *Science Translational Medicine* 4, 138ra79–138ra79 (2012).
99. Wang, Y.-Y. *et al.* Addressing the PEG mucoadhesivity paradox to engineer nanoparticles that ‘slip’ through the human mucus barrier. *Angew. Chem. Int. Ed.* 47, 9726–9729 (2008).
100. Lai, S. K., Wang, Y.-Y. & Hanes, J. Mucus-penetrating nanoparticles for drug and gene delivery to mucosal tissues. *Adv. Drug Deliv. Rev.* 61, 158–171

(2009).
101. Jokerst, J. V., Lobovkina, T., Zare, R. N. & Gambhir, S. S. Nanoparticle PEGylation for imaging and therapy. *Nanomedicine* 6, 715–728 (2011).
102. Özcan, I. *et al.* Pegylation of poly (γ-benzyl-L-glutamate) nanoparticles is efficient for avoiding mononuclear phagocyte system capture in rats. *International Journal of Nanomedicine* 5, 1103 (2010).
103. Mann, J. F. S. *et al.* Transferrin conjugation confers mucosal molecular targeting to a model HIV-1 trimeric gp140 vaccine antigen. *J Control Release* 158, 240–249 (2012).
104. Chang, J. *et al.* Characterization of endocytosis of transferrin-coated PLGA nanoparticles by the blood-brain barrier. *International Journal of Pharmaceutics* 379, 285–292 (2009).
105. Wiley, D. T., Webster, P., Gale, A. & Davis, M. E. Transcytosis and brain uptake of transferrin-containing nanoparticles by tuning avidity to transferrin receptor. *Proc Natl Acad Sci USA* 110, 8662–8667 (2013).
106. Pridgen, E. M. *et al.* Transepithelial transport of Fc-targeted nanoparticles by the neonatal Fc receptor for oral delivery. *Science Translational Medicine* 5, 213ra167–213ra167 (2013).
107. Kuo, T. T., Baker, K., Yoshida, M. & Qiao, S. W. Neonatal Fc Receptor: From Immunity to Therapeutics - Springer. *Journal of Clinical …* (2010).
108. Manolova, V. *et al.* Nanoparticles target distinct dendritic cell populations according to their size. *Eur J Immunol* 38, 1404–1413 (2008).
109. Zhao, L. *et al.* Nanoparticle vaccines. *Vaccine* 32, 327–337 (2014).
110. Fifis, T. *et al.* Size-dependent immunogenicity: therapeutic and protective properties of nano-vaccines against tumors. *J. Immunol.* 173, 3148–3154 (2004).
111. Hardy, C. L. *et al.* Differential uptake of nanoparticles and microparticles by pulmonary APC subsets induces discrete immunological imprints. *J. Immunol.* 191, 5278–5290 (2013).
112. Foged, C., Brodin, B., Frokjaer, S. & Sundblad, A. Particle size and surface charge affect particle uptake by human dendritic cells in an in vitro model. *International Journal of Pharmaceutics* 298, 315–322 (2005).
113. Thiele, L. *et al.* Evaluation of particle uptake in human blood monocyte-derived cells in vitro. Does phagocytosis activity of dendritic cells measure up with macrophages? *Journal of Controlled Release* 76, 59–71 (2001).
114. Raghuwanshi, D., Mishra, V., Das, D., Kaur, K. & Suresh, M. R. Dendritic cell targeted chitosan nanoparticles for nasal DNA immunization against SARS CoV nucleocapsid protein. *Mol. Pharmaceutics* 9, 946–956 (2012).
115. Cruz, L. J. *et al.* Targeted PLGA nano-but not microparticles specifically deliver antigen to human dendritic cells via DC-SIGN in vitro. *Journal of Controlled Release* 144, 118–126 (2010).
116. Mi, W. *et al.* Targeting the neonatal fc receptor for antigen delivery using engineered fc fragments. *J. Immunol.* 181, 7550–7561 (2008).

Chapter 3: Effect of mucosal cytokine administration on selective expansion of vaginal dendritic cells to support nanoparticle transport

3.A. ABSTRACT

The capacity of antigen-carrying vaccine nanoparticles administered vaginally to stimulate local immune responses may be limited by the relatively low numbers of antigen-presenting cells (APCs) in the genital mucosa. Because inflammation is associated with increased susceptibility to sexually transmitted infections, we sought to increase APC numbers without causing inflammation. In this study, we evaluated intravaginal delivery of chemokines, growth factors, or synthetic adjuvants to expand APCs in reproductive tissues. We found that granulocyte macrophage-colony stimulating factor (GM-CSF) stimulated expansion of CD11b+ dendritic cells within 24 h of intravaginal administration, with no effect on Langerhans cells or macrophages. Expansion of the CD11b+ DC population was not associated with increased inflammatory cytokine production, and these cells retained phagocytic function. Our data suggest that non-inflammatory expansion of mucosal APCs by intravaginal GM-CSF could be used as an adjuvanting strategy to potentiate the genital immune response to nanoparticulate mucosal vaccines.

3.B. INTRODUCTION

Overcoming the tightly down-regulated immune environment at mucosal sites has significant implications for the design of mucosal vaccines[1]. An additional challenge in the lower female reproductive tract is the tissue's unique anatomy, including the limited network of lymphatic structures and secondary lymphoid structures, which restricts migration of immune cells in the absence of inflammation[2-6]. In general, this predisposes the female reproductive tract to weak immune responses to intravaginal vaccination.

Antigen presenting cells (APCs), specifically dendritic cells (DCs), are important for maintaining the balance between tolerance and pathogen-induced inflammation. A critical role for DCs in shaping genital immunity is suggested by the observation that strong adjuvants are required to boost genital immune responses to non-replicating

subunit vaccines[7,8]. Since DCs are not a homogeneous population, targeting vaccines to specific DC subsets could allow effector T cell functions to be tailored to the relevant pathogen. However, targeting DCs is challenging given that they constitute a small fraction of cells in the vaginal mucosa, typically 5-10% of the cells in the basal vaginal epithelium and lamina propria of women without an active infection[9]. As such, strategies that recruit or expand mucosal DC subsets *in situ* may enhance immunity to vaginally administered vaccines.

Several approaches have been investigated to modulate DC numbers and activation state at immunization sites. Molecular adjuvants, such as the TLR9 agonist CpG, upregulate expression of co-stimulatory molecules[10-13]. Mucosal vaccines delivered in the presence of CpG induced cytokine secretion and increased infiltration of activated CD8+ T-cells[14]. Furthermore, intravaginally-delivered CpG transiently recruited MHC II+ CD11b+ antigen presenting cells to the vaginal submucosal[15]. However, molecular adjuvants like CpG cause strong, non-specific immune stimulation[16,17]. Such generalized inflammation can break down the natural mucosal barrier and recruit immune cells that serve as targets for mucosal pathogen transmission[18,19].

In addition to synthetic adjuvants, cytokines or growth factors can be used to enhance DC populations in the mucosa. This strategy minimizes non-specific inflammation by specifically recruiting immature or precursor APCs. Chemokines, such as MIP-3α, can promote chemotaxis of APCs to the site of administration[20-23]. Growth factors, such as granulocyte-macrophage stimulating factor (GM-CSF), may specifically stimulate the differentiation of DCs from local undifferentiated monocytes[24,25]. In fact, recombinant GM-CSF (Leukine®) is used in the clinic to reconstitute myeloid cell populations in blood after chemotherapy[26,27].

In vaccination studies, GM-CSF alone and in combination with other cytokines has been shown to differentiate monocytes into fully functional DCs that can stimulate T cell immune responses. For example, *in vivo* transfection with a GM-CSF encoded plasmid successfully expanded liver CD11c+ dendritic cells that were highly efficient in priming T cells[28]. In CSF2-null mice, which cannot make GM-CSF, DCs and macrophages in the murine uterus express less MHC class II on their surface and are

less effective in priming antigen-specific CD4+ and CD8+ T cells[29]. Cultures of PBMC with GM-CSF and other cytokines yields DCs that show high expression of HLA-DR and co-stimulatory molecules that efficiently present antigen and stimulate CD4+ T cell responses[30-32]. These results suggest that GM-CSF is important for DC function.

While many studies have evaluated the use of chemokines and growth factors in the context of systemic injections, few studies have evaluated their use for recruiting cells into the vaginal mucosa following topical administration. The need for mucosal adjuvants that modulate immunity in the reproductive mucosa motivates the discovery and application of agents that can expand key immune cell populations without causing concomitant local inflammation. Our goal is an intravaginal administration strategy focused on chemokine- or growth factor-mediated expansion of mucosal DCs. Here, we evaluate the numbers and phenotypes of mucosal DCs that arise from topical administration of a synthetic adjuvant (CpG) or a growth factor (GM-CSF), either alone or in combination with the chemokine MIP-3α, to the vaginal mucosa. Our results demonstrate that low doses of GM-CSF expanded *in situ* a functionally phagocytic mucosal DC population without eliciting inflammatory cytokine production. Furthermore, we show that GM-CSF specifically expanded CD11b+ dendritic cells but not Langerhans cells. Fluorescent nanoparticles administered intravaginally were phagocytosed by this mucosal DC population. Therefore, expanding functional DC subsets by topical administration of GM-CSF may be a promising strategy to potentiate protective immune responses to mucosal vaccines.

3.C. Materials and Methods

3.C.1. Materials

Recombinant murine MIP-3α was purchased from Peprotech (Rocky Hill, NJ) and GM-CSF from Cell Sciences (Canton, MA). Chemokines and growth factors were resuspended in sterile Dulbecco's Phosphate-Buffered Saline (DPBS) to a concentration of 1 mg/ml. Murine TLR9 ligand CpG ODN 1826, a Class B CpG oligonucleotide, was purchased from Invivogen (San Diego, CA). CpG was formulated in endotoxin-free water at 1 mg/ml. Calginate swabs used to remove mucus from mouse vaginal tracts were obtained from Fisher Scientific (Waltham, MA). Medroxyprogesterone acetate was

obtained through the University of Washington pharmacy from Greenstone LLC (Peapack, NJ). Murine TNF-α and IL-1β Standard ELISA kits were purchased from Peprotech. Fluorescent yellow/green 200 nm nanoparticles (FluoSpheres) 505/515 nm (excitation/emission) were purchased from Invitrogen.

3.C.2. Animals and intravaginal delivery of materials

Female C57Bl/6J mice (8-12 weeks old) were purchased from Jackson Laboratories. Prior to intravaginal administration, mice were subcutaneously administered 2 mg of medroxyprogesterone acetate (Depo-Provera®) formulated in sterile DPBS to reduce variability resulting from differences in stage of estrus cycle. All mice receiving treatments were anesthetized with isoflurane in an induction chamber. Genital tracts were flushed out three times with 50 µl sterile DPBS and vaginal lumens were swabbed with Calginate swabs to remove mucus. Mice were intravaginally administered 10 µg of chemokines, growth factors, adjuvants, or sterile DPBS (negative control) in 10 µl using a micropipette. Mice were transferred back to the induction chamber and hung upside down for 10 min to improve vaginal retention of materials. Animals were euthanized 24 h after treatments by carbon dioxide followed by cervical dislocation. Treatment groups, dosing, and animal experiment timelines are described in Figure 3-1a. All animal studies were approved by and in compliance with guidelines set by the University of Washington Institutional Animal Care and Use Committee.

3.C.3. Antibodies

All antibodies were purchased from BD Biosciences (Franklin Lakes, NJ) unless otherwise indicated. Primary antibody-fluorochrome pairs used for staining and identifying cell populations included: APC anti-mouse CD11c, PE anti-mouse I-Ad/I-Ed (MHC II), PerCP-Cy5.5 anti-mouse CD45, APC-Cy7 anti-mouse CD11b, PE-Cy7 anti-mouse CD8, and FITC anti-mouse F4/80 were purchased from eBioscience. Isotype antibodies used were APC Hamster IgG1 λ1, PE Rat IgG2b κ, APC-Cy7 Rat IgG2b κ PerCP-Cy5.5 Rat IgG2b κ FITC Rat IgG2a κ and PE-Cy7 IgG2a κ. LIVE/DEAD Fixable Green dead cell stain kit was purchased from Molecular Probes (Eugene, OR). For nanoparticle uptake studies, the following additional stains were used: Brilliant Violet-421 anti-mouse CD86 (BioLegend) and LIVE/DEAD Fixable Near-IR dead cell stain kit.

Purified rat anti-mouse CD16/CD32 was used to block Fc receptors (Fc block) on cells prior to cell surface staining. One Comp eBeads were purchased from eBioscience for antibody compensation and ArC amine reactive compensation bead kit was purchased from Molecular Probes for live/dead compensation.

3.C.4. Isolation of single cells from vaginal tissue and staining

Single cell suspensions were prepared from excised spleens and vaginal tissues using established techniques. Splenocytes were isolated by mechanical digestion of spleens with a syringe plunger in a 70 μm cell strainer on a petri dish with 5 ml of cRPMI (complete RPMI – RPMI 1640 + 10% heat inactivated FBS). Suspensions were restrained through a second 70 μm filter and centrifuged in cRPMI at 1200 rpm for 5 min. Cells were subsequently incubated for 5 min with red blood cell (RBC) lysis buffer and further washed by centrifugation in cRPMI. Vaginal tracts including cervix, but not uterine horns, were dissected, placed in sterile DPBS on ice, and cut into small pieces (~2 mm diameter). Organs within each group (n = 3-6) were pooled to reduce variability. Cell isolation from vaginal tissues was adapted from previously published protocols[33]. Vaginal tissues were placed in 3 ml of digestion media, made with a 1:1 ratio of PBS and R15 (RPMI 1640 with FBS, 1% Penicillin Streptomycin) at a final collagenase from clostridium histolyticum (Sigma-Aldrich) concentration of 1 mg/ml. 3 μl of DNAse at 1 Unit/ml was added to tissue digestion preparations. Tissues were agitated for 30 min on an orbital shaker (New Brunswick Scientific, Incubator Shaker Series). Cell isolation suspensions were subject to further mechanical digestion through a blunt-end, 16-gauge needle and filtered through a 70-μm cell strainer. Vaginal tissues were subjected to two rounds of chemical and mechanical digestion.

Cell suspensions were stained with a LIVE/DEAD Fixable Cell stain kit, washed, incubated with Fc block at 4°C for 15 min, and stained with antibody cocktails before washing and fixation with 1% paraformaldehyde. Samples were acquired on a FACSCanto2 with a 405-nm violet laser, a 488-nm blue laser, and a 633-nm red laser.

3.C.5. Tissue homogenization and cytokine measurements

The vaginal tract, including cervix, but not uterine horns was dissected 24 h after delivery of chemokines, growth factors, or adjuvants for tissue homogenization. Tissues

were frozen at -80°C until use. Vaginal tracts were massed and placed in 0.5 ml of homogenization buffer (0.05% Triton X-100 in Hank's Balanced Salt Solution - HBSS buffer) and 2 ml of protease inhibitor. Tissues were fully homogenized using a Tissue Tearor (Biospec Products, Inc). Murine standard ELISA development kits for TNF-α and IL-1β (Peprotech Rocky Hill, NJ) were used to determine cytokine levels in tissue homogenates using standard procedures provided by the vendor.

3.C.6. Identification of draining lymph nodes

Draining lymph nodes, including the inguinal and iliac lymph nodes (Figure 3-1b,c), were identified by dye-guided lymph node mapping. Briefly, mice were subcutaneously injected in the footpad with a 5% (w/v) solution of Evans Blue prepared in sterile PBS. Mice were euthanized by CO_2 and cervical dislocation after 15 minutes, to allow for lymphatic trafficking of the dye. As described by Ruddell et al., draining inguinal and iliac lymph nodes were identified visually[34].

3.C.7. FluoSphere preparation and quantification

FluoSpheres (supplied at 2%, w/w) were buffer exchanged to remove sodium azide. Briefly, nanoparticles were washed three times with 70% EtOH in Amicon filters (10 KDa molecular weight cutoff) and twice with endotoxin-free water by centrifugation at 4,000 x g for 20 min. FluoSpheres were collected and the concentration was determined using a TECAN fluorescence microplate reader. All particles were resuspended in endotoxin-free water to a final concentration of 0.5% (w/w) for intravaginal administration.

3.C.8. Intravaginal FluoSphere administration and imaging

Depo-provera treated mice were administered DPBS, GM-CSF, or CpG 24 h prior to intravaginal administration of nanoparticles. Mice were anesthetized using isoflurane in an induction chamber and intravaginally administered 10 µl of 0.5% (w/w) FluoSpheres. After 24 h, mice were euthanized by CO_2 and cervical dislocation. Vaginal tracts and the iliac and inguinal draining lymph nodes were dissected and placed on ice for imaging and flow cytometry analysis. A xenogen *in vivo* imaging system (iVis) was used to measure fluorescence at 505/515 nm (ex/em) for evaluating nanoparticle distribution in the vaginal tract, and in iliac and inguinal lymph nodes. Samples were acquired on a

FACSCanto2. Samples were subsequently processed using an ImagestreamX Mark II imaging cytometer (Amnis, Seattle, WA) to visualize and evaluate cell internalization of nanoparticles.

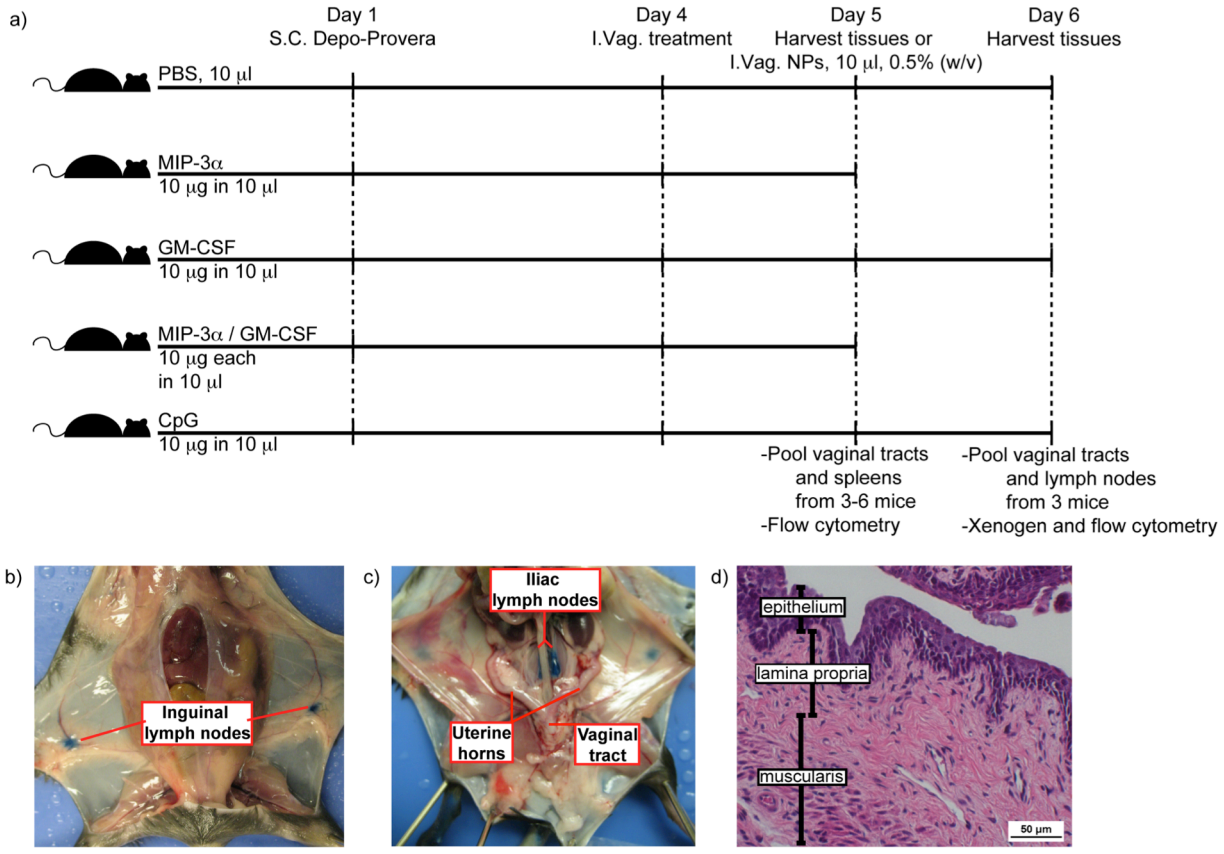

Figure 3 - 1 Administration timeline, lymph node mapping, and histologic features. Mice were cycled with Depo-Provera on Day 1 and intravaginally administered chemokines, growth factors, and adjuvants on Day 4. On day 5, tissues were harvested for cell analysis from all treatment groups; Nanoparticles (NPs) were administered to indicated mouse groups (continuing lines), which were further followed by fluorescence imaging to detect nanoparticle distribution and tissue processed for flow cytometry analysis on Day 6 (a). Evans Blue was subcutaneously injected in the footpad to map the inguinal (b) and iliac (c) lymph nodes. The uterine horns and vaginal tract are identified upon necropsy (c). Photomicrograph of H&E-stained mouse vaginal mucosa during progesterone-induced diestrous shows a thinned epithelium (d).

3.D. RESULTS

*3.D.1. Mucosal APC subsets at homeostasis in the genital tract of female mice*Female mice treated with progesterone were maintained in the diestrous phase of the menstrual cycle. During diestrous, histological analysis shows that the murine lower female genital tract is comprised of a thinned epithelium overlying the lamina propria (Figure 3-1d). Phenotypic analysis of murine vaginal cells by flow cytometry revealed that leukocytes (CD45+) accounted for up to 15% (11.03 ± 5.07 / mean ± S.D.) of the total cell population (Figure 3-2a). Total mucosal DCs (CD45+MHCII+CD11c+) accounted for <1% (0.95 ± 1.16) of the total cells but up to 5% (3.93 ± 1.54) of total CD45+ leukocytes (Figure 3-2b). Of this mucosal DC population, we observed that ~75% (75.33 ± 7.77) expressed the CD11b+ marker typical of subepithelial DCs whereas ~25% (24.68 ± 7.73) were CD11b negative (Figure 3-2c), which is characteristic of Langerhans cells (LCs)[35] ($p < 0.0001$, Student's t-test). Macrophages (CD45+MHCII+CD11c-CD11b+F4/80+) accounted for ~1% (0.67 ± 0.71) of the total cells and ~5% (5.78 ± 3.97) of the CD45+ cell population. In summary, we found that macrophages and dendritic cells have similar abundance of total mucosal leukocytes in the lower genital tract of female mice during diestrous.

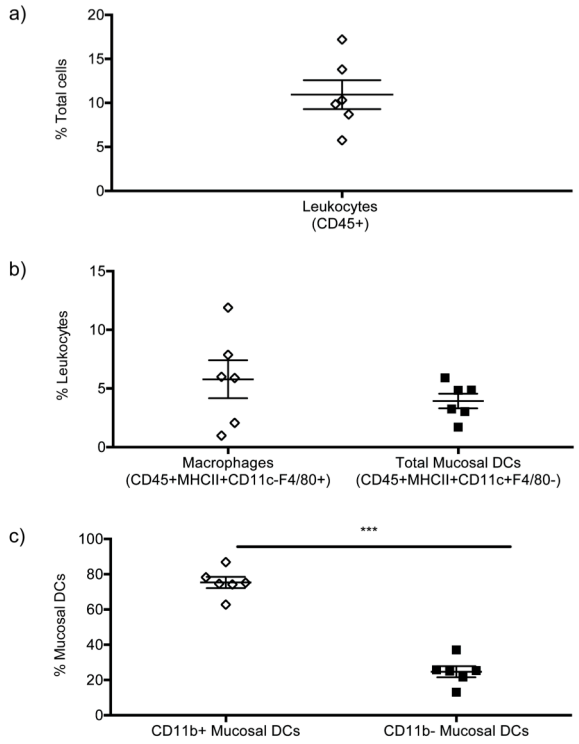

Figure 3 - 2 Vaginal immune cell populations at homeostasis during diestrus. Distinct cell populations in the mouse vaginal tract were identified by flow cytometry. Total leukocytes are displayed as a percentage of the total vaginal cells (a). Macrophages and mucosal DCs are displayed as a percentage of these total leukocytes (b). CD11b+ and CD11b- DCs are displayed as a percentage of the total mucosal DCs (c). Each symbol represents vaginal tracts pooled from 3-6 mice to reduce mouse-to-mouse variability. Six independent experiments were performed. Data were analyzed for statistical significance by a student's t test (*** $p<0.0001$) and are displayed as mean ± S.E.M.

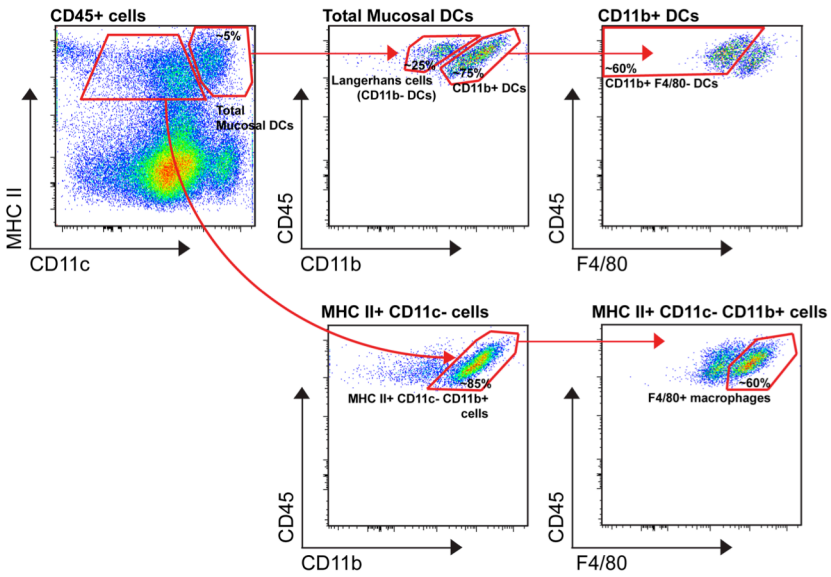

Figure 3 - 3 Gating strategy for identifying vaginal CD11b+ DCs. Gating was performed from PBS treatment groups by excluding dead cells and selecting for CD45+ leukocytes. Total mucosal dendritic cells were identified as MHC II+ CD11c+, and further gated as CD11b+ and F4/80- to quantify CD11b+ DCs. MHC II+ CD11c- leukocytes were further gated as CD11b+ and F4/80+ to identify macrophages.

3.D.2. GM-CSF treatment selectively enriches for CD11b+ dendritic cells.

We tested the effect of delivering different agents topically to the vaginal mucosa to enrich for mucosal APCs. MIP-3α and GM-CSF were administered alone or in combination and compared to CpG, a synthetic adjuvant that recruits DCs by triggering local inflammation[19] (Figure 3-1a). Flow cytometry was used to measure the quantity and phenotype of different APC populations amongst total leukocyte cells (CD45+) collected from the vaginal tissue at 24 h post-administration. Live, CD45+ cells were gated on MHC II, CD11c, CD11b, and F4/80 cell surface markers as described in Figure 3-3.

At the doses used in our studies, the CpG and MIP-3α treatment groups did not significantly affect the magnitudes of any of the APC populations compared to the PBS controls (Figure 3-4). Mucosal macrophages (CD45+MHC II+CD11c-CD11b+F4/80+) did not change in response to any of the intravaginal administrations (Figure 3-4a). In contrast, we found that the total mucosal DC (CD45+/MHCII+/CD11c+) population doubled to nearly 10% of the CD45+ leukocyte population upon administration of GM-CSF alone or in combination with the MIP-3α chemokine compared to the MIP-3α treatment group (Figure 3-4b). Surprisingly, we found that GM-CSF significantly expanded the CD11b+ DC populations compared to the synthetic adjuvant CpG used at an equivalent dose. In particular, CD11b+ mucosal dendritic cells (CD45+MHC

II+CD11c+CD11b+F4/80-) were expanded an average of two fold by GM-CSF as compared to the PBS treatment group, and constituted up to 5.5% of the CD45+ leukocyte population (Figure 3-4c). We did not observe significant changes in the magnitude of mucosal Langerhans cells (CD45+/MHC II+/CD11c+/CD11b-) (Figure 3-

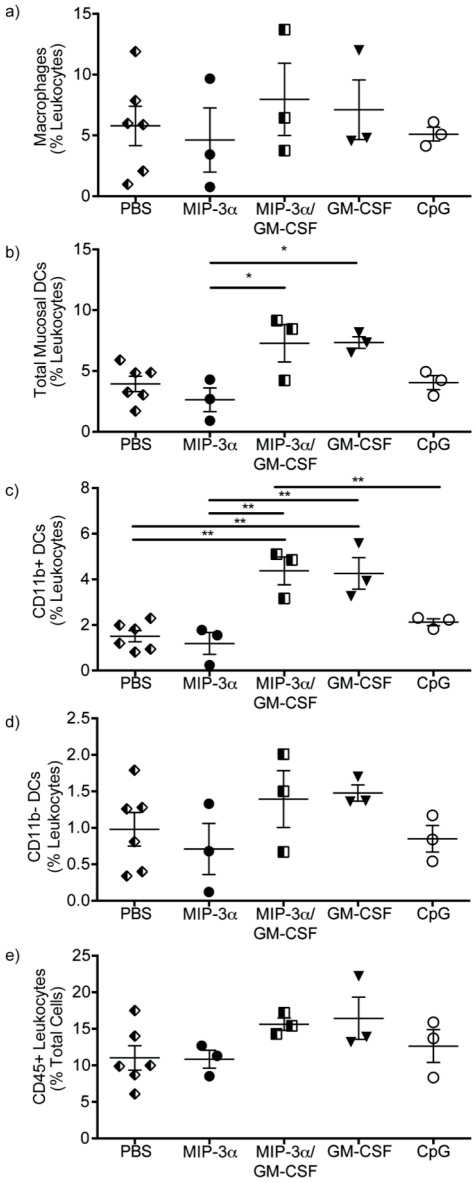

Figure 3 - 4 Identification of expanded immune cell populations in the vagina. Murine vaginal cells were isolated and stained to identify cell populations 24 hours post-vaginal administration of PBS, MIP-3α, GM-CSF, MIP-3α and GM-CSF, or CpG-ODN 1826. Each symbol represents vaginal tracts pooled from 3-6 mice to reduce mouse-to-mouse variability, and at least 3 independent experiments were performed per treatment. Effects of treatments are described on macrophages (a), total mucosal DCs (b), CD11b+ DCs (c), CD11b- DCs (d), and CD45+ leukocytes (e). Data were analyzed for statistical significance by a one-way ANOVA followed by a Bonferroni post-test (* $p<0.05$, ** $p<0.01$)

4d). Although total tissue leukocytes (CD45+) appeared to increase in GM-CSF-treated mice, the difference was not statistically significant (Figure 3-4e).

3.D.3. Chemokines and growth factors do not impact systemic cell populations or vaginal cytokines

The reproductive mucosal tissues are highly vascularized, allowing for systemic distribution of intravaginally delivered agents. To understand if intravaginal administration of MIP-3α, GM-CSF, or CpG impacts systemic APC populations, we measured the magnitude of APC populations in the spleen by flow cytometry. At the doses used in our studies, we did not observe a significant difference in the total number of leukocytes or DCs (CD45+ MHC II+ CD11c+) in the spleen between any of our treatment groups (Figure 3-5a,b). Leukocytes constituted about 50% of the total splenic cells and DCs represented only 1-3% abundance of these cells. Subpopulations of cells expressing CD11b and F4/80 were not observed in splenocyte-derived dendritic cells. These results suggest that the delivered factors did not impact systemic levels of leukocytes and dendritic cells.

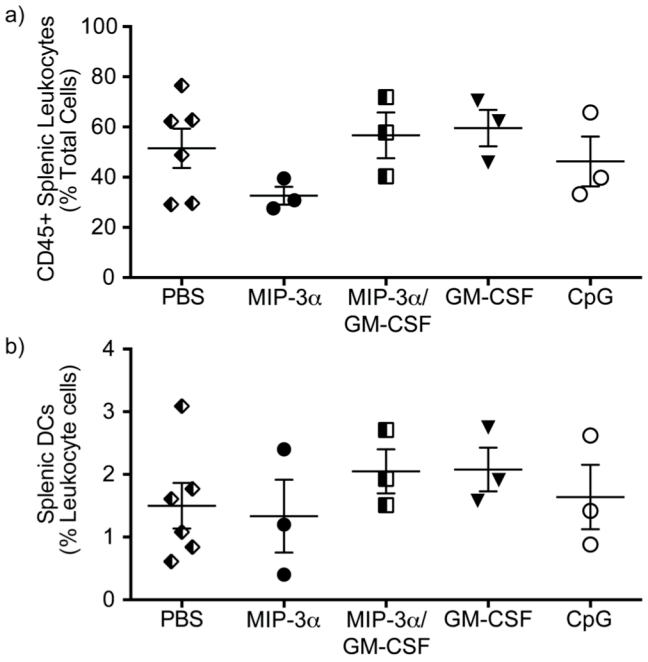

Figure 3 - 5 Spleen immune cell populations. Murine splenocytes were isolated and stained to identify immune cell populations following vaginal administration of PBS, MIP-3a, GM-CSF, MIP-3α and GM-CSF, or CpG-ODN 1826. Each symbol represents spleens pooled from 3-6 mice to reduce mouse-to-mouse variability, and 3 or more independent experiments were performed per group. Effects of treatments are described on leukocytes (CD45+) (a) and splenic DCs (MHC II+ CD11c+) (b). Data were analyzed for statistical significance by a one-way ANOVA followed by a Bonferroni post-test and are displayed as mean ± S.E.M. No significant differences between any groups were found.

During mucosal infections, expansion of APCs also results in production of inflammatory signals to modulate local immune responses[36-38]. We measured TNF-α and IL-1β cytokine levels in the vaginal tract 24-h post-topical administration of GM-CSF and CpG to evaluate if delivery of these agents and the resulting changes in the local

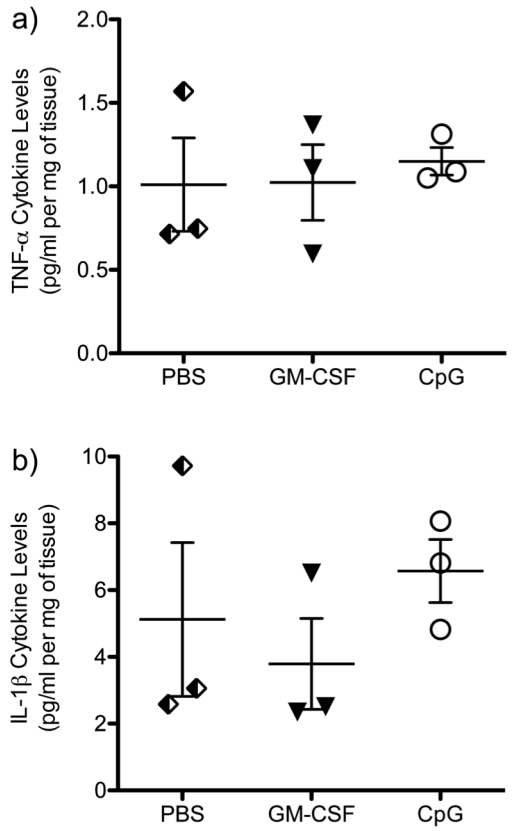

Figure 3 - 6 Inflammatory cytokine levels in vaginal tissues. TNF-a and IL-1b cytokine production was measured in reproductive tissues using an ELISA. Tissues were homogenized and quantified by comparison to a standard, and normalized to tissue mass. No significant differences were observed in TNF-α (a) or IL-1β (b) cytokine levels between PBS, GM-CSF, and CpG topical administrations. Data were analyzed for statistical significance by a one-way ANOVA followed by a Bonferroni post-test and are displayed as mean ± S.E.M.

immune cell populations caused inflammation. Our treatment groups show concentrations of TNF-α at ~1 pg/ml/mg and of IL-1β at ~5 pg/ml/mg, expressed per mass of vaginal tissue (Figure 3-6). A trend towards increased IL-1β levels was observed in the CpG treatment group. We found no significant differences in the levels of these pro-inflammatory cytokines between mice that received GM-CSF compared to control mice treated with PBS. Therefore, despite significant enrichment of DCs and CD11b+ DCs up to 2-3 fold, we did not observe evidence of pro-inflammatory cytokine secretion.

3.D.4. Fluorescent nanoparticles distribute in the vaginal tract and accumulate in draining lymph nodes.

To evaluate if APCs retained their functional capacity to associate with or phagocytose nanoparticles, we measured uptake and trafficking of 200 nm fluorescent nanoparticles 24 hours after vaginal tissues were administered with PBS, GM-CSF, or CpG. Fluorescence in the vaginal tract and iliac lymph nodes was quantified using LivingImage Software, and autofluorescence was normalized to the respective tissues from control mice. We observed high fluorescence intensity in the vaginal tract for all mice receiving nanoparticle administrations (Figure 3-7a). Quantification of fluorescence in the vaginal tracts demonstrated significant retention of intravaginally delivered nanoparticles in the genital lumen after 24 hours, with a trend towards CpG-treated mice retaining the most

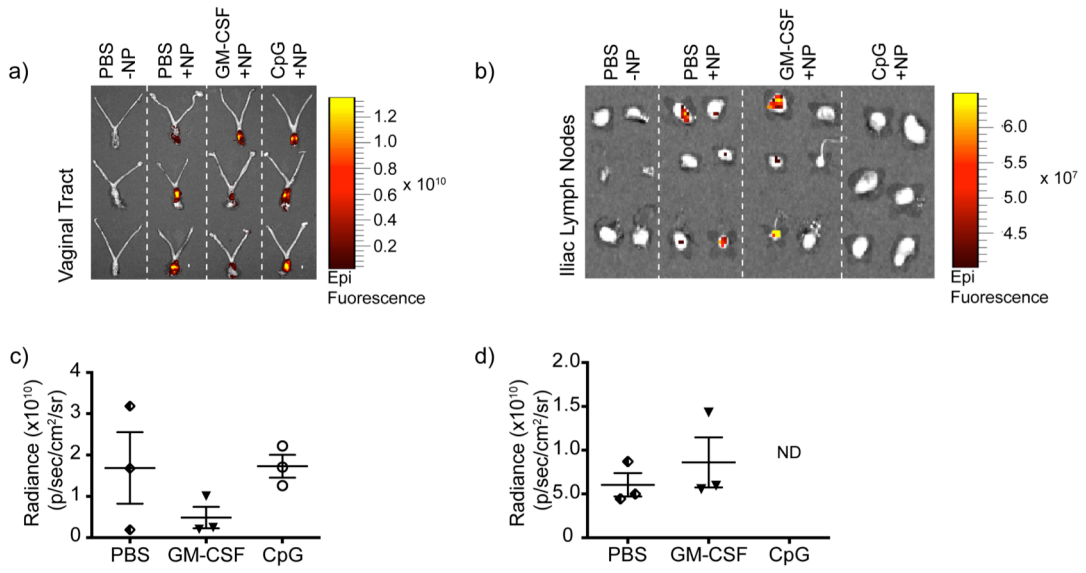

Figure 3 - 7 Xenogen imaging and fluorescence quantification. Vaginal tracts and draining lymph nodes were dissected 24-h after nanoparticle administration of mice pre-treated with PBS, GM-CSF, and CpG (n=3 per group). Tissues were imaged using a Xenogen *in vivo* imaging system (iVIS). Fluorescence was observed in the vaginal tract in all treatment groups (a) and in the iliac lymph nodes (b) in PBS and GM-CSF treated animals. Fluorescence in the vaginal tract and iliac lymph nodes was quantified using the LivingImage Software (c,d). ND indicates that fluorescence was "not detected." Data are displayed as mean ± S.E.M.

fluorescent nanoparticles (Figure 3-7c). We also analyzed for the presence of fluorescent nanoparticles in the iliac and inguinal lymph nodes, which drain the lower female genital tract. No fluorescence was observed in inguinal lymph nodes of mice from any treatment group (data not shown). However, we found fluorescent nanoparticles in the iliac lymph nodes of mice treated with PBS and GM-CSF but not CpG (Figure 3-7b). Although the mean fluorescence in the iliac lymph nodes was higher for GM-CSF treated mice, we observed no significant difference between our treatment groups (Figure 3-7d). In summary, nanoparticles delivered into the vagina were well retained for at least 24 hours and distributed to the iliac but not inguinal lymph nodes.

3.D.5. Dendritic cells internalize nanoparticles.

To evaluate the function and phagocytic capacity of the total mucosal DC (CD45+/MHC II+/CD11c+) population that was expanded in the vaginal tract by GM-CSF treatment, we assessed accumulation of fluorescent nanoparticles in these cells by flow cytometry. Fluorescent nanoparticles (10 μL of 0.5%, w/w) were administered intravaginally at 24h following initial treatment with PBS, CpG, or GM-CSF. After allowing an additional 24h for nanoparticle trafficking, the mice were sacrificed and total

mucosal dendritic cells (MHC II+ CD11c+) were quantified for NP fluorescence. In comparison to mice that did not receive NPs, we found that ~30% of DCs were NP+ (Figure 3-8a). At 48h post-administration of growth factors or adjuvants, total mucosal

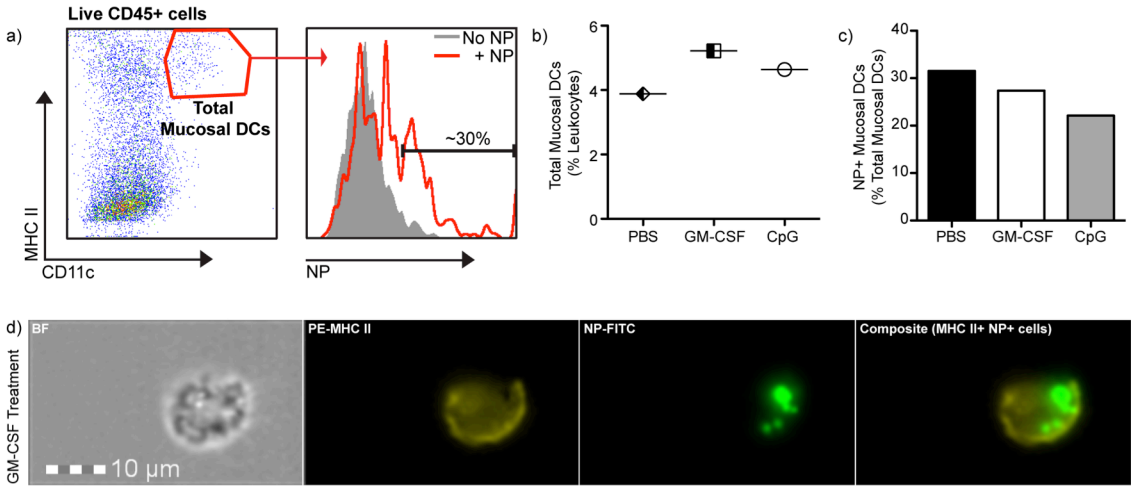

Figure 3 - 8 Nanoparticle uptake in vaginal mucosal DCs. Total mucosal DCs were identified and nanoparticle uptake by these cells was quantified (a). Vaginal tracts from 3 mice were pooled within each group. GM-CSF treated animals displayed increased levels of total mucosal DCs (MHC II+ CD11c+) (b), but no significant difference was observed in NP phagocytosis by mucosal DCs between treatment groups (c). ImageStream imaging flow cytometry was performed to evaluate if nanoparticles were internalized in mucosal MHC II+ cells. A representative image of nanoparticle internalization in MHC II+ cells is shown (d). Bright field (BF), PE, and FITC channels show live cells, MHC II cell surface staining, and internal NP fluorescence, respectively. The composite image shows punctate NPs in MHC II+ cells.

DCs remained elevated in GM-CSF treated mice compared to mice administered PBS or CpG (Figure 3-8b). We did not observe a difference in phagocytosis of NPs by mucosal DCs between treatment groups, indicating that treatment with GM-CSF did not stimulate enhanced uptake of particulates (Figure 3-8c).

To ascertain if the cell-associated fluorescence in our nanoparticle uptake studies was due to internalized or cell surface-associated nanoparticles, we analyzed samples from each treatment group on an Amnis ImageStream imaging flow cytometer. In these experiments, after nanoparticle treatment and cell isolation, cells were stained for viability and MHC II+ expression. Intracellular total fluorescence intensity was normalized to the total cell fluorescence to calculate an internalization score using the Amnis software. Cell surface intensity was defined by PE fluorescence, indicating MHC II+ antigen presenting cells. We calculated internalization scores of 1.7 for PBS,

and 1.9 for GM-CSF and CpG treatment groups. These values indicate that approximately 65% of nanoparticle fluorescence was due to internal fluorescence in MHC II+ cells. The internalized particles were observed as punctate fluorescence in MHC II+ cells captured by the imaging flow cytometer (Figure 3-8d).

3.E. DISCUSSION

In this study, we examined if intravaginal delivery of DC chemokines, growth factors, or synthetic adjuvants could expand mucosal dendritic cells and facilitate nanoparticle biodistribution to distal sites. We found that a low dose of GM-CSF doubled the frequency of total mucosal DCs (CD45+ MHC II+ CD11c+) to 10% of the leukocyte population in the vaginal mucosa. Furthermore, we observed a specific enrichment of subepithelial dendritic cells, which were identified by the presence of the CD11b surface marker from ~2% to ~5% of leukocytes. No change was observed in mucosal F4/80+ macrophages or CD11b- mucosal Langerhans cells. Overall, we observed a trend towards increased CD45+ leukocytes in GM-CSF-treated mice, but the difference was not statistically significant. Because DCs constitute only 2-5% of the CD45+ cell population, even a doubling of DCs would cause only a small change in the CD45+ leukocyte population, explaining why total leukocytes increased only marginally. Given what is known and described in the literature about GM-CSF, it is likely that increased proliferation or differentiation of local DCs and their precursors contributed to the expanded CD11b+ DC population, rather than recruitment from the periphery. However, our data do not distinguish between these possibilities, and future work will need to elucidate if GM-CSF acts strictly on mucosal cells to influence cellular infiltration of immune cells into the vagina.

While the exact function of each DC subset remains controversial, CD11b+ DCs have been previously demonstrated to be important for priming protective CD4+ T responses to vaginal infection by HSV-2[39]. In this study by Zhao et al., mucosal Langerhans cells did not exhibit the ability to migrate to draining lymph nodes and prime T cells, implicating a potential tolerogenic role for these cells in the reproductive tissues. Evidence has also showed that GM-CSF-induced dendritic cells are monocyte-derived and are generated under inflammatory conditions. Unlike steady-state dendritic cells,

which are CD11b-, these inflammatory dendritic cells are CD11b+ and play an important role in shaping immunity[40,41]. Staining for other DC subset surface markers, such as CD14, may help further elucidate the specific polarization of these expanded DCs towards Th1 versus Th2[42]. Thus, the GM-CSF-expanded population of CD11b+ dendritic cells in our study may play a role in enriching a cell population that has phagocytic and migratory capacity. As such, our results demonstrate that GM-CSF can be used to expand the local mucosal dendritic cell population in the vaginal tract within a 24-hour window.

Reproductive tissues are highly vascularized, potentially allowing for systemic delivery from topical administrations. To evaluate if vaginal administration of chemokines, growth factors, and adjuvants at the doses used in our animal models modulated immune cell populations in the periphery, we analyzed cell populations in the spleen. We found no statistically significant difference in levels of leukocytes and dendritic cells in the spleen between all treatment groups, suggested that intravaginally delivered agents acted locally and did not influence systemic immune cell populations.

Although MIP-3a is a well-defined DC chemoattractant, we found no significant increase in the total mucosal DC population in response to this chemokine, but this may be due to the low dose used in our studies. To our surprise we also found that the CpG-ODN 1826, a synthetic adjuvant that has been previously described to expand MHC II+ CD11b+ cells after intravaginal delivery, had no significant effect on the antigen presenting cell population in our study. This is likely a consequence of the lower dose used in our study as compared to other studies that deliver CpG at 20-100 μg[15,43,44]. That CpG was likely dosed too low in our study is also reflected by the finding that it did not stimulate TNF-α and IL-1β.

In general, the levels of TNF-α and IL-1β were consistent with published data measuring these cytokines in the mouse reproductive mucosa at steady-state after Depo-Provera administration[45]. We did not observe an increase in TNF-α and IL-1β upon GM-CSF treatment, suggesting that while GM-CSF was able to expand the CD11b+ DC population, it did not stimulate increased cytokine secretion. This does not

rule out, however, that increased dosing or co-delivery of GM-CSF and other maturation agents would induce cytokine secretion[46,47].

Whole animal fluorescent imaging allowed us to macroscopically visualize biodistribution of fluorescent nanoparticles in the vaginal tract and lymph node tissues. Polystyrene nanoparticles were retained in the vaginal tract for at least 24-h post-topical administration. Furthermore, fluorescence imaging demonstrated that nanoparticles distributed to the iliac lymph nodes. As the iliac lymph nodes are one of the major draining lymph nodes from the reproductive tissues, we expect intravaginally administered materials to reach these tissues either by cell-associated or cell-free trafficking. Previous studies evaluating biodistribution of quantum dots demonstrated cell-free trafficking to the lumbar lymph nodes after intravaginal delivery[48]. Other studies have shown that nanoparticles in the range of 20-200 nm are able to drain to lymph nodes where they are taken up by cells whereas NPs larger than 500nm were associated with tissue resident DCs originating from the site of injection[49]. In our study, we did not distinguish between cell-free and cell-associated trafficking of the nanoparticles. Future work may focus on differentiating between NP fluorescence in lymph node resident immune cells versus migratory immune cells to elucidate modes of NP trafficking from the genital mucosa.

By analyzing the cell populations that showed nanoparticle fluorescence, we found that within all treatment groups about 30% of mucosal dendritic cells (MHC II+ CD11c+) associated with NPs. We observed no statistically significant difference in NP association with cells between treatment groups, indicating that phagocytic function of mucosal DC populations was not altered by any of the pre-treatments. We employed the Amnis ImageStream X imaging flow cytometer to ascertain if nanoparticle fluorescence in antigen presenting cells (MHC II+) was surface associated or intracellular. Our analysis showed that ~65% of nanoparticle fluorescence was localized inside MHC class II+ cell populations for all treatment groups. This indicates that 24 hours after intravaginal administration, nanoparticles were still localized inside MHC II+ APCs. Punctate nanoparticle fluorescence in MHC II+ cells suggests that nanoparticles were likely sequestered in intracellular vesicles. Although we observed fluorescence in lymph

nodes by Xenogen imaging, we were unable to detect nanoparticles in lymph node preparations after staining for mucosal DCs by conventional flow cytometry (data not shown). Given the low percentage of mucosal DCs in lymph nodes, it is likely that cell-associated nanoparticles were lost during sample staining and washing. Other groups that have attempted to detect particulates by flow cytometry after intravaginal administration of materials have also noted limited success identifying cell populations with particles in draining lymph nodes[48]. In conclusion, GM-CSF induced a greater number of DCs in the vaginal mucosa, but it did not alter their individual phagocytic capabilities. Thus, intravaginal administration of GM-CSF can be used to increase the number of nanoparticle-processing DCs in the vagina, which may be a useful strategy to improve the presentation and immunogenicity of topically delivered particulate vaccine antigens.

3.F. CONCLUSION

Our study aimed to describe the effect of exogenously delivered chemokines and growth factors on the local immune cell populations of the murine genital tract. We found that GM-CSF increased the total mucosal DC population, specifically CD11b+ dendritic cells. Further, we found that the effects of GM-CSF were localized to the vaginal tract and did not impact systemic leukocyte levels. Finally, our results demonstrate that the enriched APC population in the vaginal tract is functional and able to phagocytose nanoparticulate materials. Extensions of our work will aim to optimize the *in situ* expansion of DCs using GM-CSF as a function of dose and administration schedule, and establish that its co-delivery with an antigen improves immune responses to a mucosal vaccine.

3.G. ACKNOWLEDGEMENTS

This work is funded by an NIH Director's New Investigator Award to K.A.W. (1DP2HD075703) and with the support of a UW STD/AIDS Training Fellowship to R.R. (NIHT32AI07140).

3.H. REFERENCES

1. Woodrow KA, Bennett KM, Lo DD. Mucosal Vaccine Design and Delivery. Annu Rev Biomed Eng. 2012 Aug 15;14(1):17–46.
2. Shin H, Iwasaki A. A vaccine strategy that protects against genital herpes by establishing local memory T cells. Nature. 2012 Nov 15;491(7424):463–7.
3. Cuburu N, Chackerian B. Genital delivery of virus-like particle and pseudovirus-based vaccines. Expert Rev Vaccines. 2011 Sep;10(9):1245–8.
4. Russell MW, Mestecky J. Tolerance and Protection against Infection in the Genital Tract. Immunol Invest. 2010 Jan;39(4-5):500–25.
5. Pavot VV, Rochereau NN, Genin CC, Verrier BB, Paul SS. New insights in mucosal vaccine development. Vaccine. 2012 Jan 5;30(2):142–54.
6. Yu M, Vajdy M. Mucosal HIV transmission and vaccination strategies through oral compared with vaginal and rectal routes. Expert Opin Biol Ther. 2010 Aug 1;10(8):1181–95.
7. Tengvall S, Lundqvist A, Eisenberg RJ, Cohen GH, Harandi AM. Mucosal administration of CpG oligodeoxynucleotide elicits strong CC and CXC chemokine responses in the vagina and serves as a potent Th1-tilting adjuvant for recombinant gD2 protein vaccination against genital herpes. J Virol. 2006 Jun;80(11):5283–91.
8. Luci C, Hervouet C, Rousseau D, Holmgren J, Czerkinsky C, Anjuère F. Dendritic cell-mediated induction of mucosal cytotoxic responses following intravaginal immunization with the nontoxic B subunit of cholera toxin. J. Immunol. 2006 Mar 1;176(5):2749–57.
9. Bhoopat L, Eiangleng L, Rugpao S, Frankel SS, Weissman D, Lekawanvijit S, et al. In Vivo Identification of Langerhans and Related Dendritic Cells Infected with HIV-1 Subtype E in Vaginal Mucosa of Asymptomatic Patients. Modern Pathology. Nature Publishing Group; 2001 Dec 1;14(12):1263–9.
10. Krieg AM. Antiinfective applications of toll-like receptor 9 agonists. Proc Am Thorac Soc. 2007 Jul;4(3):289–94.
11. Vollmer J, Krieg AM. Immunotherapeutic applications of CpG oligodeoxynucleotide TLR9 agonists. Adv. Drug Deliv. Rev. 2009 Mar 28;61(3):195–204.
12. McCluskie MJ, Davis HL. CpG DNA as mucosal adjuvant. Vaccine. 1999 Sep;18(3-4):231–7.
13. Bode C, Zhao G, Steinhagen F, Kinjo T, Klinman DM. CpG DNA as a vaccine adjuvant. Expert Rev Vaccines. 2011 Apr;10(4):499–511.
14. Jiang JQ, Patrick A, Moss RB, Rosenthal KL. CD8+ T-cell-mediated cross-clade protection in the genital tract following intranasal immunization with inactivated human immunodeficiency virus antigen plus CpG oligodeoxynucleotides. J Virol. 2005 Jan;79(1):393–400.
15. Sajic D, Patrick AJ, Rosenthal KL. Mucosal delivery of CpG oligodeoxynucleotides expands functional dendritic cells and macrophages in the vagina. Immunology. 2005 Feb;114(2):213–24.
16. BenMohamed L, Wechsler SL, Nesburn AB. Lipopeptide vaccines--yesterday,

today, and tomorrow. Lancet Infect Dis. 2002 Jul 1;2(7):425–31.
17. Zhang X, Issagholian A, Berg EA, Fishman JB, Nesburn AB, BenMohamed L. Th-cytotoxic T-lymphocyte chimeric epitopes extended by Nepsilon-palmitoyl lysines induce herpes simplex virus type 1-specific effector CD8+ Tc1 responses and protect against ocular infection. J Virol. 2005 Dec 1;79(24):15289–301.
18. de Jong MAWP, de Witte L, Oudhoff MJ, Gringhuis SI, Gallay P, Geijtenbeek TBH. TNF-α and TLR agonists increase susceptibility to HIV-1 transmission by human Langerhans cells ex vivo. J. Clin. Invest. 2008 Oct 1;118(10):3440–52.
19. Wang Y, Abel K, Lantz K, Krieg AM, McChesney MB, Miller CJ. The Toll-Like Receptor 7 (TLR7) Agonist, Imiquimod, and the TLR9 Agonist, CpG ODN, Induce Antiviral Cytokines and Chemokines but Do Not Prevent Vaginal Transmission of Simian Immunodeficiency Virus When Applied Intravaginally to Rhesus Macaques. J Virol. 2005 Oct 27;79(22):14355–70.
20. Schutyser E, Struyf S, Van Damme J. The CC chemokine CCL20 and its receptor CCR6. Cytokine & Growth Factor Reviews. 2003 Oct;14(5):409–26.
21. Mackay CR. Chemokines: immunology's high impact factors. Nat. Immunol. Nature Publishing Group; 2001;2(2):95–101.
22. Le Borgne M, Etchart N, Goubier A, Lira SA, Sirard JC, van Rooijen N, et al. Dendritic cells rapidly recruited into epithelial tissues via CCR6/CCL20 are responsible for CD8+ T cell crosspriming in vivo. Immunity. 2006 Feb;24(2):191–201.
23. Song R, Liu S, Leong KW. Effects of MIP-1α, MIP-3α, and MIP-3β on the Induction of HIV Gag-specific Immune Response with DNA Vaccines. Mol Ther. Nature Publishing Group; 2007 Mar 13;15(5):1007–15.
24. Inaba K, Inaba M, Romani N, Aya H. Generation of large numbers of dendritic cells from mouse bone marrow cultures supplemented with granulocyte/macrophage colony-stimulating factor. 1992 Dec 1;176(6):1693–702.
25. Khatami S, Brummer E, Stevens DA. Effects of granulocyte-macrophage colony stimulating factor (GM-CSF) in vivo on cytokine production and proliferation by spleen cells. Clinical & Experimental Immunology. Wiley Online Library; 2001;125(2):198–201.
26. Apte SM, Vadhan-Raj S, Cohen L, Bassett RL, Gordon IO, Levenback CF, et al. Cytokines, GM-CSF and IFNgamma administered by priming and post-chemotherapy cycling in recurrent ovarian cancer patients receiving carboplatin. J Transl Med. 2006;4:16.
27. Vadhan-Raj S, Broxmeyer HE, Hittelman WN, Papadopoulos NE, Chawla SP, Fenoglio C, et al. Abrogating chemotherapy-induced myelosuppression by recombinant granulocyte-macrophage colony-stimulating factor in patients with sarcoma: protection at the progenitor cell level. J. Clin. Oncol. 1992 Aug;10(8):1266–77.
28. Wang Y, Zheng N, Lu Z, Wu W, Wang L, Nakao A, et al. In vivo expansion of two distinct dendritic cells in mouse livers and its impact on liver immune regulation. Liver Transpl. 2006 Dec;12(12):1850–61.
29. Moldenhauer LM, Keenihan SN, Hayball JD, Robertson SA. GM-CSF is an

essential regulator of T cell activation competence in uterine dendritic cells during early pregnancy in mice. J Immunol. 2010 Dec 1;185(11):7085–96.
30. Romani N, Gruner S, Brang D, Kämpgen E, Lenz A, Trockenbacher B, et al. Proliferating dendritic cell progenitors in human blood. J. Exp. Med. 1994 Jul 1;180(1):83–93.
31. Paquette RL, Hsu NC, Kiertscher SM, Park AN, Tran L, Roth MD, et al. Interferon-alpha and granulocyte-macrophage colony-stimulating factor differentiate peripheral blood monocytes into potent antigen-presenting cells. J. Leukoc. Biol. 1998 Sep;64(3):358–67.
32. Pulendran B, Smith JL, Caspary G, Brasel K, Pettit D, Maraskovsky E, et al. Distinct dendritic cell subsets differentially regulate the class of immune response in vivo. Proc Natl Acad Sci USA. 1999 Feb 2;96(3):1036–41.
33. McKinnon LR, Hughes SM, De Rosa SC, Martinson JA, Plants J, Brady KE, et al. Optimizing viable leukocyte sampling from the female genital tract for clinical trials: an international multi-site study. PLoS ONE. 2014;9(1):e85675.
34. Harrell MI, Iritani BM, Ruddell A. Lymph node mapping in the mouse. J. Immunol. Methods. 2008 Mar;332(1-2):170–4.
35. Iwasaki A. Mucosal dendritic cells. Annu. Rev. Immunol. 2007.
36. Bebell LM, Passmore J-A, Williamson C, Mlisana K, Iriogbe I, van Loggerenberg F, et al. Relationship between levels of inflammatory cytokines in the genital tract and CD4+ cell counts in women with acute HIV-1 infection. J INFECT DIS. 2008 Sep 1;198(5):710–4.
37. Prantner D, Darville T, Sikes JD, Andrews CW, Brade H, Rank RG, et al. Critical Role for Interleukin-1 (IL-1) during Chlamydia muridarum Genital Infection and Bacterial Replication-Independent Secretion of IL-1 in Mouse Macrophages. Infection and Immunity. 2009 Nov 13;77(12):5334–46.
38. Iijima N, Mattei LM, Iwasaki A. Recruited inflammatory monocytes stimulate antiviral Th1 immunity in infected tissue. Proc Natl Acad Sci USA. 2011 Jan 4;108(1):284–9.
39. Zhao X, Deak E, Soderberg K, Linehan M, Spezzano D, Zhu J, et al. Vaginal Submucosal Dendritic Cells, but Not Langerhans Cells, Induce Protective Th1 Responses to Herpes Simplex Virus-2. 2003.
40. Shortman K, Naik SH. Steady-state and inflammatory dendritic-cell development. Nat Rev Immunol. 2006 Dec 15;7(1):19–30.
41. Naik SH. Demystifying the development of dendritic cell subtypes, a little. Immunol. Cell Biol. 2008 Jul;86(5):439–52.
42. Duluc D, Gannevat J, Anguiano E, Zurawski S, Carley M, Boreham M, et al. Functional diversity of human vaginal APC subsets in directing T-cell responses. Mucosal Immunol. 2013 May;6(3):626–38.
43. Sajic D, Ashkar AA, Patrick AJ, McCluskie MJ, Davis HL, Levine KL, et al. Parameters of CpG oligodeoxynucleotide-induced protection against intravaginal HSV-2 challenge. J. Med. Virol. 2003 Oct 6;71(4):561–8.
44. Pettini E, Prota G, Ciabattini A, Boianelli A, Fiorino F, Pozzi G, et al. Vaginal immunization to elicit primary T-cell activation and dissemination. PLoS ONE.

2013;8(12):e80545.
45. Ensign LM, Tang BC, Wang YY, Tse TA, Hoen T, Cone R, et al. Mucus-Penetrating Nanoparticles for Vaginal Drug Delivery Protect Against Herpes Simplex Virus. Science Translational Medicine. 2012 Jun 13;4(138):138ra79–9.
46. Min L, Mohammad Isa SAB, Shuai W, Piang CB, Nih FW, Kotaka M, et al. Cutting edge: granulocyte-macrophage colony-stimulating factor is the major CD8+ T cell-derived licensing factor for dendritic cell activation. J Immunol. 2010 May 1;184(9):4625–9.
47. Danis VA, Franic GM, Rathjen DA, BROOKS PM. Effects of granulocyte-macrophage colony-stimulating factor (GM-CSF), IL-2, interferon-gamma (IFN-γ), tumour necrosis factor-alpha (TNF-α) and IL-6 on the production of immunoreactive IL-1 and TNF-α by human monocytes. Clinical & Experimental Immunology. 2008 Jun 28;85(1):143–50.
48. Ballou B, Andreko SK, Osuna-Highley E, McRaven M, Catalone T, Bruchez MP, et al. Nanoparticle transport from mouse vagina to adjacent lymph nodes. PLoS ONE. 2012;7(12):e51995.
49. Manolova V, Flace A, Bauer M, Schwarz K, Saudan P, Bachmann MF. Nanoparticles target distinct dendritic cell populations according to their size. Eur J Immunol. 2008 May;38(5):1404–13.

Chapter 4: Antibody functionalized nanoparticle immune complexes for *in vivo* targeting of draining lymph nodes and antigen presenting cells

4.A. ABSTRACT

The intravaginal delivery of drug and vaccine loaded nanoparticles faces unique biological challenges that preclude effective drug transport to the target tissues and cells. Exploiting existing biological processes, including IgG binding, translocation, and endocytosis, may facilitate improved vaginal nanoparticle delivery. The Fcγ receptor is expressed by antigen presenting cell subsets, and has been shown to play a key role in uptake of opsonized pathogens, cross-presentation, and shaping the activation state of DCs. The neonatal Fc receptor (FcRn) is expressed on mucosal surfaces, including the gut, nasal, and vaginal epithelium. FcRn has been uniquely implicated in active transcytosis of IgG bidirectionally across the vaginal epithelium by binding the Fc region. This chapter examines the capability of intravaginally administered IgG-functionalized nanoparticles to engage eplithelial Fc receptors and to subsequently facilitate active transcytosis. We found that these surface functionalized nanoparticle immune complexes (NP-ICs) achieved more efficient transcytosis across the vaginal epithelium, improving drainage to lymph nodes, and increasing access to critical immune cells in the vaginal submucosa.

4.B. INTRODUCTION

Barriers to vaginal nanoparticle delivery include low retention time within the tract, nanoparticle entrapment in mucus, and an impenetrable barrier posed by the vaginal epithelium in the absence of inflammation-inducing adjuvants. Numerous groups have investigated strategies to improve mucus penetration of polymeric, drug-loaded nanoparticles[1-3]. Surface modification of nanoparticles with polyethylene glycol, in particular, has emerged as a strategy to increase diffusivity in vaginal mucus and improve accumulation of nanoparticles at the vaginal epithelium[1-4]. However, to serve as effective delivery vehicles for mucosal vaccines, nanoparticle systems must access the tissue antigen presenting cells (APCs) in the subepithelial mucosa. One of the major

advantages of nanoparticle systems is the ease with which their surfaces can be modified to incorporate proteins, peptides, or polymers as a way to impart specific functionality. In this chapter, we modify nanoparticles to mimic opsonized pathogens to improve particle transport and uptake via existing IgG-Fc receptor pathways that exist in the reproductive organs.

Receptors that engage the Fc region of IgG can be broadly classified into Fcγ receptors and the neonatal Fc receptor (FcRn). The exact distribution of these receptors among cell types, surface density, function, and binding activity is highly complex and remains a major topic for elucidation. However, it is well known that the Fcγ receptors are responsible for internalization of immune complexes, such as opsonized pathogens, and influence the activation state of APCs towards inflammation or tolerance[5,6]. The family of Fcγ receptors in mice includes FcγRI, FcγRIIB, FcγRIII, and FcγRIV[6]. With the exception of the inhibitory FcγRIIB receptor, all Fcγ receptors can activate and promote immunogenic processes. FcγRI is restricted to mouse monocyte-derived dendritic cells (DCs), FcRIIB has been characterized on all myeloid cell populations and B cells, FcγRIII has been found on natural killer (NK) cells and natural killer T (NKT) cells, and FcγRIV has been identified on $Ly6C^{lo}$ monocytes, macrophages, and neutrophils.

The specificity of these receptors for various IgG subsets, however, can be variable across species. While mouse Fc receptors have various binding affinities for the mouse IgG subsets (e.g., IgG1, 2a, 2b, and 3), all mouse Fc receptors (i.e., FcγRs and FcRns) efficiently bind all subsets of human IgG[5,6]. In contrast human Fc receptors inefficiently bind, or do not bind, mouse IgG subsets. While FcγRIA has high affinity for binding IgG (near 10^8 - 10^9 M^{-1}), all other Fcγ receptors are reported to exhibit a 100-1000 fold decrease in affinity for their target IgG subsets[5]. This decreased affinity may rationalize the inability of most Fcγ receptors to bind monomeric IgG, and further highlights the potential of immune complexes to exploit binding through avidity effects.

The role of FcRn in the active transport of IgG was first postulated in response to studies observing passive transfer of immunity from mother to child and was later isolated from rat small intestinal epithelial cells[7,8]. Since, FcRn-IgG interactions have been a major source of study, reflected by the widespread success of antibody therapy

for several disease indications. Pinocytosed IgG binds FcRn tightly once in an endosome that is being acidified for lysosomal degradation[9-14]. FcRn binding of IgG rescues antibodies from degradation and recycles it back to the same surface membrane or transcytosed to the opposite surface membrane.

FcRn is composed of a molecule akin to MHC class I and is also associated with beta-2-microglobulin. Its main function is to protect IgG from catabolism (degradation) and, as such, FcRn is considered to be a critical aspect of the prolonged half-life of IgG. While human FcRn is able to bind human and rabbit IgG, murine FcRn is thought to be "promiscuous" and can bind multiple IgG species, including human IgG. Proetzel and colleagues have also developed humanized FcRn mouse models to study the pharmacokinetics of IgG in a more clinically relevant murine model[15]. In 1997, one group performed RT-PCR amplification and identification of human FcRn on human fetal intestine and adult intestine[16]. It was identified that these FcRn were similar in structure and function to what had been previously identified in mice and rats. Furthermore, IHC revealed that FcRn was highly expressed on the apical side of epithelial cells. Studies in FcRn knockout mice showed that neonatal mice were unable to absorb IgG from maternal milk and had lower levels of IgG in systemic circulation after immunization[17,18].

Targeting both Fc receptor pathways has been shown to be a unique and effective strategy to improve immune responses, systemically and mucosally. Fcγ is expressed on antigen presenting cells and has been found to be key in cross-presentation and the mediation of protective immune responses[19,20]. Targeting the Fcγ receptor has shown to be a promising strategy to improve presentation and cross-presentation to promote functional T cell responses[21,22]. Antigen-antibody complexes, termed immune complexes (ICs), have been researched for their ability to influence the maturation and functional state of DCs. These studies recently showed that OVA/anti-OVA IgG ICs induced greater maturation of DCs, as measured by increased expression of the CD86 co-stimulatory molecule. Furthermore, in DC and T cell co-cultures, DCs that were primed with OVA ICs induced greater secretion of IL-12 and IL-2 cytokine secretion[22]. In a separate study OVA-IC pulsed BMDCs, which were intravenously injected into mice, significantly prevented subsequent tumor formation upon challenge

by injection of MO-4 cells[21]. *In vitro* assays showed that lymph-node derived T cells from mice treated with OVA-IC-pulsed BMDCs showed increase proliferative responses after *ex vivo* restimulation. OVA-IC-pulsed BMDCs stimulated better proliferative responses in CD4+ and CD8+ T cells. Furthermore, while OVA-IC uptake in wild-type BMDCs was comparable to FcγR -/- BMDCs, only the former showed an increase in co-stimulatory markers including CD40, CD54, CD86, CD80, ICAM-1, and MHCII. Together, these results highlight that the Fcγ receptors are essential in shaping the activation state of functional DCs.

Another study investigated FcRn for implementation as an innovative antibody-based therapy. An influenza HA mAb was applied basolaterally to canine kidney cells, which were shown to express FcRn[23]. When challenged with influenza virus on the apical side, cells were protected by FcRn mediated binding of IgG, preventing virus from fusing with endosomal membranes. This study illustrated intracellular neutralization in epithelial cells, dependent on FcRn[23]. Studies have shown that albumin and IgG were rescued from lysosomal degradation by FcRn in kidney proximal tubular cells and that receptor-mediated transport of IgG was bidirectional[24,25]. A separate study showed that in the human intestinal T84 cell line, IgG is transported bidirectionally by receptor-mediated transcytosis[26]. In another study it was found that FcRn plays a significant role in protecting pathogens that infect epithelium. In mice lacking FcRn in the intestine, animals showed increased sensitivity to *C. rodentium* and host defense was restored by reconstitution with transgenic FcRn[27]. In one study, the p24 protein from HIV Gag was fused the heavy chain of IgG and administered intranasally with a CpG adjuvant. Potent immune responses were elicited including protection against intravaginal challenge with a recombinant virus expressing HIV Gag.

In the context of the genital submucosa, a significant amount of research has highlighted the role of FcRn in vaginal immune responses. FcRn was shown to be expressed in the female human uterus and reproductive tract as well as murine uterus and reproductive tract[28]. IgG was shown to be transported bidirectionally by FcRn. Furthermore, systemically administered IgG was not found in the vaginal lumen of FcRn knockout mice, and these wild-type mice showed higher protection when intravaginally

immunized with an HSV-2-specific polyclonal serum sample following intravaginal challenge with HSV-2. In another study, HSV-2 glycoprotein D was fused to an IgG Fc fragment and administered intranasally with a CpG adjuvant[29]. These studies showed that in wild-type, but not FcRn knockout mice, the HSV-2 vaccine protected against HSV-2 intravaginal challenge. Moreover, four important observations laid precedent for the potency of an FcRn targeted mucosal vaccine. First of all, germinal centers structures were formed in the mediastinal lymph nodes for a longer period of time than other vaccination groups and higher levels of B cells were found in these germinal centers. Secondly, after vaccination, BALT structures were observed in the lung and were similar to germinal centers. Third, glycoprotein D-specific IgG was found in mucosal lavages from the bronchial and vaginal tracts, but not in FcRn knockout mice. Finally, the combination of CpG and an FcRn targeted vaccine were found to boost levels of a Th1 type response inducing IFN-g producing CD4+ and CD8+ T cells.

The presence of the FcRn receptor has significant implications for mucosal delivery of biologics. At many mucosal surfaces, for example the lung, penetration of larger molecules or protein biologics through the epithelium remains a challenge. As such, active transport mechanisms, which promote transepithelial transport of proteins, may be significant for drug delivery. Several proteins have been successfully fused to Fc including Fc erythropoietin (which had pharmacokinetics equivalent to subcutaneous administration, after pulmonary delivery), IFN-b-Fc, IFN-a-Fc, Factor IX-Fc, and FSH-Fc[17]. Vaginal epithelium and human uterine tissue has been shown to express FcRn, and furthermore, it is notable that vaginal pH is low enough (4-4.5 in human, 6-6.5 in mice) to enable FcRn-mediated IgG binding by epithelial cells[28].

In the context of acting as delivery vehicles for vaccines, nanoparticles must access APCs in the submucosal space of the vaginal epithelium. We propose that the development of antibody-nanoparticle immune complexes (NP-ICs) to leverage the FcRn and Fcγ receptors will promote efficient transepithelial delivery, uptake by vaginal tissue APCs, and improve antigen delivery. Modification of nanoparticle surfaces with Fc protein to engage epithelial receptors that promote transepithelial transport after oral mucosal delivery has shown promise as a strategy for insulin delivery across the

intestinal epithelium[30]. We investigated a similar strategy for delivery of nanoparticles across the vaginal epithelium. Our studies focused on developing IgG immobilization strategies on fluorescent NPs (Fluor-NPs) to generate fluorescent nanoparticle immune complexes (Fluor-NP-ICs), and evaluated their distribution within the reproductive organs and trafficking to draining lymph nodes. We further evaluated uptake of Fluor-NP-ICs by tissue APC subsets. We hypothesize that Fluor-NP-ICs, synthesized by IgG adsorption of nanoparticles, will more efficiently traverse the vaginal epithelium, efficiently traffic to draining lymph nodes, and show increased uptake by tissue APCs.

4.C. Materials and methods

4.C.1. Materials

IgG from human serum was purchased from Sigma Aldrich (St. Louis, MO). Fluorescent red, amine functionalized 200 nm polystyrene nanoparticles (FluoSpheres) 580/605 (excitation/emission) were purchased from ThermoFisher Scientific (Waltham, MA). Calginate swabs used to remove vaginal mucus were obtained from FisherScientific (Indianapolis, IN). Medroxyprogesterone acetate was purchased through the UW pharmacy from Greenstone LLC (Peapack, NJ). Immunofluorescence studies were carried out using Phalloidin (ThermoFisher Scientific, Waltham, MA) and 2-(4-amidinophenyl)-1H-indole-6-carboxamidine (DAPI) Fluoromount-G (Southern Biotech, Birmingham, AL). DyLight™ 680 NHS-Ester was purchased from ThermoFisher Scientific (Waltham, MA). Maleimide (MAL)-PEG-Succinimidyl Valerate (SVA) (MW 5,000) was purchased from Laysan Bio (Arab, AL). Zeba spin columns (MWCO 7,000) were obtained from ThermoFisher Scientific (Bothell, WA).

4.C.2. Antibodies

All antibodies were purchased from BD Biosciences (Franklin Lakes, NJ) unless indicated. Primary antibody-fluorochrome used for cell surface marker staining included: APC anti-mouse CD11c, APC-Cy7 anti-mouse CD11b), Alexa-488 anti-mouse I-Ad/I-Ed (MHC II), PE-Cy5 anti-mouse F4/80, and PE-Cy7 anti-mouse CD45. LIVE/DEAD Fixable Violet dead cell stain kit was obtained from ThermoFisher Scientific (Bothell, WA). Purified rat anti-mouse CD16/CD32 was purchased from BD Biosciences to block non-specific Fc receptor binding of primary antibody-fluorochrome pairs. Compensation

was performed using One Comp eBeads (eBioscience, San Diego, CA) and the ArC amine reactive compensation bead kit (ThermoFisher Scientific, Waltham, MA).

4.C.3. Animal and vaginal NP delivery

Female C57Bl/6J (4-6 weeks old) were purchased from the Jackson Laboratories. Four days prior to vaginal administration of NPs, all mice were subcutaneously administered 100 µl medroxyprogesterone acetate (Depo-Provera®) to synchronize estrous cycle stage and reduce mouse-to-mouse variability. Depo-Provera® was formulated at 20 mg/ml in sterile Dulbecco's Phosphate-Buffered Saline (DPBS). Mice were anesthetized with isoflurane in an induction chamber. Prior to NP administration, mice genital tracts were flushed out with 80 µl of endotoxin-free water three times using a micropipette, and two Calginate swabs were used to remove mucus from the vaginal lumen. All mice were taped around the abdomen using two pieces of Fisherbrand tape (Fisher Scientific, Waltham, MA) to prevent self-grooming. Mice were intravaginally administered 10 µl of fluorescent polystyrene nanoparticles (Fluor-NPs) at 0.5% (w/v) formulated in endotoxin-free water using a micropipette. Mice were placed in dorsal recumbence for 15 minutes in the induction chamber to improve vaginal retention of administered treatments. After recovery from anesthetization, mice were individually caged to prevent grooming between animals. All animal studies were approved and monitored under guidelines set by the University of Washington Institutional Animal Care and Use Committee (IACUC).

4.C.4. Synthesis of IgG-modified FluoSphere nanoparticles

IgG modification of Fluor-NPs was performed using two synthetic strategies. Amine-functionalized Fluor-NPs supplied at 2% (w/v), were diluted to 0.5% (w/v) in 50 mM sodium phosphate buffer, pH 8. IgG adsorption was carried out by adding IgG at a 1000 molar excess to Fluor-NPs and incubating overnight to generate Fluor-NP-ICs. Adsorbed Fluor-NP-ICs were purified by 3 rounds of centrifugation at 18,000 x g for 6 minutes. Adsorbed Fluor-NP-ICs were resuspended in 50 mM sodium phosphate for *in vitro* studies and sterile, endotoxin-free water for *in vivo* studies. Conjugated Fluor-PEG NP ICs were synthesized using a multi-step synthetic strategy, modified from established protocols[31]. First, amine-functionalized Fluor-NPs were reacted with MAL-

PEG-SVA at a 1000 molar excess by incubating 0.5% Fluor-NPs (w/v) in 50 mM sodium phosphate (pH 8) for 2.5 hours on a plate shaker at room temperature. Fluor-PEG NPs were then purified by centrifugation at 10,000xg for 15 min. IgG from human serum was thiolated using Traut's Reagent as per instructions from the manufacturer. Briefly, a stock solution of IgG was made at 10 mg/ml in DPBS with 2-5 mM EDTA, pH 8. Traut's Reagent was brought to 2 mg/ml in DPBS in 2-5 mM EDTA and 46 µl was added for every 1 mL of IgG stock solution. The solution was incubated on a shaker at room temperature for one hour, and thiolated IgG was purified using a 7K MWCO Zeba spin column equilibrated with 50 mM sodium phosphate. Purified thiolated protein concentration was determined using a Nanodrop system (ThermoFisher Scientific, Waltham, MA). Finally thiolated IgG was added to Fluor-PEG NPs at a 1000 molar excess and placed on a shaker at room temperature overnight. Fluor-PEG NP ICs were finally purified by three rounds of centrifugation at 18.000xg for 6 minutes.

4.C.5. Physical characterization by dynamic light scattering

Hydrodynamic size, polydispersity (PDI), and zeta potential of unmodified and modified Fluor-NPs was determined by dilution in 10 mM NaCl, pH 4 by dynamic light scatter (DLS) techniques with a Malvern Zetasizer (Malvern Instruments, Malvern, UK). NP stability over time was assessed by incubation at 4°C and 37°C, and measurements at a range of timepoints. NP concentration after IgG surface modification was quantified by comparison to a standard PS NP curve using TECAN fluorescence plate reader (Mannedorf, Switzerland) and used to normalize all treatment groups to the same fluorescence dose delivered in all *in vivo* studies.

4.C.6. IgG Leaching

IgG was modified with DyLight™ 680 NHS-Ester (ex/em, 682/715) to produce fluorescent IgG following standard protocols provided by the manufacturer for protein labeling. IgG-DyLight™ 680 was adsorbed to Fluor-NPs, following the synthetic strategy for IgG adsorption. Protein leaching from the surface of Fluor-NP-ICs was quantified by incubating particles in a 1% (w/v) BSA solution. At designated timepoints, Fluor-NP-ICs were centrifuged at 18,000 x g for 10 min, and fluorescence in supernatants were measured using a TECAN fluorescence plate reader.

4.C.7. Fluorescence imaging post-vaginal administration of NPs

NP vaginal dosing in female mice was determined by evaluating fluorescence post-administration for 10 µl doses of NPs at 0.5%, 0.1% and 0.05% (w/v) in sterile, endotoxin-free water. After 24-hours, mice were euthanized by CO_2 followed by cervical dislocation. Reproductive organs, including the vagina, cervix and uterine horns, and iliac and inguinal draining lymph nodes were necropsied. Reproductive organs and draining lymph nodes were placed on ice until imaging or flow cytometry. The Xenogen *in vivo* imaging system (iVis) was used to measure fluorescence to evaluate NP retention in the vaginal tract and NP trafficking to draining lymph nodes. Living Image In Vivo Imaging Software was used to select regions of interest (ROI) and quantify average or maximum radiance.

4.C.8. Isolation of single cell suspensions and staining

Single cell suspensions were prepared from reproductive organ and lymph node tissues using previously established methods[32]. Briefly, reproductive tissues were cut into small pieces and placed into 1 ml of digestion media, composed of 1.5 mg/ml Collagenase D and 40 µg/ml DNAse I in cRPMI. Lymph node tissues were incubated in 0.5 ml of digestion media and all tissues were incubated at 37°C on an orbital shaker (New Brunswick Scientific, Incubator Shaker Series) for 30-45 minutes. After collagenase digestion of tissues, 10 µl of a 0.5M stock solution of EDTA (Sigma Aldrich, St. Louis, MO) was added to reproductive tissues and 5 µl was added to lymph node tissues. Reproductive tissues underwent additional mechanical disruption by passing samples through a blunt-end, 16-gauge needle and were filtered through a 70 µm cell strainer. Lymph node tissues were directly transferred were further mechanically disrupted with a syringe plunger and filtered through a 70 µm cell strainer. NP fluorescence in single cell suspensions were quantified for dosing studies by flow cytometry and were acquired on a FACSCanto2 equipped with a 405-nm violet laser, a 488-nm blue laser, and a 633-nm red laser. NP uptake in vaginal cell populations was determined by staining reproductive tissue-derived cell suspensions with a LIVE/DEAD Fixable dead cell staining kit. Cells were washed, incubated with Fc block at 4°C for 5 min, and stained with antibody cocktails prior to washing and fixation in 1.6% paraformaldehyde. These samples were

acquired on an LSRII with a 488-nm blue laser, 561 nm yellow/green laser, 640-nm red diode laser, 405-nm violet laser, and a 350-nm UV laser.

4.C.9. Fluorescence staining and microscopy of vaginal tissue sections

Reproductive tissues were dissected from 3-4 mice per group, and frozen in Tissue-Tek OCT Compound (Sakura Finetek, Torrance, CA) on dry ice. Frozen tissues were sectioned with a cryo-microtome into 3-5 samples, each at a 5 µm thickness using a Leica CM1850 cryostat (Leica Biosystems, Buffalo Grove, IL). Transverse sections were taken from the middle of the frozen tissue block along the length of the reproductive organs. Sections were pressed onto glass slides and covered with a glass cover slip. Each section was observed under a microscope in three different areas – lower vaginal tract, upper vaginal tract/cervix, uterine horns) for immunofluorescence and histological analysis. For immunofluorescence image analysis, cryo-microtomed tissues were stained for Phalloidin and counterstained with Fluormount-G DAPI. Images were taken in the FITC channel to visualize the Phalloidin cytoskeletal stain, the DAPI channel to visualize cell nuclei, and the TRIT-C channel to image NPs. Fluorescence images were acquired on a Nikon Eclipse Ti microscope fitted with a camera. Hematoxylin and eosin staining was carried out using standard techniques and imaged by phase contrast (Nikon Eclipse Ti).

4.D. RESULTS

4.D.1. IgG functionalization and physical characterization of protein-modified NPs

Two strategies, passive adsorption and covalent bioconjugation, were tested to evaluate IgG immobilization on amine-modified PS NP surfaces. Dynamic light scattering was used to evaluate size, polydispersity (PDI), and surface charge of both unmodified and modified NPs. Fluor-NPs had a hydrodynamic diameter of 270 nm with a low PDI < 0.1 and a positive surface charge of ~40 mV (Table 4-1). Passive adsorption results in

Table 4 - 1 Size, polydispersity, and surface charge of IgG-modified PSNPs

	Fluor-NPs	Fluor-NP-ICs	Fluor-PEG-NP-ICs
Size (d, nm)	271 ± 2	328 ± 9	486 ± 15
PDI	0.04 ± 0.02	0.11 ± 0.03	0.31 ± 0.01
ζ-potential	40.4 ± 1.3	14.5 ± 0.4	-6.2 ± -0.4

Fluor-NP-ICs at ~330 nm with a low PDI ~0.1 and a near neutral surface charge of ~15 mV. PEGylation of Fluor-NPs and bioconjugation to IgG resulted in Fluor-PEG NP ICs near ~490 nm in hydrodynamic radius, a higher PDI ~0.3, and a near neutral surface charge of ~-6 mV.

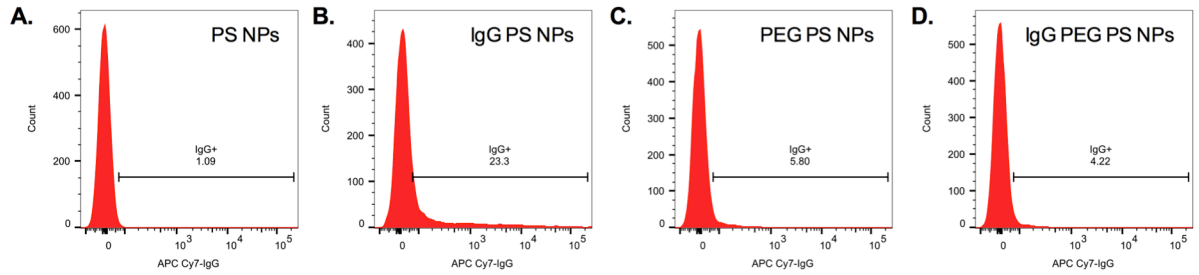

Figure 4 - 1 Nanoparticle surface coverage with IgG Fluorescent nanoparticles (Fluor-NPs) were functionalized with a dye-labeled IgG by passive adsorption and bioconjugation via a PEG crosslinker. Extent of surface functionalization was determined by flow cytometry. Histograms show IgG fluorescence for Fluor-NPs (A), adsorbed Fluor-NP ICs (B), PEG-conjugated Fluor-NPs (C), and conjugated Fluor-PEG NP ICs (D).

To evaluate the extent of surface functionalization, IgG was fluorescently labeled with a DyLight™ 680 NHS-Ester dye. The extent of dye labeling was determined by Nanodrop to be ~7 dye molecules per IgG. Dye labeled IgG was adsorbed and conjugated to Fluor-NPs as described above. Fluor-NP-ICs and Fluor-PEG NP ICs were quantified for co-localization of particle and IgG fluorescence using flow cytometry. NPs were identified as positive in the PE channel, and histograms were evaluated in the APC-Cy7 channel for IgG fluorescence (Figure 4-1). Our results demonstrate that protein adsorption resulted in greater IgG fluorescence associated with nanoparticles as

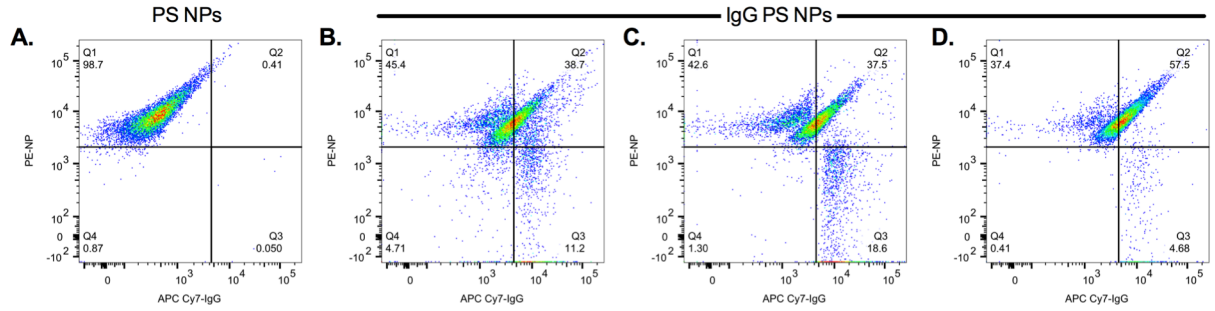

Figure 4 - 2 Surface coverage of IgG adsorbed Fluor-NP-ICs Flow cytometry dot plots show unmodified, polystyrene nanoparticles (Fluor-NPs) (A) and triplicate syntheses of IgG adsorbed Fluor-NP ICs (B-D), Extent of coverage is seen by a shift from the top left quadrant (PS+IgG-) into the top right quadrant (PS+IgG+).

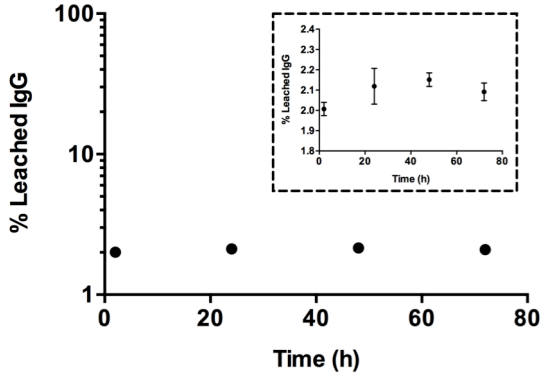

Figure 4 - 3 IgG leaching Dye-labeled IgG was adsorbed to Fluor-NPs, and leaching was determined by centrifuging Fluor-NP ICs at various timepoints over 72-hours and quantifying IgG fluorescence in supernatants

compared to bioconjugation of protein. Passive adsorption of IgG resulted in ~45% particle surface modification as determined by flow cytometry (Figure 4-2). Due to the higher degree of surface modification, we chose to carry forward this method to generate Fluor-NP-ICs for subsequent *in vivo* studies. To further characterize passive IgG adsorption to particle surfaces, we evaluated leaching of dye-labeled IgG from Fluor-NP-ICs over time in a 1% BSA solution. Our results showed that minimal IgG leached from particle surfaces, even in the presence of another protein (Figure 4-3).

4.D.2. Fluor-NP vaginal dose determination

We tested a range of Fluor-NP doses delivered topically to the vaginal mucosa by detecting the range of bulk fluorescence signal in the reproductive and lymph node tissues using Xenogen iVis imaging and flow cytometry. Animals were vaginally administered Fluor-NPs at 0.5%, 0.1%, and 0.05% solids formulated in endotoxin-free water and caged for 24 hours. Reproductive tracts were dissected to include the vagina, cervix and uterine horns (Figure 4-4). Fluorescence images were taken using the iVis system and normalized to the respective control group to remove tissue autofluorescence. We observed that vaginal fluorescence was greatest in mice dosed at 0.5% (w/v) Fluor-NPs (Figure 4-4A). Fluorescence signal appeared strongest in the lower vagina. LivingImage Software was used to quantify fluorescence in the vaginal tract and the data showed a dose dependent decrease in max radiance as Fluor-NP dose was lowered (Figure 4-4B). Bulk fluorescence was also quantified by determining Fluor-NP fluorescence in single cell suspensions after cell isolation by flow cytometry. The NP+ gate was set in reference to control group mice, which received endotoxin-free water and mean fluorescence intensity (MFI) was quantified (Figure 4-4C). We again

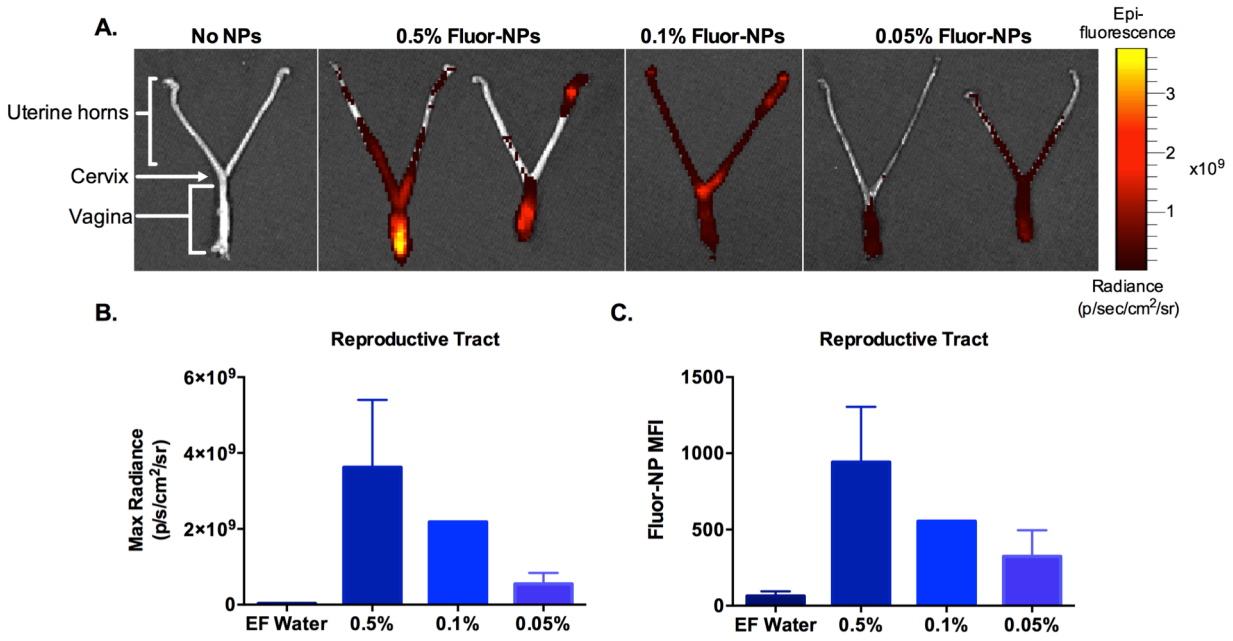

Figure 4 - 4 Bulk fluorescence imaging of reproductive organs PSNPs were vaginally dosed at 0.5%, 0.1%, and 0.05% and allowed to traffick for 24-hours. Fluorescence in the reproductive organs was visualized using the Xenogen iVis Imaging System (A). Max fluorescence in reproductive organs was quantified with the LivingImage Software (B), and NP mean fluorescence intensity (MFI) in single cell suspensions derived from reproductive organs was quantified by flow cytometry.

observed a dose dependent decrease in MFI of reproductive tract-derived single cell suspensions as PS NP dose was lowered.

Fluorescence signal in iliac draining lymph nodes was qualitatively most clear in mice, which received the highest vaginal Fluor-NP dose of 0.5% (w/v) (Figure 4-5). Quantification of max radiance in each node demonstrated that nearly all particle doses were very near the background bulk fluorescence signal in water-treated mice, though radiance was highest in mice dosed at 0.5% Fluor-NPs (Figure 4-5A). No distinguishable fluorescence was observed or quantified above background in the inguinal draining lymph nodes in any of the treatment groups (Figure 4-5C,D). All iliac and inguinal draining lymph nodes within a single mouse were pooled and single cell suspensions were isolated and quantified for fluorescence by flow cytometry (Figure 4-5E). Draining lymph node-derived single cell suspensions did not exhibit fluorescence signal above background in any of the treatment groups. Based on these data, we moved forward with the highest particle dose (0.5% w/v) for all subsequent studies to maximize the detectable fluorescence signal.

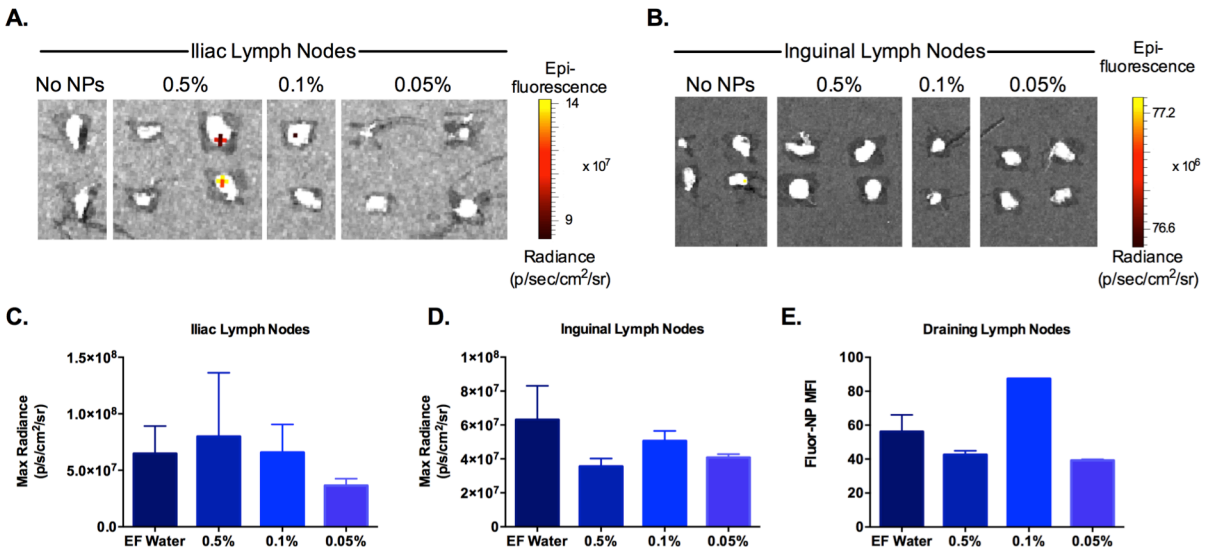

Figure 4 - 5 Bulk fluorescence imaging of tissue draining lymph nodes Fluorescence in iliac and inguinal draining lymph nodes (DLNs) was imaged using the Xenogen iVis Imaging System (A,B). Max fluorescence in iliac and inguinal DLNs was quantified using the LivingImage Software (C,D). DLNs were pooled and NP mean fluorescence intensity in single-cell suspensions was quantified by flow cytometry.

4.D.3. Bulk fluorescence imaging in reproductive and draining lymph node organs

We tested the effect of IgG surface functionalization of Fluor-NPs on particle trafficking to draining lymph nodes after topical, vaginal administration. We imaged and quantified bulk tissue fluorescence in animals treated with water, Fluor-NPs, and Fluor-NP-ICs. Fluor-NPs and Fluor-NP-ICs were formulated at 0.5% (w/v) and fluorescence concentration was confirmed using a TECAN plate reader (Männedorf, Switzerland). After vaginal administration, treatments were allowed to traffic out to 6-hours, 24-hours, 48-hours, and 72-hours. Bulk fluorescence imaging showed that Fluor-NPs and Fluor-NP-ICs were retained within the reproductive tract up to three days following vaginal administration (Figure 4-6A). Fluorescence from both particles decayed significantly in the reproductive tissues over time.

Iliac and inguinal draining lymph nodes were also imaged at 6, 24, 48, and 72 hours following vaginal administration. We observed the appearance of particle fluorescence as early as 6 hours post-vaginal administration in the iliac lymph nodes, and continued to observe sustained fluorescence up to 72 hours in Fluor-NP and Fluor-NP IC-treated mice (Figure 4-6B,C). In contrast, we observed particle fluorescence in inguinal lymph nodes beginning at 24 hours post-vaginal administration in Fluor-NP IC

treated mice and were observed in all mice receiving treatment up to 48-hours post-vaginal administration.

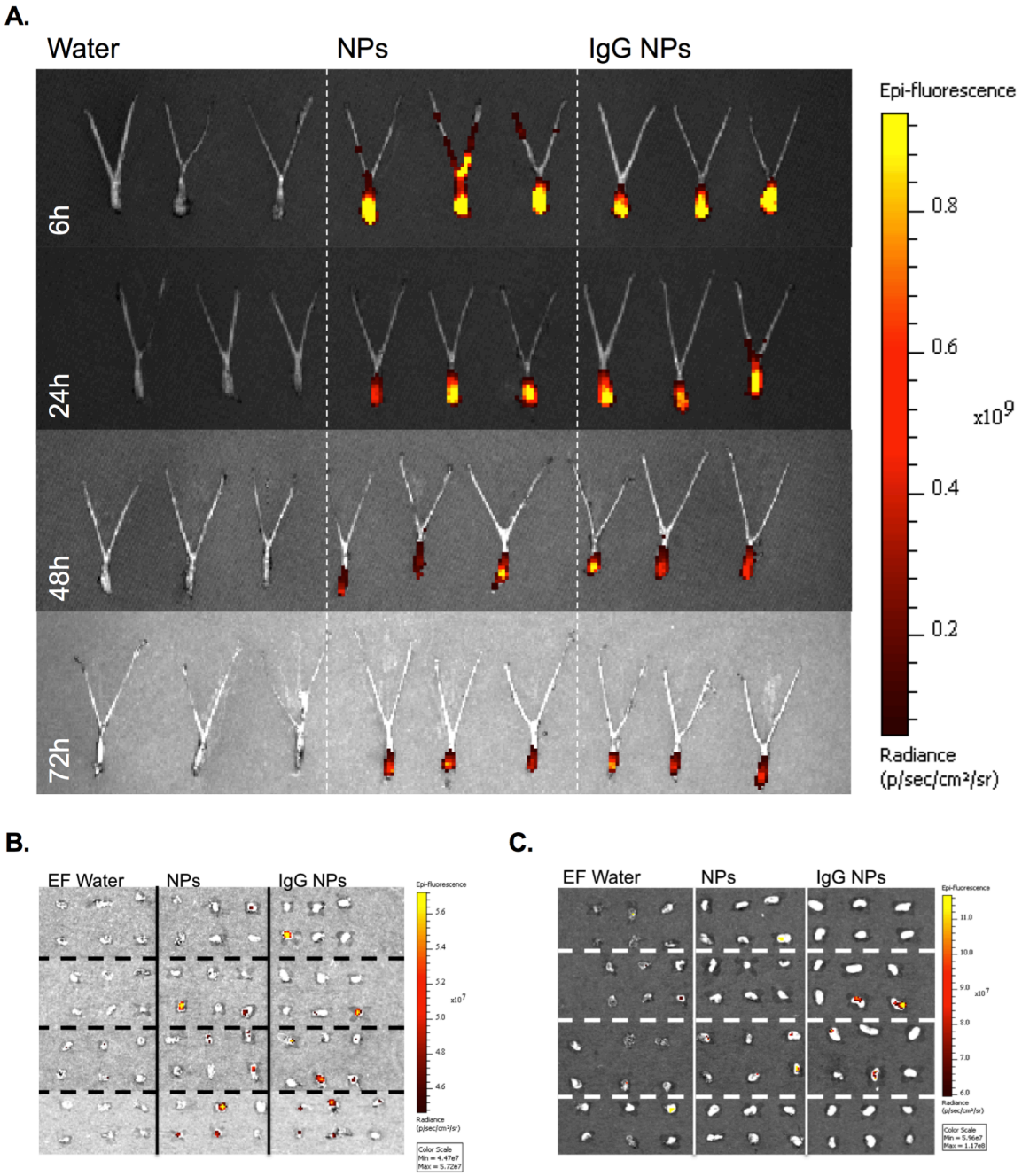

Figure 4 - 6 Nanoparticle distribution in reproductive tract and tissue draining lymph nodes PSNPs and IgG PSNPs (Op PSNPs) were vaginally administered at 0.5% (w/v) particle mass. Bulk fluorescence in the reproductive tract (A) and iliac and inguinal lymph nodes (B, C) was determined over 72-hours using the Xenogen iVis System.

To understand if there were any statistically significant differences in lymph node draining between Fluor-NPs and Fluor-NP-ICs, we scaled up evaluation of trafficking at 24 hours after vaginal administration. We used the LivingImage Software to quantify average and maximum fluorescence observed in lymph nodes. The PS NP treatment group did not display significant average or maximum fluorescence signal over the negative control mice, which were administered water (Figure 4-7). We found that Fluor NP-ICs displayed up to a ~3.5-fold increase in average fluorescence and up to a ~8-fold increase in maximum detected fluorescence in iliac lymph nodes as compared to Fluor-NPs (Figure 4-7D). We observed a trend towards increased average fluorescence in inguinal lymph nodes from mice treated with Fluor-NP-ICs (Figure 4-7A). Quantification of maximum fluorescence in inguinal lymph nodes revealed up to a ~4-fold increase in

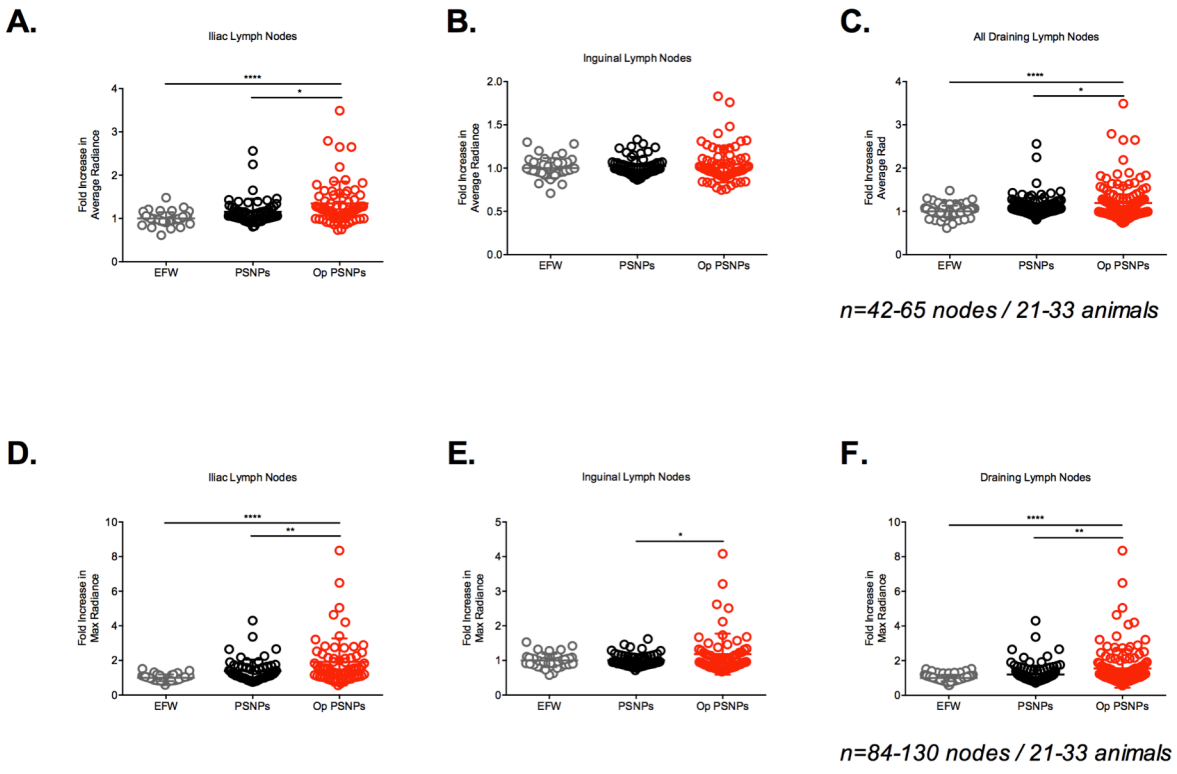

Figure 4 - 7 Nanoparticle trafficking to tissue-draining lymph nodes Fold increase in average and maximum fluorescence was quantified using the LivingImage Software with the Xenogen iVis Imaging System in iliac lymph nodes (A, D) and inguinal lymph nodes (B, E), 24 hours post-vaginal administration. Quantification of max fluorescence in all draining lymph nodes was pooled to highlight the overall changes in draining patterns (C,F). Statistical significance was determined using GraphPad Prism6 by a one-way ANOVA with a post-Tukey test.

animals, which received Fluor-NP-ICs (Figure 4-7E). To understand the overall impact on particle trafficking to draining lymph nodes, we pooled all of our data from iliac and inguinal tissues (Figure 4-7C,F). Overall, Fluor-NP-ICs displayed statistically significantly increased average and maximum bulk fluorescence signal in draining lymph nodes, 24 hours post-vaginal administration of materials.

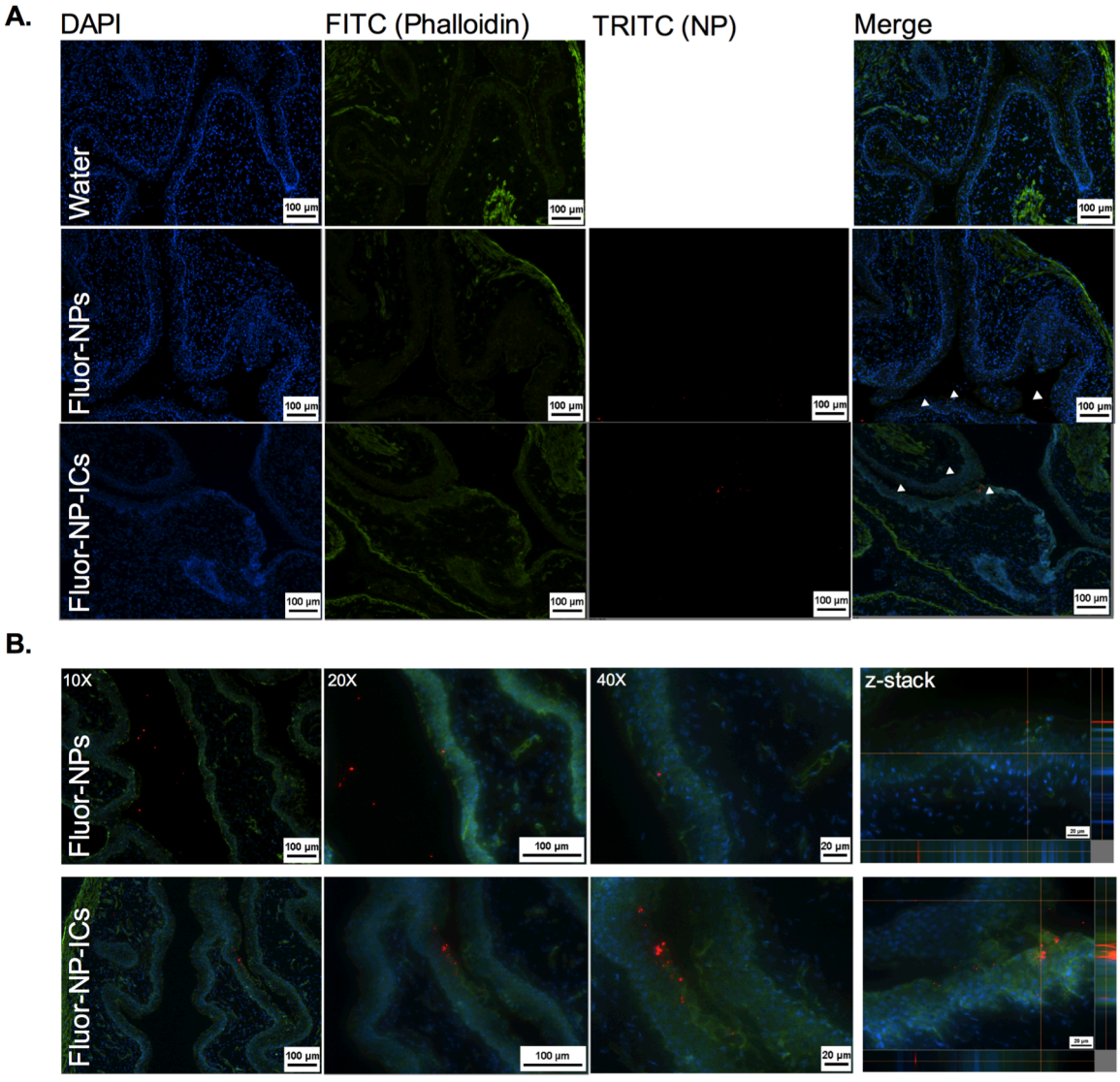

Figure 4 - 8 Immunofluorescence images of reproductive tract Reproductive tracts were sectioned and stained 24-hours after vaginal administration of nanomaterials. Sections were counterstained with DAPI (nuclei) and stained with Phalloidin (FITC, cytoskeleton). NPs are visualized in the TRIT-C channel. Independent DAPI, FITC, TRIT-C, and composite images are shown in (A) from water, PSNP, and IgG PS NP treatment groups. Composite images are shown at 10X, 20X, and 40X magnification for the NP and IgG PS NP treatment groups. Optical

4.D.4. Immunofluorescence imaging of vaginal tissues

Immunofluorescence imaging of reproductive tissues was conducted 24-hours after vaginal administration of treatment groups. NP fluorescence was generally observed in the lower vaginal tract. We observed very little to no fluorescence near the cervix and uterine horns (data not shown). As such, the presented representative images were all taken from the vaginal tract, below the cervix. Generally, we observed that Fluor-NPs were sequestered to the vaginal lumen (Figure 4-8). We were rarely able to visualize punctate Fluor-NPs associated with the vaginal epithelium. Qualitatively, we consistently visualized significant numbers of Fluor-NP-ICs cluster on the vaginal epithelium (Figure 4-8B). In both treatment groups, with this method of fluorescence imaging, we were unable to definitively visualize particles in the subepithelial vaginal mucosa. To confirm that the observed fluorescence signal was from NPs within the tissue, we performed optical sectioning of tissues. Optical sectioning confirmed that NPs were indeed embedded within the plane of tissue sections (Figure 4-8B).

4.D.5. NP uptake in vaginal antigen presenting cell subsets

To evaluate the impact of IgG surface functionalization on particle uptake in vaginal APC subsets, we assessed the percentage of NP+ cells 24 hours post-vaginal delivery of materials. Dead cells were excluded from analysis. CD45+ leukocytes were gated on MHC II, F4/80, CD11c, and CD11b to identify APC subsets. The PS NP treatment group

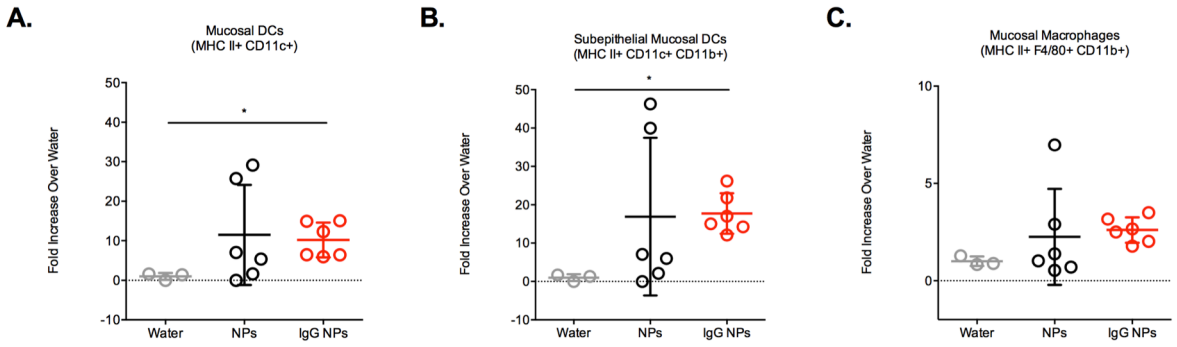

Figure 4 - 9 Nanoparticle uptake in vaginal antigen presenting cells NP fluorescence in antigen presenting cell (APC) subsets are shown as fold increase over the water treatment group. Fold increase over water is displayed for mucosal DCs (A), subepithelial mucosal DCs (B), and tissue-resident macrophages (C). Statistical significance was determined using GraphPad Prism 6 with a non-parametric Kruskall-Wallis test comparing the mean of each column to the control treatment group (water). (* indicates $p<0.05$).

did not display significant average or maximum fluorescence signal over the negative control mice for any APC subsets (Figure 4-9). The percentage of NP+ cells is displayed as fold increase over the control water treatment group. Mucosal macrophages (CD45+ F4/80+ CD11b+ CD11c-) displayed a trend towards increased particle uptake in mice, which received Fluor-NP-ICs, however the data is not statistically significant (Figure 4-9C). Mucosal DCs (CD45+ MHC II+ CD11c+) exhibited a statistically significant (~10-fold) increase in the average percentage of NP+ cells for the Op-NP treatment group compared to the control group (Figure 4-9A). Fluor-NP-ICs displayed a clear trend towards increased uptake by mucosal DCs as compared to Fluor-NPs, however the results were not significant due to the high variability in the PS NP treatment group. Finally, CD11b+ mucosal DCs (CD45+ MHC II+ CD11c+ CD11b+) displayed a statistically significant increase in Op-NP uptake by ~12-fold compared to the control group, and a trend towards ~2-fold increase in particle uptake compared to PS NP uptake (Figure 4-9B). Overall these data demonstrate that Fluor-NP-ICs are more readily taken up by vaginal APC subsets compared to unfunctionalized Fluor-NPs.

4.D.6. Histological analysis of vaginal tissues

Progesterone treated female mice were maintained in the diestrous phase of the menstrual cycle, which is characterized by a thinned vaginal epithelium as compared to naïve mice, which did not receive progesterone (Figure 4-10A). We performed haematooxylin and eosin (H&E) staining and histological analysis of tissues from mice receiving vaginal nanoparticle treatments to ascertain if there were any gross changes in epithelial structure, which might artificially boost delivery to draining lymph nodes or

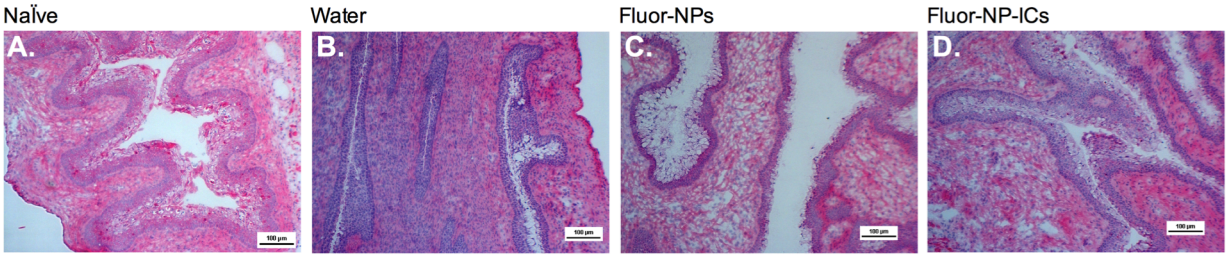

Figure 4 - 10 Histological analysis of reproductive tracts Tissues were sectioned using a cryomicrotome and H&E stained to visualize epithelial integrity. Reproductive tracts from mice that did not receive Depo-Provera® (A) were analyzed alongside mice which did receive Depo-Provera® (B-D) as well as vaginal administration of water (B), NPs (C), or IgG PS NPs (D).

increased access to underlying vaginal APCs. In mice that received progesterone, no differences in the integrity of the vaginal epithelium were observed between treatment groups (Figure 4-10).

4.E. DISCUSSION

In this report, we demonstrate the successful surface modification of dye-loaded, polystyrene nanoparticles with IgG to generate fluorescent, nanoparticle immune complexes (Fluor-NP-ICs). Our surface functionalization techniques were adapted to maximize surface coverage with IgG. To this end, we explored two methods of surface modification including bioconjugation and passive adsorption to amine-modified FluoSpheres, which have been previously used to track vaginal NP delivery[1]. Using established techniques for bioconjugation, we employed a heterobifunctional PEG crosslinker to conjugate IgG to the PEGylated Fluor-NPs. In agreement with previous literature findings, we found that unmodified 200-nm Fluor-NPs were ~270 nm in hydrodynamic diameter, and had a positive surface charge from the solvent accessible amine groups[33]. Further, PEG modification of NP surfaces results in a near neutral surface charge, as expected[1,31]. Conjugation of IgG to Fluor-PEG NP ICs resulted in a neutral surface charge. Our results also demonstrated that IgG surface modification by adsorption resulted in Fluor-NP-ICs that still had a positive surface charge, though it was significantly reduced from unmodified, Fluor-NPs. Importantly, the isoelectric point of human IgG subsets ranges from 7.2-8.6[34]. In the pH 8 buffer in which adsorption and conjugation was performed, IgG proteins would be near neutral or negative in overall charge. As such, electrostatic interactions are likely to drive IgG adsorption to the NP surface in this system.

Importantly, our synthesis was focused on maximizing NP surface coverage with IgG. Previous studies have employed radiolabeling of antibodies to compare conjugation of IgG to PEG NPs at a 900 molar excess and passive adsorption of IgG to PEG NPs[31]. Interestingly, these studies showed that even with PEGylated NP surfaces, passive adsorption resulted in 62 antibodies per PEG NP. This shows that IgG adsorption to polystyrene NPs is very efficient, even in the presence of polymer that has been employed to minimize surface adsorption of proteins[35]. We aimed to characterize

surface coverage by using a dye-conjugated IgG for subsequent modification of Fluor-NPs by bioconjugation or passive adsorption. Co-localization of fluorescence signals was measured by flow cytometry and was used as a metric to compare the efficiency of each modification strategy. Our results demonstrated that passive adsorption of IgG to Fluor-NPs resulted in nearly a five-fold increase in surface modification as compared to bioconjugation. Moreover, we were able to modify up to a maximum of ~60% of all Fluor-NPs by IgG adsorption. Importantly, dye modification of IgG was performed by conjugation to solvent accessible amines, and resulted in ~7 dye molecules per protein. Prior to IgG conjugation to PEG NPs bearing maleimide head groups, proteins are thiolated using a reagent that targets primary amines for conversion to sulfhydryl groups. As such, it is conceivable that the reduced conjugation efficiency seen in this system is due to a reduced number of amine groups in the dye-labeled IgG protein for conversion to sulfhydryls. Finally, to ensure that the majority of adsorbed IgG would remain adsorbed and not be out competed by another protein, we evaluated IgG desorption from Fluor-NP IC surfaces in the presence of BSA. Our results demonstrate that ~98% of surface adsorbed IgG remained adsorbed to Fluor-NP-ICs over a 72 hour period, indicating that these complexes would likely remain intact over the timescales relevant for *in vivo* studies.

Several studies have utilized fluorescent NPs as contrast agents for tracking diffusivity in mucus, tissue association, and lymph node trafficking [1,4,36,37]. Previous studies have employed 100 nm fluorescent nanoparticles for tracking distribution in the reproductive organs and 150-170 nm fluorescent NPs for bulk fluorescence imaging and tissue fluorescence quantification[1,4]. Few papers have also used much smaller, quantum dots to evaluate trafficking to tissue-draining lymph nodes after vaginal administration[36]. Howe et al. recently published immunofluorescence imaging of reproductive organs on vaginal distribution of smaller 20 nm and 40-nm sized fluorescent NPs, demonstrating that uterine and vaginal epithelial cells efficiently take up these NPs within 6-12 hours of vaginal administration[37]. Furthermore, these previous studies show data supporting drainage of these small NPs within the lymphatic ducts of the reproductive tract and in iliac and mesenteric lymph nodes within 5 hours of

administration. However, these studies do not focus on draining patterns of ~200 nm NPs from vaginal tissues to the tissue draining iliac and inguinal lymph nodes. Our vaginal dosing studies with Fluor-NPs were designed to investigate the capability of unmodified particles to distribute within the reproductive organs, associate with reproductive tract cells, and traffic to the iliac and inguinal lymph nodes. We hypothesized that Fluor-NPs would need to be delivered at a high dose in order to observe the background trafficking of 200-nm NPs to draining lymph nodes. Our results showed a dose dependent reduction of maximum bulk fluorescence measured in the reproductive tract, including the vagina, cervix, and uterine horns. In agreement with works of others, we found that the majority of Fluor-NP signal was observed in the lower vaginal tract[4]. Fluor-NPs delivered at 0.5%, 0.1%, and 0.05% correspond to 50 μg, 10 μg and 5 μg of NPs formulated in 10 μl of water. The highest dose showed a near ~100-fold increase in measured bulk fluorescence over the water control treatment group and a near ~15-fold increase in mean fluorescence intensity in reproductive tract-derived cell populations over the negative control. However, the highest dose showed only a ~1.23 fold increase in maximum bulk fluorescence observed in the iliac draining lymph nodes and no clear signal observed in the inguinal draining lymph nodes. Furthermore, these results showed that Xenogen image quantification of bulk fluorescence corroborated the same trends observed in flow cytometry fluorescence quantification of tissue-derived cells and, as such, both metrics were reliable for comparing treatment groups. It is also notable that tissue digestion and cell isolation prior to flow cytometry results in possible loss of signal in sample processing. From these results, we chose to move forward the highest dose of vaginal Fluor-NP administration (0.5%) for comparison to Fluor-NP-ICs.

Fluor-NPs and Fluor-NP-ICs were tracked over a 72-hour period for retention in the reproductive tract for draining to iliac and inguinal lymph nodes. Our results suggest that all nanoparticle formulations were detectable in the reproductive tract out to 72 hours, and were primarily sequestered to the lower vaginal tract. Other studies that rigorously quantified NP retention in the lavage showed that unmodified NPs associated with vaginal tissue was ~0.1% of the total dose delivered 6 hours post-administration[4]. Moreover, PEG NPs exhibited a ~10-fold increase in vaginal tissue retention at 6 hours

post-administration. Dose retention in vaginal tissues dropped off significantly at later time points. In addition, Cu et al. observed that levels of NPs collected in cervicovaginal lavages were also near ~1% of the total initial dose delivered 24 hours post-administration. In contrast, the bulk fluorescence images from the present study show detectable doses of Fluor-NPs and Fluor-NP-ICs out to 72 hours.

An important difference in these studies, which may result in enhanced vaginal retention at later time points, is that we performed swabbing of vaginal mucus prior to NP administration that may allow overall improved association with the vaginal tissue. In fact, Ensign et al. showed that unmodified NPs equally associated with the vaginal epithelium as compared to PEG NPs once mucus had been swabbed[1]. Mucus swabbing was essential to our studies, as we aimed to characterize the contribution of IgG to aid in transepithelial transport and uptake by mucosal DCs. Other groups have shown using alcain staining of mucin proteins that extensive washing with sterile PBS is sufficient to remove the majority of luminal mucus[38]. Future work may focus on the development of NPs that impart mucus-penetrating properties and functionality that allows for transeptihelial transport.

While some reports have reported transport of smaller vehicles such as quantum dots or 20-40 nm NPs to lumbar, inguinal, iliac, and mesenteric lymph nodes [36,37], none to our knowledge have evaluated larger NPs for trafficking from vaginal tissues after mucosal administration. It is well acknowledged that the iliac and inguinal lymph nodes drain the vaginal tissues[39], and as such, cell-free and cell-mediated draining of vaginal NP-ICs to these nodes is essential for routing antigen to sites of T cell priming by DCs. Our results demonstrate that Fluor-NP-ICs appeared in iliac lymph nodes by 6 hours, and fluorescence signal was visualized after Fluor-NP or Fluor-NP IC vaginal administration over a period of 72 hours. Fluor-NP-ICs appeared in inguinal lymph nodes between 24-48 hours post-vaginal administration. Scale-up of trafficking patterns at 24-hours showed up to an eight-fold increase in the maximum fluorescence signal observed in the Fluor-NP IC administration group over background. These results were statistically significantly greater than fluorescence observed in iliac lymph node from animals administered with Fluor-NPs. While Fluor-NPs showed no fluorescence signal

above background in inguinal lymph nodes, Fluor-NP-ICs showed up to a four-fold increase in maximum fluorescence. Overall, modification of NP surfaces with IgG resulted in a nearly eight-fold increase in trafficking to draining lymph nodes 24 hours post-vaginal administration. These results demonstrate that IgG modified protein surfaces are more efficient in transepithelial transport resulting in trafficking to draining lymph nodes. It is important to note that our results do not discern between cell-free and cell-associated transport for NPs.

Immunofluorescence imaging was employed to visualize the general location of Fluor-NPs and Fluor-NP-ICs within the reproductive organs 24-hours after vaginal administration. We were unable to image any nanoparticles near the cervix or in the uterine horns, and found that most fluorescence signal was sequestered to the vaginal tract[37]. This finding is in contrast to previous groups who have shown trafficking to the uterine epithelial cells; however, this is likely due to the fact that the administered NPs were five- to 10-fold smaller than what was used in our studies. In the vaginal tract, we found little to no Fluor-NPs in most of the images that were obtained. When Fluor-NPs were observed, our results suggest that they remained sequestered to the lumen or minimally associated with the epithelium. In contrast, Fluor-NP-ICs were observed to cluster in large complexes at and within the vaginal epithelium. Importantly, FcRn is largely considered to be an endosomal rescue receptor of IgG, but in the acidic environment of the vaginal lumen (pH 4 in humans, pH 6.2-6.5 in mice), FcRn may be able to capture IgG at the cell surface via receptor-mediated endocytosis[28]. As such, clustering of Fluor-NP-ICs may be due to endocytosis of large complexes or crosslinking of FcRn receptors at the cell surface and clustering of Fluor-NP-ICs at the vaginal epithelium. Ensign et al. showed that 10 minutes after administration of unmodified NPs, post-mucus swab NPs were able to coat the vaginal epithelium similarly to PEG-modified NPs[1]. However, Ensign et al. do not report if post-euthanization lavages were performed to remove NPs that aren't fully associated with the epithelium. In contrast, it is notable that we performed a post-euthanization lavage to maximize removal of Fluor-NPs and Fluor-NP-ICs from the vaginal lumen and focus on NPs that are most associated with the epithelium.

To understand if Fluor-NPs and Fluor-NP-ICs differentially gain access to mucosal APCs, we evaluated NP uptake in DC subsets and macrophages. While a number of groups have evaluated delivery of NPs or drugs loaded in NPs to vaginal tissues, none to our knowledge have characterized the selective association of NPs with mucosal APC subsets. Our results describe for the first time a comparison of Fluor-NP and Fluor-NP IC uptake by mucosal DCs and macrophages. Although the variability in the Fluor-NP treatment group was high, we found that Fluor-NP-ICs showed a clear trend towards increased uptake by MHC II+ antigen presenting cells including mucosal DCs (CD11c+), subepithelial DCs (CD11c+ CD11b+), and mucosal macrophages (F4/80+ CD11b+). Importantly, our results demonstrate that unlike unmodified NPs, Fluor-NP-ICs showed a statistically significant increase in uptake by mucosal DCs and subepithelial DCs. Since our results to do not separate the contributions of FcRn mediated-enhancements in transepithelial transport and Fcγ-mediated enhancements in uptake of Fluor-NP-ICs, we believe that enhanced uptake may be a result of increased NPs in the submucosa due to improved transcytosis, increased uptake via Fcγ-expressing mucosal cells, or a combination of both these phenomena. Future studies must focus on separating the contribution of both these receptors using knockout models. Finally, our histology electron micrographs suggest that while the epithelium is thinned from subcutaneous hormone administration, vaginal NP delivery does not compromise the integrity of the epithelial layer. This ensures that the differences we observed between particle treatment groups are truly an effect of the differences in NP surface functionalization. Taken together, our data serve as a proof-of-concept that NP surface modification with IgG enhances delivery across the vaginal epithelium to underlying immune cells and draining lymph nodes. Formation of NP-ICs may be a key strategy in efficient delivery of particle-formulated vaccine antigens at mucosal sites.

4.F. CONCLUSION

Our study aimed to describe the impact of IgG modification of nanoparticles on vaginal delivery across the epithelium and to key cellular and organ targets that play a role in potentiating immune responses to vaccine antigens. We found that surface modification of fluorescent NPs resulted in the generation of immune complexes, which were

efficiently transported across the vaginal epithelium. Further, we found that Fluor-NP-ICs were efficiently draining to iliac and inguinal lymph nodes and exhibited increased uptake in mucosal APC subsets. Extensions of this work will focus on validating the delivery of antigens within NP ICs to facilitate enhanced functional immune responses after mucosal vaccination.

4.G. ACKNOWLEDGEMENTS

This work is funded by an NIH Director's New Investigator Award to K.A.W. (1DP2HD075703) and with the support of a UW STD/AIDS Training Fellowship to R.R. (NIHT32AI07140).

4.H. REFERENCES

1. Ensign, L. M. *et al.* Mucus-penetrating nanoparticles for vaginal drug delivery protect against herpes simplex virus. *Science translational medicine* **4,** 138ra79–138ra79 (2012).
2. Yang, M. *et al.* Vaginal Delivery of Paclitaxel via Nanoparticles with Non-Mucoadhesive Surfaces Suppresses Cervical Tumor Growth. *Advanced healthcare materials* **3,** 1044–1052 (2014).
3. Cu, Y. & Saltzman, W. M. Controlled surface modification with poly (ethylene) glycol enhances diffusion of PLGA nanoparticles in human cervical mucus. *Molecular pharmaceutics* **6,** 173–181 (2008).
4. Cu, Y., Booth, C. J. & Saltzman, W. M. In vivo distribution of surface-modified PLGA nanoparticles following intravaginal delivery. *Journal of controlled release* **156,** 258–264 (2011).
5. Nimmerjahn, F. & Ravetch, J. V. Fcγ receptors as regulators of immune responses. *Nature Reviews Immunology* **8,** 34–47 (2008).
6. Bruhns, P. Properties of mouse and human IgG receptors and their contribution to disease models. *Blood* **119,** 5640–5649 (2012).
7. Brambell, F. W. The transmission of immune globulins from the mother to the foetal and newborn young. *Proceedings of the Nutrition Society* **28,** 35–41 (1969).
8. Simister, N. E. & Mostov, K. E. An Fc receptor structurally related to MHC class I antigens. (1989).
9. Yoshida, M. *et al.* Neonatal Fc receptor for IgG regulates mucosal immune responses to luminal bacteria. *The Journal of clinical investigation* **116,** 2142 (2006).
10. Spiekermann, G. M. *et al.* Receptor-mediated immunoglobulin G transport across mucosal barriers in adult life functional expression of FcRn in the mammalian lung. *The Journal of experimental medicine* **196,** 303–310 (2002).
11. Kuo, T. T. & Aveson, V. G. Neonatal Fc receptor and IgG-based therapeutics. **3,** 422–430 (2011).
12. Yoshida, M. *et al.* Human neonatal Fc receptor mediates transport of IgG into

luminal secretions for delivery of antigens to mucosal dendritic cells. *Immunity* **20,** 769–783 (2004).
13. McCarthy, K. M., Yoong, Y. & Simister, N. E. Bidirectional transcytosis of IgG by the rat neonatal Fc receptor expressed in a rat kidney cell line: a system to study protein transport across epithelia. *Journal of Cell Science* **113,** 1277–1285 (2000).
14. Neutra, M. R. & Kozlowski, P. A. Mucosal vaccines: the promise and the challenge. *Nature Reviews Immunology* **6,** 148–158 (2006).
15. Proetzel, G. & Roopenian, D. C. Humanized FcRn mouse models for evaluating pharmacokinetics of human IgG antibodies. *Methods* **65,** 148–153 (2014).
16. Israel, E. J. *et al.* Expression of the neonatal Fc receptor, FcRn, on human intestinal epithelial cells. *Immunology* **92,** 69–74 (1997).
17. Baker, K. *et al.* Immune and non-immune functions of the (not so) neonatal Fc receptor, FcRn. **31,** 223–236 (2009).
18. Roopenian, D. C. & Akilesh, S. FcRn: the neonatal Fc receptor comes of age. *Nature Reviews Immunology* **7,** 715–725 (2007).
19. Hessell, A. J. *et al.* Fc receptor but not complement binding is important in antibody protection against HIV. *Nature* **449,** 101–104 (2007).
20. Baker, K., Rath, T., Lencer, W. I., Fiebiger, E. & Blumberg, R. S. Cross-presentation of IgG-containing immune complexes. *Cellular and Molecular Life Sciences* **70,** 1319–1334 (2013).
21. Rafiq, K., Bergtold, A. & Clynes, R. Immune complex-mediated antigen presentation induces tumor immunity. *Journal of Clinical Investigation* **110,** 71–80 (2002).
22. Schuurhuis, D. H. *et al.* Antigen-antibody immune complexes empower dendritic cells to efficiently prime specific CD8+ CTL responses in vivo. *The Journal of Immunology* **168,** 2240–2246 (2002).
23. Bai, Y. *et al.* Intracellular neutralization of viral infection in polarized epithelial cells by neonatal Fc receptor (FcRn)-mediated IgG transport. *Proceedings of the National Academy of Sciences* **108,** 18406–18411 (2011).
24. Kobayashi, N. *et al.* FcRn-mediated transcytosis of immunoglobulin G in human renal proximal tubular epithelial cells. *American Journal of Physiology-Renal Physiology* **282,** F358–F365 (2002).
25. Tenten, V. *et al.* Albumin is recycled from the primary urine by tubular transcytosis. *Journal of the American Society of Nephrology* **24,** 1966–1980 (2013).
26. Dickinson, B. L. *et al.* Bidirectional FcRn-dependent IgG transport in a polarized human intestinal epithelial cell line. *Journal of Clinical Investigation* **104,** 903 (1999).
27. Yoshida, M. *et al.* IgG transport across mucosal barriers by neonatal Fc receptor for IgG and mucosal immunity. **28,** 397–403 (2006).
28. Li, Z. *et al.* Transfer of IgG in the female genital tract by MHC class I-related neonatal Fc receptor (FcRn) confers protective immunity to vaginal infection. *Proceedings of the National Academy of Sciences* **108,** 4388–4393 (2011).
29. Ye, L., Zeng, R., Bai, Y., Roopenian, D. C. & Zhu, X. Efficient mucosal vaccination mediated by the neonatal Fc receptor. *Nature biotechnology* **29,** 158–163 (2011).

30. Pridgen, E. M. *et al.* Transepithelial transport of Fc-targeted nanoparticles by the neonatal fc receptor for oral delivery. *Science translational medicine* **5,** 213ra167–213ra167 (2013).
31. Chan, L. W. *et al.* Synthesis and characterization of anti-EGFR fluorescent nanoparticles for optical molecular imaging. *Bioconjugate chemistry* **24,** 167–175 (2013).
32. Ramanathan, R. *et al.* Effect of Mucosal Cytokine Administration on Selective Expansion of Vaginal Dendritic Cells to Support Nanoparticle Transport. *American Journal of Reproductive Immunology* **74,** 333–344 (2015).
33. Fleischer, C. C. & Payne, C. K. Nanoparticle surface charge mediates the cellular receptors used by protein–nanoparticle complexes. *The Journal of Physical Chemistry B* **116,** 8901–8907 (2012).
34. Hamilton, R. G. The human IgG subclasses. (1994).
35. Walkey, C. D., Olsen, J. B., Guo, H., Emili, A. & Chan, W. C. Nanoparticle size and surface chemistry determine serum protein adsorption and macrophage uptake. *Journal of the American Chemical Society* **134,** 2139–2147 (2012).
36. Ballou, B. *et al.* Nanoparticle transport from mouse vagina to adjacent lymph nodes. (2012).
37. Howe, S. E. & Konjufca, V. H. Protein-coated nanoparticles are internalized by the epithelial cells of the female reproductive tract and induce systemic and mucosal immune responses. *PloS one* **9,** e114601 (2014).
38. Neves, das, J. *et al.* Biodistribution and pharmacokinetics of dapivirine-loaded nanoparticles after vaginal delivery in mice. *Pharmaceutical research* **31,** 1834–1845 (2014).
39. Iwasaki, A. Mucosal dendritic cells. *Annu. Rev. Immunol.* **25,** 381–418 (2007).

Chapter 5: Physical and immunological characterization of polymer nanoparticle immune complexes for the enhancement of antigen cross-presentation to effector T cells

5.A. ABSTRACT

Our previous research has shown that the development of nanoparticle immune complexes by surface adsorption of IgG can be used as a strategy to promote transepithelial transport, draining to lymph nodes, and uptake by vaginal antigen presenting cells (APCs). We hypothesize that existing Fc receptor pathways mediate interactions with IgG that ultimately promote transport across the vaginal epithelium and targeting of innate immune cells. Here we evaluate the synthesis of polymer nanoparticle systems for encapsulation of a model protein antigen, ovalbumin (OVA), surface modification to generate nanoparticle immune complexes (NP ICs), and delivery to the vaginal mucosa. We show that particle formulation of OVA enhances Th1 cytokine secretion in co-cultures of BMDCs and primed CD8+ cytolytic T cells. Finally, we address whether *in vivo* vaginal protein delivery can be evaluated using *ex vivo* co-culture systems with effector CD4+ helper T cells.

5.B. INTRODUCTION

To extend our work towards the development of an intravaginal mucosal vaccine for HIV, our goal in this aim is to test the hypothesis that host Fc receptors may be leveraged to promote stronger mucosal immune responses to antigens delivered by nanocarriers. Previous immunizations with recombinant proteins expressing an Fc domain have demonstrated the ability to mount mucosal immune responses[1,2]; however, the generation of a significant immune response after intravaginal vaccination remains elusive. We hypothesize that by encapsulating antigen within a nanoparticle carrier functionalized to specifically engage Fc receptors, we will be able to transport protected antigenic cargo to the submucosa where they may be more efficiently internalized into dendritic cells, processed, and trafficked to lymph nodes.

Poly(lactic-co-glycolic acid) (PLGA) nanoparticle systems have been commonly used to formulate proteins including bovine serum albumin (BSA) and a model antigen,

ovalbumin (OVA), using double emulsion techniques[3-6]. Various groups have also showed that PLGA surfaces can be further modified with IgG[7,8]. As such, these systems show promise as materials that can be used in the synthesis of OVA-loaded, IgG-modified PLGA nanoparticles or OVA nanoparticle immune complexes (OVA NP ICs). Applications using antigen-antibody immune complexes are described in 4.B. and have been shown to shape the activation state of DCs and influence T cell priming. Our work is focused on extending the application of ICs to nanoparticle systems, which have been described to optimize antigen dosing, minimize toxicity, and provide sustained release of protein cargo[9]. While vaginal immunization with OVA has been somewhat characterized for functional responses, nanoparticle formulation of antigen has not been evaluated for promoting cellular responses – only for humoral antibody responses[10-12].

To evaluate the potential functional benefits of encapsulating antigen in NP ICs, we developed a general strategy for generating OVA-NP ICs using a double emulsion method followed by surface modification with human serum IgG. Transepithelial transport of Fc-protein-modified nanoparticles (analogous to the NP ICs we are testing) has been described to improve drug delivery after oral mucosal administration[13]. In our research, we seek to understand if NP ICs can leverage existing mechanisms of FcRn transepithelial transport pathways or Fcγ receptor-mediated uptake (see 4.B. for extended discussion), to promote functional, T cell responses after vaginal immunization with OVA.

5.C. MATERIALS AND METHODS

5.C.1. Materials

Acid-terminated, 50:50 Poly(DL-lactide-co-glycolide) (PLGA), 31.3-57.6 kDa in molecular weight were purchased from Lactel Absorbable Polymers (Birmingham, AL). Poly(vinyl alcohol) (PVA), 87-90% hydrolyzed and at an average molecular weight of 30-70 kDa was obtained from Sigma Aldrich (St. Louis, MO). 1-ethyl-3-(3-dimethylaminopropyl)carbodiimide (EDC) and IgG from human serum were also purchased from Sigma Aldrich (St. Louis, MO). Albumin from chicken egg white (OVA) (Sigma Aldrich) was used for *in vitro* validation of protein loading in PLGA nanoparticles and EndoFit OVA (Invivogen, San Diego, CA) was used for all formulations delivered *in*

vivo and in *ex vivo* immune studies. Protein quantification was determined using a Micro BCA Protein Assay Kit (Thermo Fisher Scientific, Bothell, WA) and Protein A-FITC used in binding studies was obtained through Sigma Aldrich (St. Louis, MO). Endotoxin-free water was used for rehydration of soluble or particle formulated protein in all studies with immunological endpoints. Ovalbumin, Alexa Fluor 647® Conjugate was used for dosing studies (Thermo Fisher Scientific, Bothell, WA). Black construction paper was used as a background for Xenogen iVis bulk fluorescence imaging. Materials and reagents used in cell isolation include 70-micron cell filters (company, location), 16-gauge blunt-end needles (Stem Cell Technologies, Vancouver, Canada), Collagense D (Roche, Indianapolis, IN), and DNAse I (Roche, Indianapolis, IN). CD11c MicroBeads, CD4+ T Cell Isolation Kit, CD8a+ T Cell Isolation Kit, MS/LS magnets and columns were all purchased through Miltenyi Biotec (Bergisch Gladbach, Germany). Granulocyte macrophage colony-stimulating factor (GM-CSF) used in co-culture assays was purchased from Peprotech (Rocky Hill, NJ), and lipopolysaccharide (Sigma Aldrich, St. Louis, MO) was used as an *ex vivo* adjuvant. CpG oligodeoxynucleotide (ODN) 1826 used as an *in vivo* adjuvant was purchased through Invivogen (San Diego, CA). IFN- γ, IL-12, IL-10, and IL-4 enzyme-linked immunosorbent assay (ELISA) kits were purchased through Peprotech (Rocky Hill, NJ).

5.C.2. Antibodies

Primary antibody-fluorochromes used for cell surface marker staining of host cells (derived from C57BL/6J mice) include APC anti-mouse CD11c and Alexa-488 anti-mouse I-Ad/I-Ed (MHC II) (BD Biosciences, Franklin Lake, NJ). Purified rat anti-mouse CD16/CD32 was purchased from BD Biosciences to block non-specific Fc receptor binding of primary antibody-fluorochrome pairs to host cells. APC anti-mouse CD8a and APC anti-mouse CD4 antibodies used to stain CD8a+ and CD4+ T cells (derived from OTI and OTII mice) were purchased from BioLegend (San Diego, CA). Vybrant® CFDA SE Cell Tracer Kit (CFSE) used to label T cells was bought through ThermoFisher Scientific (Bothell, WA). LIVE/DEAD Fixable Violet dead cell stain kit was obtained from ThermoFisher Scientific (Bothell, WA).

5.C.3. Synthesis of PLGA NPs, OVA loading, and functionalization with IgG

PLGA nanoparticles (NPs) were prepared using previously published methods[14,15]. Briefly, NPs were synthesized using a double emulsion method. PLGA was dissolved in dichloromethane (DCM) to create a polymer/organic phase (oil). To generate OVA-loaded PLGA NPs (OVA NPs), OVA was resuspended in sterile, 1X PBS at 40 mg/mL and added to the polymer/organic phase to create the initial water-in-oil emulsion (W/O). Initial OVA protein loading in PLGA was 10% (w/w). This water-in-oil emulsion was vortexed and tip sonicated three times at 50% amplitude. Solutions were placed on ice between each sonication to prevent protein denaturation. The PLGA/OVA solution was then added dropwise into a new glass tube containing 2 mL of 5% (w/v) PVA while vortexing, to create the water-in-oil-in-water (W/O/W) double emulsion. The W/O/W solution was tip sonicated as described above. Finally, the PLGA/OVA/PVA solution was poured into 30 mL of 0.3% PVA (w/v) and placed on a magnetic stir plate over night to allow residual DCM to evaporate. NPs and OVA NPs were purified by three rounds of centrifugation at 10,000xg for 20 min at 4°C. Particles were rehydrated in DI water between centrifugation steps and purified through a 2-micron syringe filter to remove aggregates. The resulting NPs and OVA NPs were resuspended in DI water for *in vivo* studies and endotoxin-free water for *ex vivo* and *in vivo* studies.

IgG modification was performed using methods established by Kocbek et al. for passive adsorption and bioconjugation to acid-terminated PLGA nanoparticles[8]. IgG and NPs at a mass ratio of approximately 1:1 were incubated overnight at 4C and washed three times using a benchtop centrifuge at 10,000xg for 20 minutes. EDC was added at ~15 molar excess to IgG and incubated with NPs for 2 hours at room temperature. IgG conjugated NPs were washed three times by centrifugation at 10,000xg for 20 min.

5.C.4. Physical characterization of nanoparticles, protein quantification and release, and Protein A binding

Hydrodynamic size, polydispersity (PDI), and zeta potential of all particle formulations was determined by dilution in 10 mM NaCl, pH 4 by dynamic light scatter (DLS) techniques with a Malvern Zetasizer (Malvern Instruments, Malvern, UK). NP stability over time was assessed by incubation at 4°C and 37°C, and measurements at a range

of timepoints. Mass recovery of nanoparticles was determined by lyophilizing an aliquot of the particle solution overnight. Protein quantification (OVA or IgG) was determined by dissolution of particles in 0.1M NaOH, dilution of sodium hydroxide to 10 mM, and quantification with a Micro BCA assay. Release assays were carried out by incubating aliquots of OVA NPs at 4°C and 37°C. At each time point, particles were spun at 10,000xg for 20 minutes and supernatants were saved for protein quantification using a Micro BCA assay. Binding activity was determined by flow cytometry. Briefly, Protein A-FITC was incubated with NP-ICs at a 1:4 mass ratio, particles were spun down after incubation at room temperature, and pellets were resuspended in DI water. Resuspended NP-ICs with bound Protein A were quantified for mean fluorescence intensity in the FITC channel by flow cytometry, using a FACSCanto2 equipped with a 405-nm violet laser, a 488-nm blue laser, and a 633-nm red laser.

5.C.5. Animal models and vaginal administration of materials

Female C57BL/6J mice (4-6 weeks old) and female OT-I (C57BL-6-Tg(TcraTcrb)1100Mjb/J) and OT-II (B6.Cg-Tg(TcraTcrb)425Cbn/J) mice (6-8 weeks old) were purchased from The Jackson Laboratory (Bar Harbor, ME). Four days prior to vaginal administration of materials in C57BL/6J mice (hosts), all animals were subcutaneously administered 100 µl medroxyprogesterone acetate (Depo-Provera®) to synchronize estrous cycle stage and reduce mouse-to-mouse variability. Depo-Provera® was purchased through the UW pharmacy from Greenstone LLC (PeaPack, NJ) and was formulated at 20 mg/ml in sterile Dulbecco's Phosphate-Buffered Saline (DPBS). Mice were anesthetized with isoflurane in an induction chamber. Prior to NP administration, mice genital tracts were flushed out with 80 µl of endotoxin-free water three times using a micropipette, and two Calginate swabs (Fisher Scientific, Hampton, NH) were used to remove mucus from the vaginal lumen. All mice were taped around the abdomen using two pieces of Fisherbrand tape (Fisher Scientific, Hampton, NH) to prevent self-grooming. Using a micropipette, mice were intravaginally administered 40 µg, 20 µg, or 10 µg fluorescent OVA for dosing studies. For *in vivo* delivery of OVA, OVA NPs, and OVA NP-ICs - 20 µg OVA was administered. Based on changes in nanoparticles mass recovery and OVA loading, the mass of nanoparticles delivered

ranged from 220-350 µg. NP-ICs (vehicle control) were dose matched to deliver the same particle mass as in OVA-formulated nanoparticles. Mice were placed in dorsal recumbence for 15 minutes in the induction chamber to improve vaginal retention of administered treatments. After recovery from anesthetization, mice were individually caged to prevent grooming between animals for 24-72 hours. All animal studies were approved and monitored under guidelines set by the University of Washington Institutional Animal Care and Use Committee (IACUC).

5.C.6. BMDC derivation and single cell isolation from host animals and transgenic mouse spleens

Bone-marrow derived stem cells (BMDCs) were generated from C57BL/6J mice using well-established methods that have been previously published[16,17]. Briefly, stem cells were isolated from the femur and tibia of C57BL/6J mice and dendritic cells (DCs) were derived in cell culture over seven to eight days. CD11c+ BMDCs were purified using magnetic activated cell sorting (MACS) techniques with the CD11c MicroBead system, according to manufacturer's protocols. Single cell suspensions were isolated from the reproductive tract and iliac and inguinal lymph nodes of host C57BL/6J mice as described in Chapter 4 (Section 4.C.8.). T cells were isolated from the spleen of OT-I or OT-II mice by perfusion of spleens with 1 mL of a Collagenase D solution (1 mg/ml in cRPMI). Spleens were cut into small pieces with sterile scissors and incubated at 37°C for 30 min. Digested spleens were placed on a 70-micron cell strainer and tissues were mechanically disrupted using a 3-mL syringe plunger. Cells were rinsed with 10 mL of pre-warmed sterile PBS. Cells were spun at 1500 rpm for 5 min at 4°C and resuspended in 5 mL of RBC lysis buffer for 2 minutes. 15-mL of sterile PBS was added and the cells were centrifuged. Pellets were resuspended in MACS buffer (0.5% BSA and 2 mM EDTA in PBS), passed through a second 70-micron cell strainer, and centrifuged. CD4+ and CD8a+ T cell isolation kits were used to purified T cells exactly according to manufacturer's protocols. T cells were labeled with CFSE. A 10 µM stock solution of CFSE was prepared in 0.1% bovine serum albumin (BSA) in PBS and 1 mL of this CFSE stock solution was added per 7.5 x 10^6 T cells. Cells were mixed and incubated at 37°C for 10 min. RPMI media was added to labeled T cells, and cells were

washed twice by centrifugation at 1500 rpm for 5 min at 4°C. Labeled T cells were resuspended in RPMI. T cells were co-cultured with BMDCs or host reproductive tract or draining lymph node cells at a 1:1 ratio of 20,000 cells each. Cells were seeded in a 96-well round bottom plate. All wells contained a final GM-CSF concentration of 10 ng/ml. For wells receiving *ex vivo* adjuvants, the co-culture was supplemented with 2 ng of LPS.

5.C.7. T cell proliferation assays

In *ex vivo* studies, BMDCs or host cells were incubated with soluble or particle-formulated OVA for 24-hours and washed by replacing the volume of media in each well ten times. CD4+ or CD8a+ T cells were added after wells were washed, and co-cultures were incubated for 72-hours. Plates were spun at 200 rpm for 5 min, and supernatants from each co-culture well were collected and stored at -20°C for cytokine analysis. Wells were washed with FACS buffer (1% FBS in PBS), and resuspended in antibody solution to stain for CD4 or CD8a. After 40 minutes of incubation on ice, wells were washed with FACS buffer, and stained with a LIVE/DEAD Fixable Dead Cell Staining Kit for 20 min on ice. Plates were washed and fixed in 1.6% paraformaldehyde and all samples were collected on an LSRII with a 488-nm blue laser, 561 nm yellow/green laser, 640-nm red diode laser, 405-nm violet laser, and a 350-nm UV laser and equipped with a high throughput sampler (HTS).

5.C.8. Cytokine analysis of co-culture supernatants

Th1 (IFN- γ and IL-12) and Th2 (IL-10 and IL-4) cytokines in co-culture supernatants were using an ELISA. Supernatants from co-cultures of host cells (reproductive tract or draining lymph node-derived) and T cells were used undiluted in the assay. Supernatants from co-cultures of BMDCs and T cells were diluted two-fold prior to ELISA analysis. All cytokine analyses were carried out as described in the manufacturer's protocols, and quantified by comparison to a standard curve using a TECAN fluorescence plate reader (Manedorf, Switzerland).

5.D. RESULTS

5.D.1. Adsorption versus conjugation of IgG to PLGA nanoparticle surface

Table 5 - 1 Size, polydispersity, surface charge, and protein loading of IgG-modified PLGA NPs

	Size (d, nm)	PDI	ζ-potential* (mV)	IgG Loading (μg IgG/mg NP)
PLGA NPs	129.3 ± 3.2	0.09 ± 0.02	-39.9 ± 1.2	-
Adsorbed IgG PLGA NPs	176.1	0.217	-21.7	20.3 ± 0.4
Conjugated IgG PLGA NPs	133.0	0.07	-19.1	15.5 ± 1.3

*1:10 dilution in water

PLGA nanoparticles were readily synthesized and modified with human serum IgG by passive adsorption and bioconjugation. PLGA nanoparticles were ~130 nm in size and were highly monodisperse with a PDI < 0.1 (Table 5-1). The surface charge of PLGA nanoparticles was measured by dynamic light scattering to be -40 mV, as a result of solvent accessible carboxyl groups. Adsorption of IgG resulted in slightly larger particles near ~180 nm in diameter with a PDI ~0.2 in contrast to conjugation of IgG, which resulted in particles near ~130 nm and a PDI < 0.1. Both particles saw an increase in surface charge to -20 mV. IgG loading on PLGA nanoparticles was measured by particle dissolution in sodium hydroxide and protein quantification with a microBCA assay (Table 5-1). IgG loading was determined to be ~20 μg IgG/mg NP for IgG adsorbed particles and ~15 μg IgG/mg NP for IgG conjugated particles. Finally, binding of FITC-Protein A was observed to be higher to IgG adsorbed PLGA nanoparticles as compared to IgG conjugated PLGA nanoparticles (Figure 5-1).

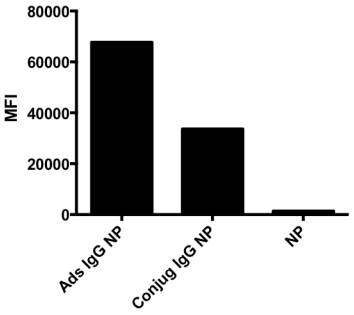

Figure 5 - 1 Protein A Binding Adsorbed IgG PLGA NPs and conjugated IgG PLGA NPs were incubated with fluorescent Protein A. Mean fluorescence intensity was quantified by flow ctyometry.

5.D.2. Physical characterization and stability of OVA NPs and OVA release

Table 5 - 2 Size, polydispersity, and surface charge of OVA-loaded PLGA NPs

	Size (d, nm)	PDI	ζ-potential* (mV)
PLGA NPs	129.3 ± 3.2	0.09 ± 0.02	-39.9 ± 1.2
OVA PLGA NPs	132.8 ± 0.3	0.1 ± 0.03	-30.7 ± 5.3

*1:10 dilution in water

Soluble OVA protein was successfully loaded into PLGA NPs using the double emulsion method. OVA PLGA NPs were near ~130 nm and had a low PDI ~0.1 and were measured to have a surface charge of ~-30 mV (Table 5-2). Mass recovery of PLGA nanoparticles and OVA PLGA NPs was ~40% (Table 5-3). OVA encapsulation within PLGA NPs was measured by accelerating dissolution of nanoparticles in a sodium hydroxide solution and quantification of protein using a microBCA assay. OVA protein loading was determined to be 97.5 µg/mg NPs. Release was determined over 72-hours, to understand the fraction of OVA protein that would be released over the relevant timescales of *in vivo* and *ex vivo* studies. At body temperature, at 72-hours only ~3% of the encapsulated protein was released (Figure 5-2). Stability of OVA PLGA NPs was determined using dynamic light scattering measurements of particles incubated at storage and body temperatures. Our data show that protein-loaded particles aggregate at 37°C, and double in size to ~400 nm 24-hours post-incubation. Adsorbed OVA NP ICs (IgG OVA PLGA NPs) were 158.7 nm in size with a PDI of 0.241 and a zeta potential of -35.2.

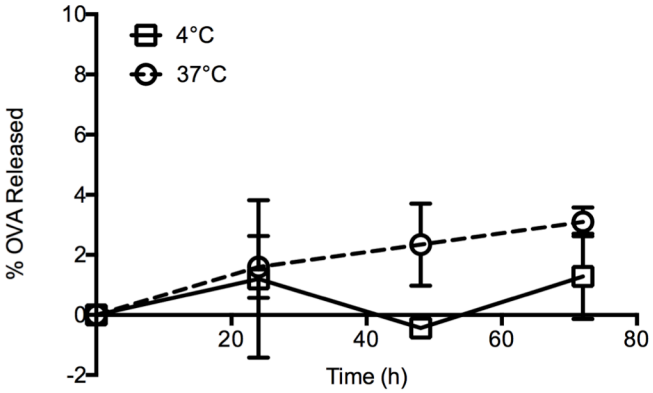

Figure 5 - 2 OVA release from PLGA nanoparticles. Protein release was measured by centrifuging NPs at each timepoint, and measuring released OVA in supernatants using a microBCA assay.

Table 5 - 3 Mass recovery and OVA loading in PLGA NPs

	% Mass Recovery	Theor. Loading* (mg OVA/mg PLGA)	Loading (mg OVA/mg NP)	% EE
PLGA NPs	38.4 ± 1.1	-	-	-
OVA PLGA NPs	43.4 ± 3.8	100	97.5 ± 5.5	97.5 ± 5.5

*PLGA NPs dissolved in 0.1 M NaOH for 24-h, OVA measured by microBCA Assay

5.D.3. Soluble OVA dosing study

To understand the appropriate vaginal dose of soluble OVA protein that would ensure draining to lymph nodes within 24-hours of topical administration, we performed a dosing study of fluorescent OVA. Animals were vaginally administered OVA-Alexa657 at

40 µg, 20 µg, and 10 µg protein formulated in endotoxin-free water and individually caged for 24-hours. Reproductive organs (including the vagina, cervix, and uterine horns) and iliac and inguinal draining lymph nodes were dissected 24-hours post-vaginal administration. All tissues were imaged using the Xenogen iVis *In Vivo* Imaging System and flow cytometry of tissue-derived single cell suspensions as a secondary metric of bulk fluorescence signal. Fluorescence images taken with the Xenogen iVis system were normalized to control treatment groups of endotoxin-free water to remove tissue autofluorescence (Figure 5-3A). Bulk fluorescence was quantified by defining a region of interest, and using the Living Image software to calculate the maximum radiance. Fluorescence signal appeared strongest in the reproductive organs from mice administered 40 µg OVA-Alexa647, and showed a dose-dependent reduction in max fluorescence signal as the dose was decreased (Figure 5-3B). Bulk tissue fluorescence was also quantified by flow cytometry of reproductive tract tissue-derived single cell suspensions. The OVA+ gate was set in reference to control group mice, which

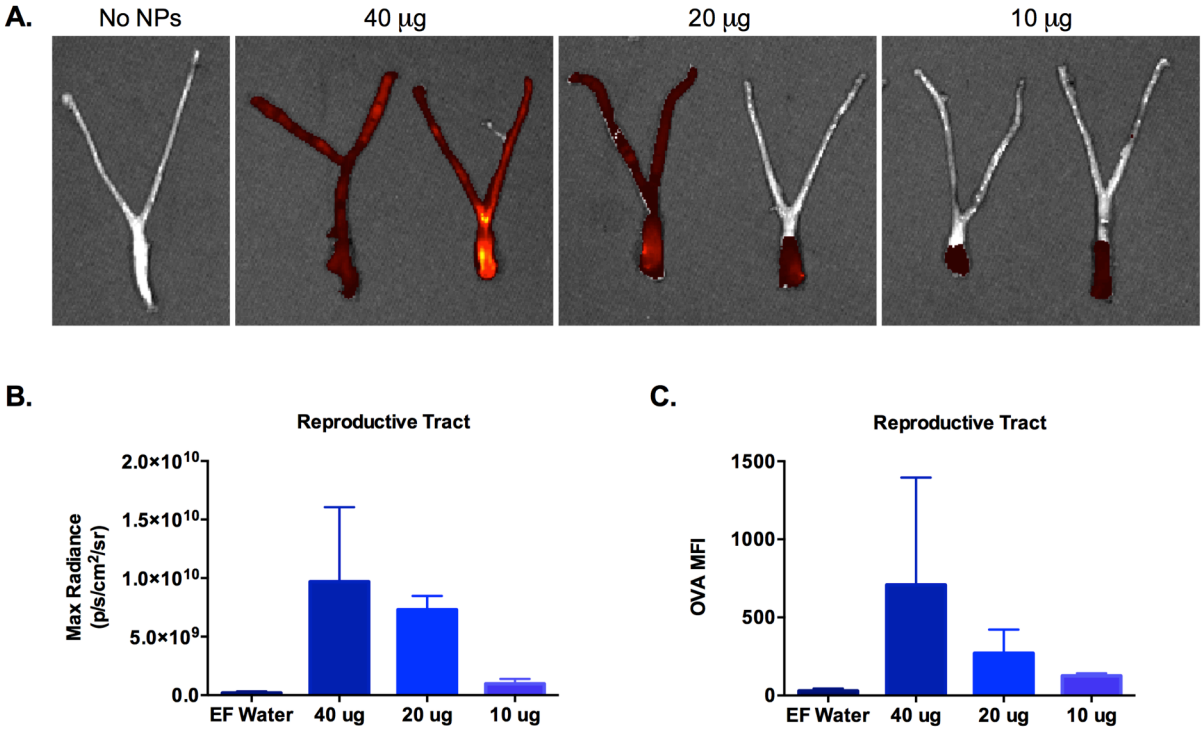

Figure 5 - 3 Fluorescence quantification of vaginal OVA dosing. Bulk fluorescence imaging of vaginal tracts was acquired using a Xenogen iVis Imaging system (A). Max fluorescence was quantified using the LivingImage software (B), and mean fluorescence intensity in single cell suspension was quantified by flow cytometry (C).

received endotoxin-free water and mean fluorescence intensity (MFI) was quantified (Figure 5-3C). We again observed a dose-dependent reduction in the MFI of single cell suspensions as the OVA dose was delivered.

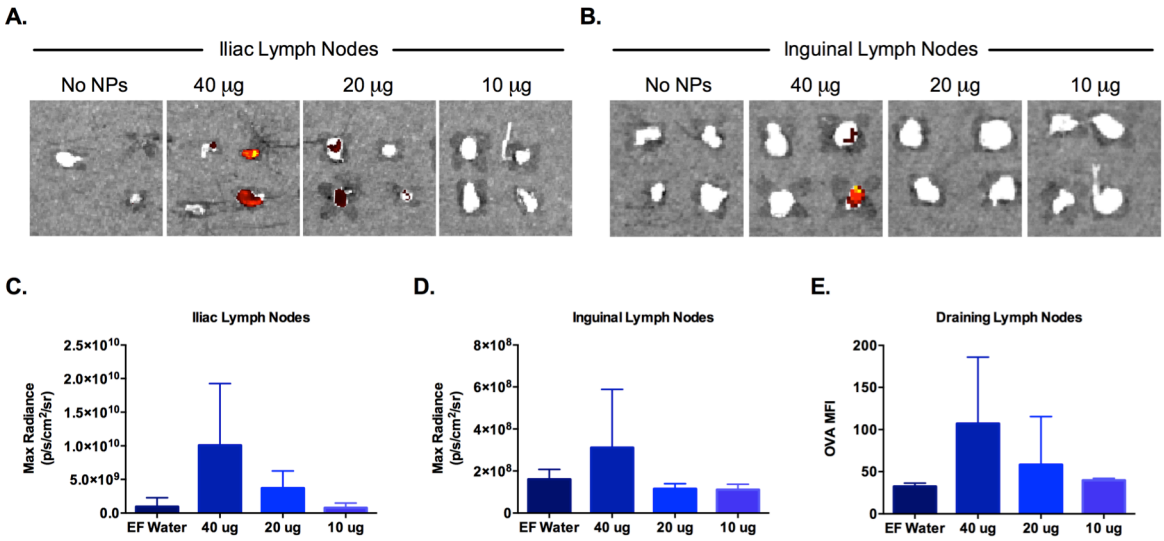

Figure 5 - 4 Fluorescence quantification of OVA trafficking to draining lymph nodes. Bulk fluorescence imaging of iliac and inguinal lymph nodes was acquired using a Xenogen iVis Imaging system (A,B). Max fluorescence was quantified using the LivingImage software (C,D), and mean fluorescence intensity in single cell suspension was quantified by flow cytometry (E).

Bulk fluorescence signal above background was clearly observed in images of iliac lymph nodes from mice vaginally dosed with 40 µg and 20 µg of OVA-Alexa647 (Figure 5-4A,C). Fluorescence signal above background was not clearly observed in mice administered the lowest OVA dose. Fluorescence signal in inguinal lymph nodes was only observed in mice administered the highest dose of soluble OVA (Figure 5-4B,D). All iliac and inguinal lymph nodes from a single mouse were pooled and single cell suspensions were isolated and quantified for OVA fluorescence by flow cytometry. OVA+ gates were again set in reference to control group mice, which did not receive soluble, fluorescent protein. Draining lymph node tissues showed clear fluorescence above background in the 40 µg and 20 µg vaginal administration treatment groups (Figure 5-4E). Given the fluorescence data on soluble OVA distribution within vaginal tissues and draining to lymph nodes, 24-hours post topical administration, we moved forward with vaginal delivery of 20 µg of soluble or particle formulated OVA in all future *in vivo* and *ex vivo* studies.

5.D.4. Ex vivo BMDC-OT1 study T Cell proliferation results

To evaluate the impact of IgG functionalization of OVA-loaded PLGA nanoparticles on BMDC uptake and stimulation of CD8+ T cells, we assessed *ex vivo* T cell proliferation in a co-culture system. Bone marrow-derived dendritic cells (BMDCs) from C57BL/6J mice were harvested and differentiated over eight days in cell culture. CD11c+ BMDCs were specifically isolated using the MACS cell separation technology and anti-mouse CD11c MicroBeads. CD11c+ BMDCs were treated with soluble OVA, PLGA-OVA, IgG-PLGA-OVA, all at 20 μg of OVA antigen. All treatment groups were formulated in endotoxin-free water. Negative controls included treatment of CD11c+ BMDCs with endotoxin-free water and IgG-PLGA, which served as the vehicle control. All treatments were incubated with CD11c+ BMDCs with and without LPS to assess the effect of an adjuvant on enhanced priming. After incubation of treatments with CD11c+ BMDCs for 24-hours, wells were washed by replacing well volume with 100 μL of media ten times. This allowed for us to remove the majority of the nanoparticle treatments, and wells were observed with each wash using a microscopy. Cells were harvested from OTI transgenic mice with T-cell receptors (TCRs) engineered to recognize ovalbumin residues 257-264 loaded on $H2K^b$. CD8+ T cells were isolated using a MACS isolation kit, stained with CFSE, and co-cultured with primed CD11c+ BMDCs for an additional 72 hours prior to flow cytometry analysis. We stained co-cultures with a LIVE/DEAD fixable dead cell stain, CD8α, and assessed T cell proliferation by dilution of the CFSE signal.

Gates were set by comparison of single-stained co-culture wells to unstained co-culture wells (Figure 5-5). Unstained cells are visualized in gray, and double peaks are the result of differences in autofluorescence of CD11c+ BMDCs and CD8α+ T cells in each channel. Overall, we observed a high degree of viability in all co-culture wells. Flow cytometry analysis was completed by excluding dead cells, selecting for CD8α+ T cells, and evaluating CFSE dilution. Example gates for all treatment groups, with and without LPS, are shown in Figure 5-6. In the FITC-CFSE channel, we have highlighted the T cell proliferation histogram from the endotoxin-free water group in gray, and displayed it for comparison to all treatment groups shown in green. We observed no T cell proliferation in the endotoxin-free water and vehicle control (PLGA-NP) negative control treatment groups. Roughly 11-20% of the co-culture population was CD8α+ in these negative control treatment wells. In contrast, over 50% of the co-culture population was CD8α+ in all treatment wells, which received OVA either in soluble or particle-formulated form. In all treatment wells, we see significant dilution of the CFSE channel. Soluble OVA and particle-formulated OVA treatment groups all show multiple generations of daughter cells. Interestingly, soluble OVA histograms display a smaller parent peak than particle-formulated OVA histograms. This result demonstrates that T cell proliferation in response to soluble OVA priming of CD11c+ BMDCs was more rapid and complete than in the case of particle-formulated OVA.

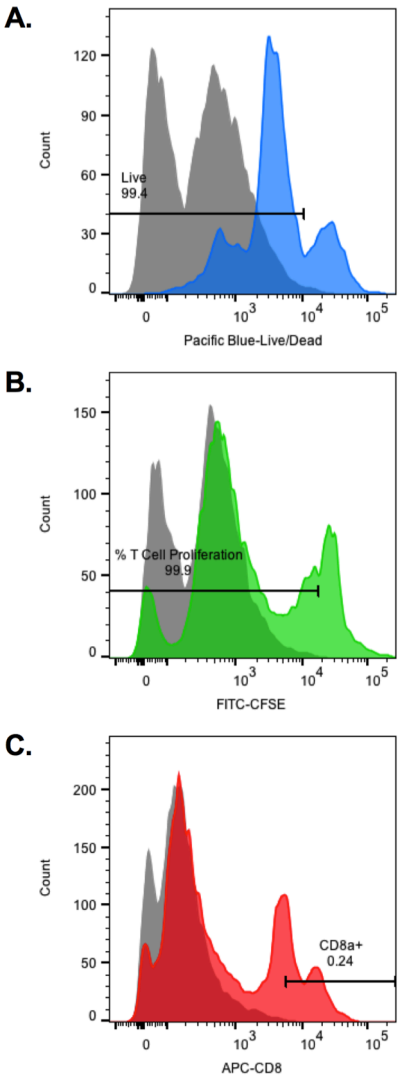

Figure 5 - 5 Single stains of BMDC-T cell co-cultures Co-cultures were stained with a Live/Dead stain (blue) (A), CFSE (green) (B), and CD8a (red) (C) and overlaid on unstained co-culture cells (gray).

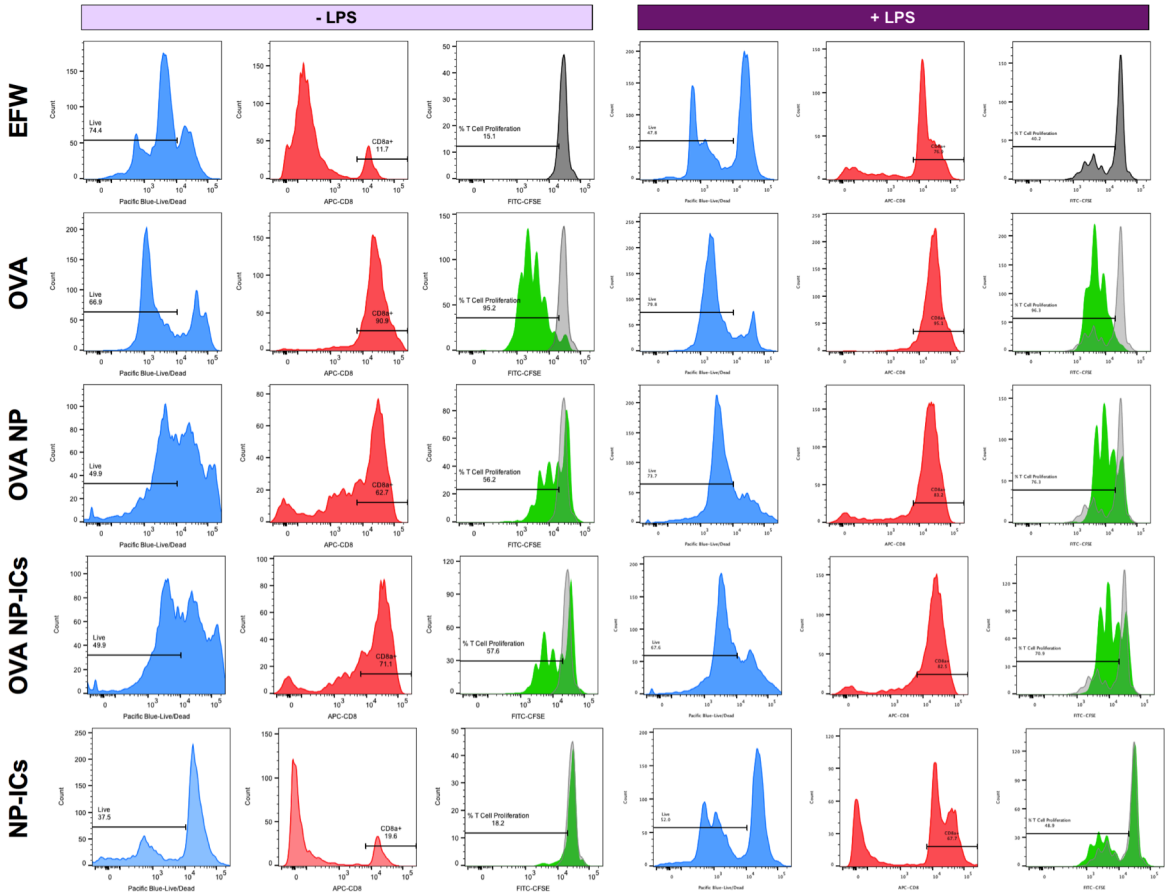

Figure 5 - 6 Gating strategies for selection of proliferating CD8a+ T cells. All treatment groups were gated by first excluding dead cells, gating for CD8a+ T cells and evaluating T cell proliferation by dilution of CFSE signal. All treatment groups are shown with and without *ex vivo* addition of LPS. Background signal of unproliferating cells from the endotoxin-free water (EFW) treatment group are shown in gray and are overlaid in all other CFSE histograms.

The addition of LPS increased the non-specific signals seen in the CFSE channel for both the negative treatment groups. Importantly, the signal from the vehicle control overlapped with the signal from endotoxin-free water treated co-culture wells indicating that non-specific proliferation was from the presence of the LPS adjuvant. The LPS adjuvant clearly enhanced T cell proliferation in all antigen-treated co-culture wells. Over 80% of the co-culture population was CD8α+ in all treatment wells receiving OVA, and T cell proliferation peaks were more similar between soluble OVA and particle-formulated OVA treatment groups. Quantification of T cell proliferation with and without LPS is shown in Figure 5-7. All treatment groups containing OVA showed a T cell proliferation signal that was statistically significant over negative control treatments, with and without LPS. Soluble OVA showed the highest degree of T cell proliferation of

~100% with and without LPS. PLGA-OVA and IgG-PLGA-OVA both showed similar levels of T cell proliferation near ~60% without LPS and ~70% with LPS.

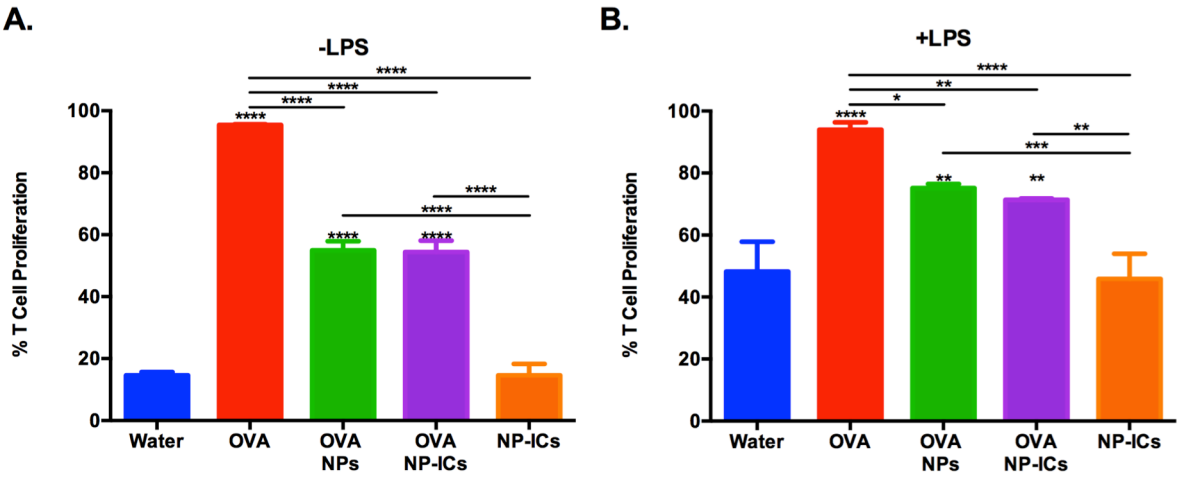

Figure 5 - 7 CD8a+ T cell proliferation to *ex vivo* cross-presentation of antigen by BMDCs. BMDCs were pulsed *ex vivo* with soluble OVA or OVA formulated in nanoparticles. NP-ICs (no OVA) and endotoxin free water were used as negative control groups. Quantification of T cell proliferation was determined using FlowJo and proliferation values are displayed in co-cultures without LPS (A) and supplemented with LPS (B). Statistical significance was determined using GraphPad Prism by a one-way ANOVA followed by Tukey's multiple comparisons test.

5.D.5. Ex vivo BMDC-OT1 study ELISA results

As a secondary metric of assessing the functional T cell response, we quantified Th1 and Th2 cytokines in co-culture supernatants with an ELISA. Regardless of the presence of LPS, we observed no signal or signals below the limit of quantification (L.O.Q.) in all co-culture supernatants for both Th2 cytokines, IL-10 and IL-4 (Figure 5-8E-H). We were able to successfully quantify to Th1 cytokines in co-culture supernatants – IFN-γ and IL-12. Negative control treatment groups were undetectable for IFN-γ and showed minimal secretion of IL-12. To our surprise, we found that particle-formulated OVA showed statistically significantly enhanced secretion of IFN-γ of up to six-fold (~550 pg/ml) as compared to soluble OVA (~90 pg/ml) (Figure 5-8A). Interestingly, the addition of LPS non-specifically increased the background secretion of IFN-γ to 100-250 pg/mL in negative control co-cultures, and equalized the secretion of IFN-γ in all OVA treated wells to ~550 pg/ml (Figure 5-8B). We observed a similar trend in IL-12 secretion. Particle-formulated OVA treatment groups showed statistically

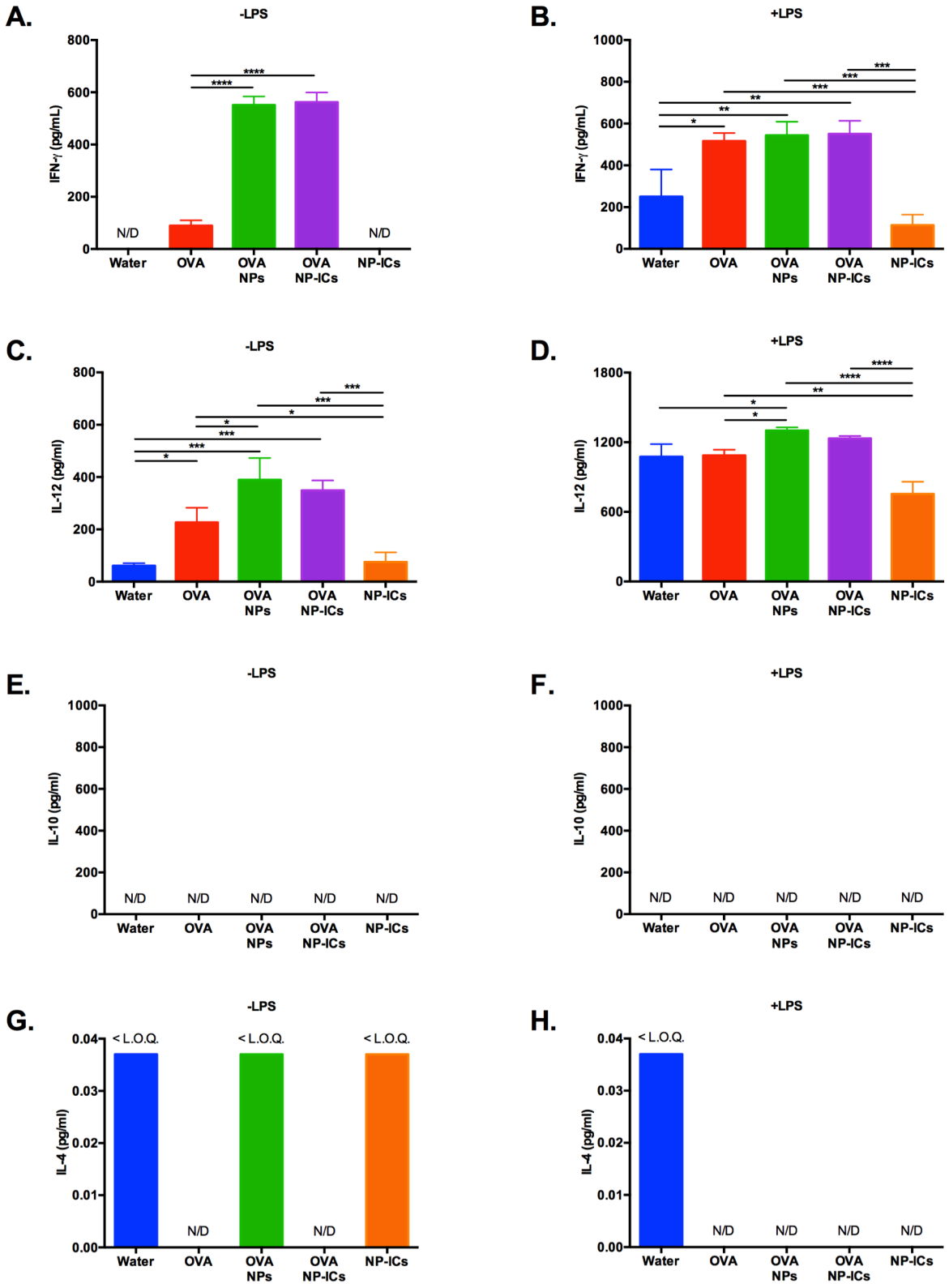

Figure 5 - 8 Th1 and Th2 cytokine quantification of BMDC-T cell co-cultures. IFN-γ (A, B), IL-12 (C, D), IL-10 (E, F), and IL-4 (G, H) were quantified by ELISA analysis, with and without additional *ex vivo* LPS stimulation. Statistical significance was determined using GraphPad Prism by a one-way ANOVA followed by Tukey's multiple comparisons test.

significantly enhanced secretion of IL-12 of ~1.7 fold (390 pg/ml) as compared to soluble OVA (230 pg/ml) (Figure 5-8C). Again the addition of LPS non-specifically increased IL-12 secretion (Figure 5-8D). However, unlike IFN-γ secretion, which only increased to the max observed cytokine concentration measured in samples without LPS, the addition of LPS magnified IL-12 secretion to very high levels. For example, without LPS, the max observed concentration in IL-12 secretion was ~390 pg/ml. With the addition of LPS, all treatment groups showed IL-12 concentrations of ~1000 pg/ml. No significant differences in cytokine secretion were observed between IgG functionalized and bare PLGA NPs encapsulating OVA.

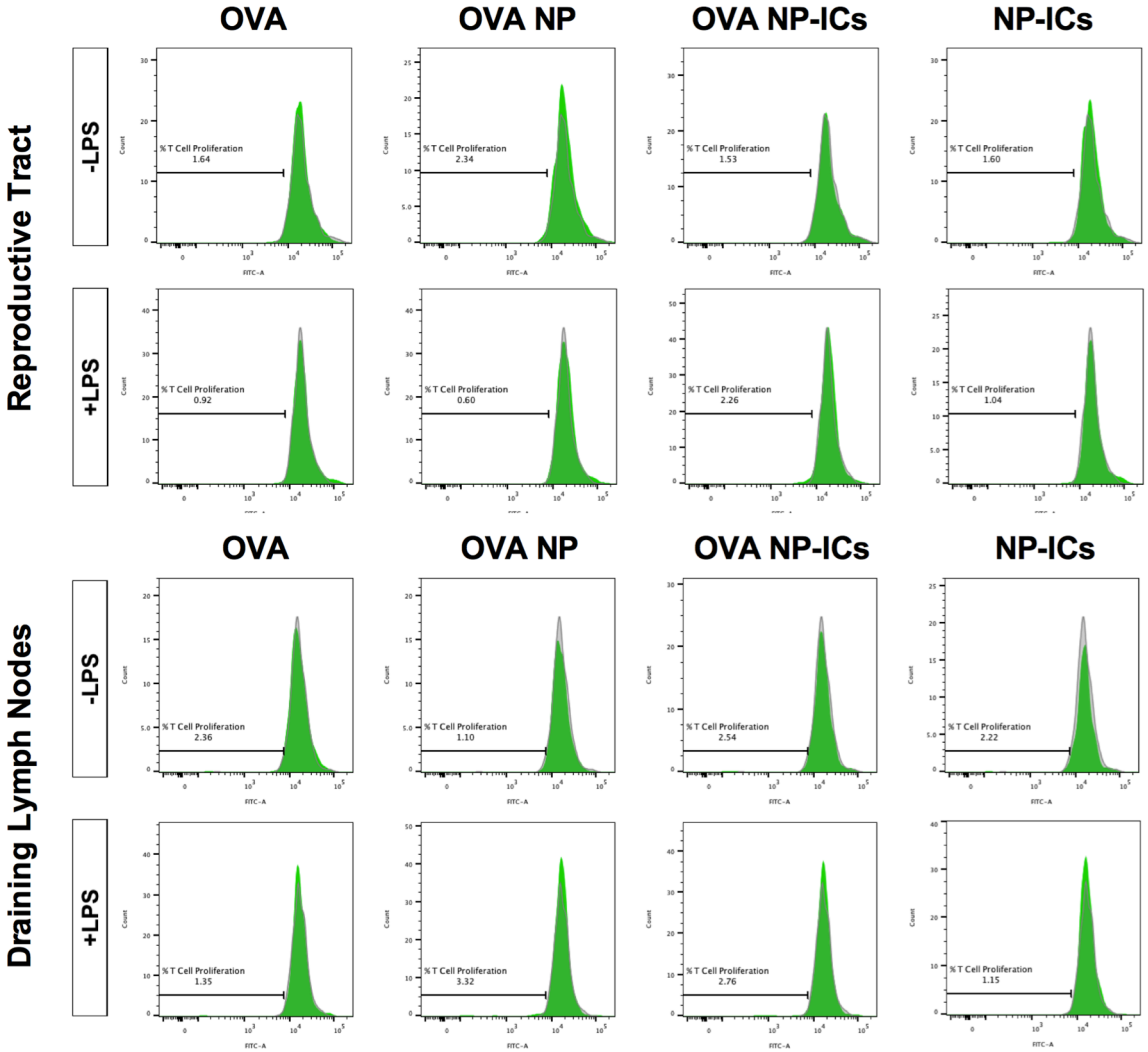

Figure 5 - 9 Cross presentation of antigen by host reproductive tract and draining lymph node cells to CD4+ T lymphocytes. CFSE histograms are shown for each treatment group (green) overlaid with the FITC channel from the water-treated negative control group (gray). Samples were acquired by flow cytometry and histograms were generated using the FlowJo software.

5.D.6. Results of in vivo validation using ex vivo T cell proliferation assays and ELISA

We aimed to evaluate the functional impact of IgG-modified, OVA-loaded PLGA NPs on *in vivo* DC priming and subsequent *ex vivo* T cell proliferation. These studies were designed to allow for topical, mucosal delivery of soluble and formulated antigen, *in vivo* trafficking through vaginal tissues and to draining lymph nodes, and *ex vivo* co-culture of DCs from host animals with CD4+ T cells from OTII transgenic mice. OVA was delivered at a 20 ug either as soluble protein or formulated within PLGA or IgG-PLGA

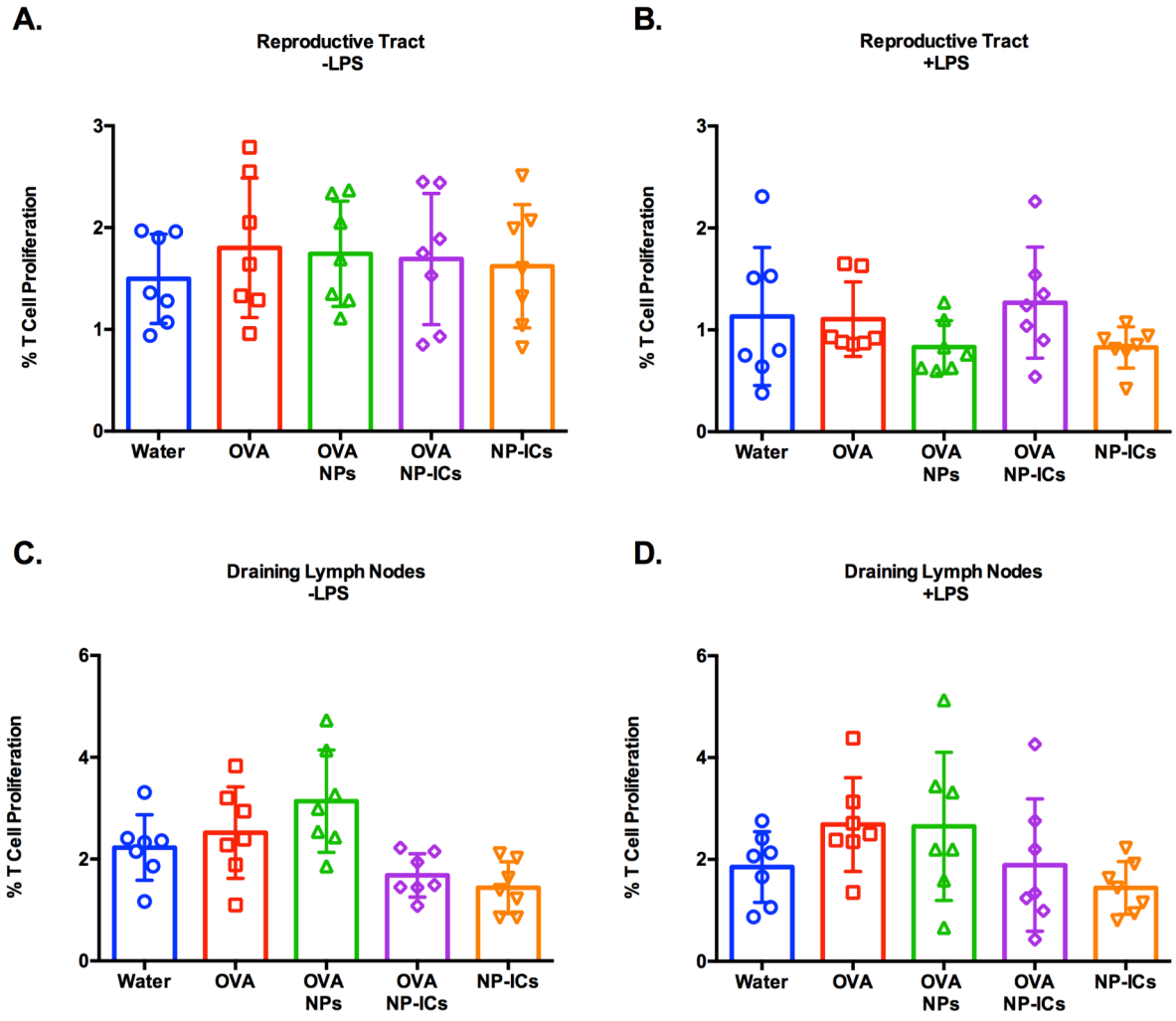

Figure 5 - 10 CD4+ T cell proliferation to *ex vivo* presentation of antigen by host cells post-*in vivo* vaginal immunization. Reproductive tract and draining lymph node cells were isolated 24-hours post-*in vivo* vaginal administration of antigen. Host cells were incubated with CD4+ T cells. Quantification of T cell proliferation was determined using FlowJo and proliferation values are displayed in co-cultures without LPS (A,C) and supplemented with LPS (B,D). Statistical significance was determined using GraphPad Prism by a one-way ANOVA followed by Tukey's multiple comparisons test.

nanoparticles. Reproductive organs and draining lymph nodes were dissected 24-hours post administration. All lymph nodes within one mouse were pooled and tissue-derived single cell suspensions were isolated using standard techniques. Single cell suspensions were also isolated from reproductive tract tissues. These single cell suspensions were co-cultured with CD4+ T cells isolated from OTII transgenic mouse spleens and purified using the MACS CD4+ T cell isolation kit. Co-cultures from all treatment groups were incubated with and without LPS for an additional 72-hours before flow cytometry analysis of T cell proliferation.

Dead cells were excluded from the analysis and co-cultures were gated to select for CD4+ T cells before assess T cell proliferation by dilution of the CFSE signal. Histograms of CFSE fluorescence from the negative control treatment group (endotoxin-free water) are shown in gray and overlaid with histograms from experimental treatment groups (Figure 5-9). Our data showed no clear peaks indicative of T cell proliferation in any of the experimental groups receiving OVA antigen. This observation was consistent whether T cells were co-cultured with draining lymph node-derived host cells or with reproductive tract-derived host cells. The addition of LPS also did not induce T cell proliferation in any of the co-cultures. Quantification of % T cell proliferation showed no

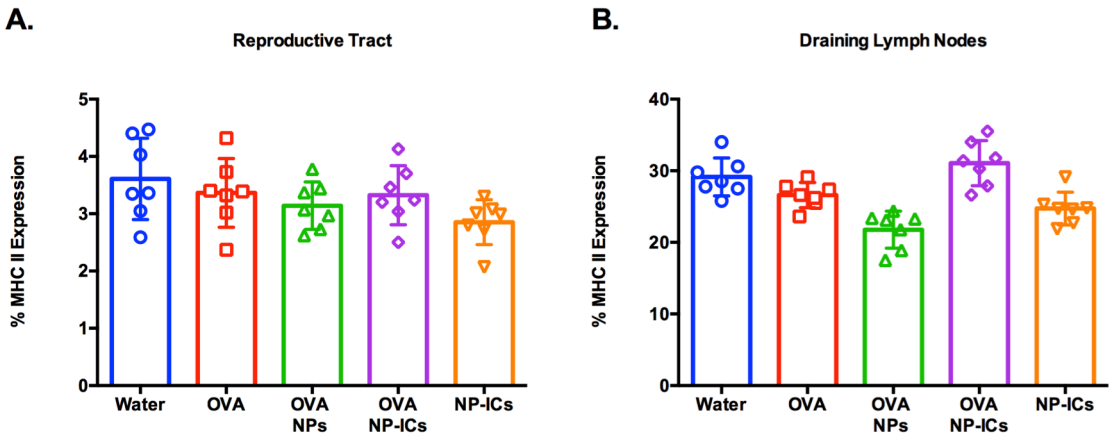

Figure 5 - 11 MHC II cell surface expression MHC II surface expression on reproductive tract cells (A) and draining lymph node cells (B) was determined by staining co-cultures and acquiring cells by flow cytometry. Surface expression was set based on unstained controls. Statistical significance was determined using GraphPad Prism by a one-way ANOVA followed by Tukey's multiple comparisons test.

statistically significant differences between any of the treatment groups, regardless of whether reproductive tract cells or draining lymph node cells were incubated with CD4+ T cells and the presence of LPS (Figure 5-10). Overall we saw no significant differences between treatment groups in MHCII on reproductive tract and draining lymph node cells (Figure 5-11). As such, T cell proliferation data was not normalized to host cell surface antigen presentation marker expression. Co-culture supernatants were measured for Th1 cytokines (IFN-γ and IL-12) and Th2 cytokines (IL-4). No Th1 or Th2 cytokines were detected above the limit of quantification in any of the co-culture wells (data not shown).

5.D.7. Results of ex vivo validation of T cell proliferation assays using tissue-harvested DCs

Based on our previous results evaluating scale-up of *in vivo* delivery of unformulated and formulated OVA, we sought to understand the inherent capacity of host cells to present antigen and promote T cell proliferation *ex vivo*. T cells were co-cultured with reproductive tract-derived cells and draining lymph node-derived cells, which were pulsed *ex vivo* with 20 ug of soluble OVA antigen for 24-hours. Co-cultures were incubated for 72-hours with and without LPS, and T cell proliferation was quantified by flow cytometry as described above. In reproductive tract-T cell co-cultures, flow cytometry histograms did not show clear dilution of CFSE signals (data not shown). Furthermore, quantification of T cell proliferation showed that reproductive tract-T cell

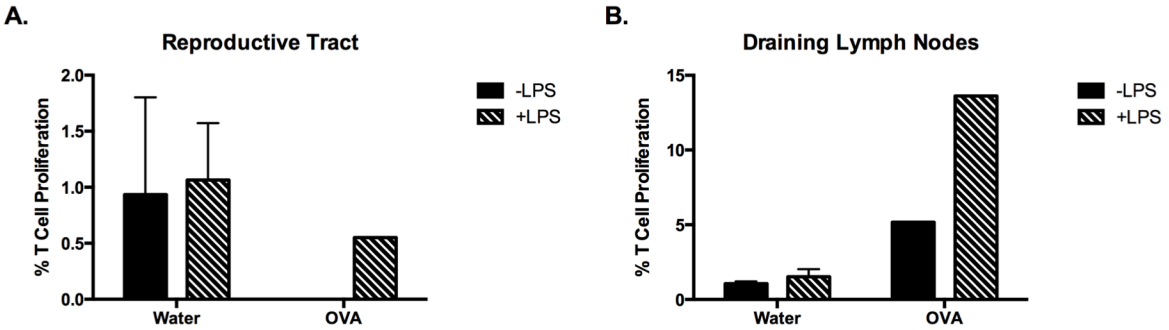

Figure 5 - 12 CD4+ T cell proliferation to *ex vivo* presentation of antigen by host cells post-*ex vivo* OVA pulsing. Reproductive tract cells (A) and draining lymph node cells (B) were isolated from host tissues and pulsed ex vivo with OVA. T cell proliferation was quantified by FlowJo with and without additional LPS stimulation.

co-cultures did not stimulate significant T cell proliferation, with or without LPS, over the negative control treatment group (endotoxin-free water). Draining lymph node histograms showed minimal dilution of the CFSE signal, and quantification showed that draining-lymph node-T cell co-cultures were able to result in minimal levels of proliferation near ~5% without LPS and ~15% with LPS (Figure 5-12).

We sought to understand if draining lymph node cell presentation of OVA to CD4+ T cells could be enhanced if CD11c+ DCs were specifically purified from host tissues and if *in vivo* materials were allowed to traffic for a longer time period of 72-hours. To this end, we conducted a parallel comparison of co-cultures in which all cells and CD11c+ DCs from host draining lymph node tissues were incubated with T cells. We further compared *in vivo* delivery of soluble protein with *ex vivo* delivery of soluble protein. Our results show that *in vivo* delivery of OVA, and subsequent isolation of draining lymph node cells did not promote T cell proliferation regardless of whether all cells or CD11c+ DCs from the host were co-cultured with CD4+ T cells (Figure 5-13A). While *ex vivo* OVA delivery showed

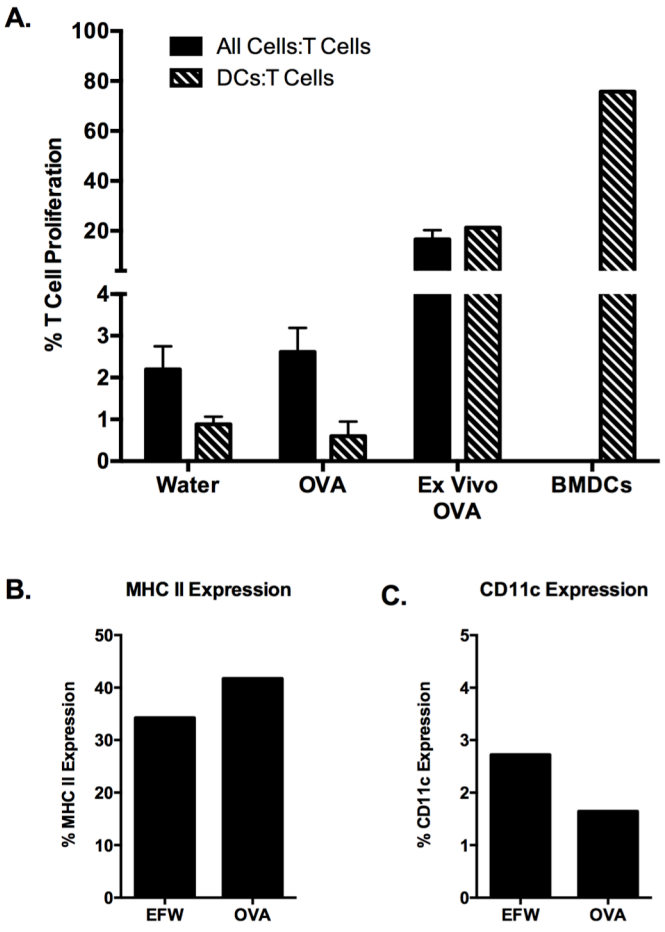

Figure 5 - 13 CD4+ T cell proliferation to *ex vivo* presentation of antigen by host cells versus host DCs post-*in vivo and ex vivo* OVA delivery. All cells and CD11c+ DCs were isolated from reproductive tracts and draining lymph nodes and pulsed ex vivo with OVA (A). T cell proliferation was quantified by FlowJo with and without additional LPS stimulation. No clear differences were observed in MHC II expression (B) In all cells and in CD11c+ purified DCs (C).

induction of ~20% T cell proliferation, no clear difference was observed between all cells and CD11c+ DCs in their capacity to stimulate T cell proliferation in co-cultures. No differences were observed in MHC II expression on all cells or CD11c expression on CD11c+ DCs isolated from animals, regardless of the *in vivo* administration (Figure 5-13B,C). Notably, *ex vivo* delivery of OVA results in variable stimulation of 5-20% T cell proliferation in co-cultures with draining lymph node cells and CD4+ T cells. In contrast, BMDCs more efficiently present *ex vivo* delivered soluble OVA, stimulation up to 80% CD4+ T cell proliferation (Figure 5-14).

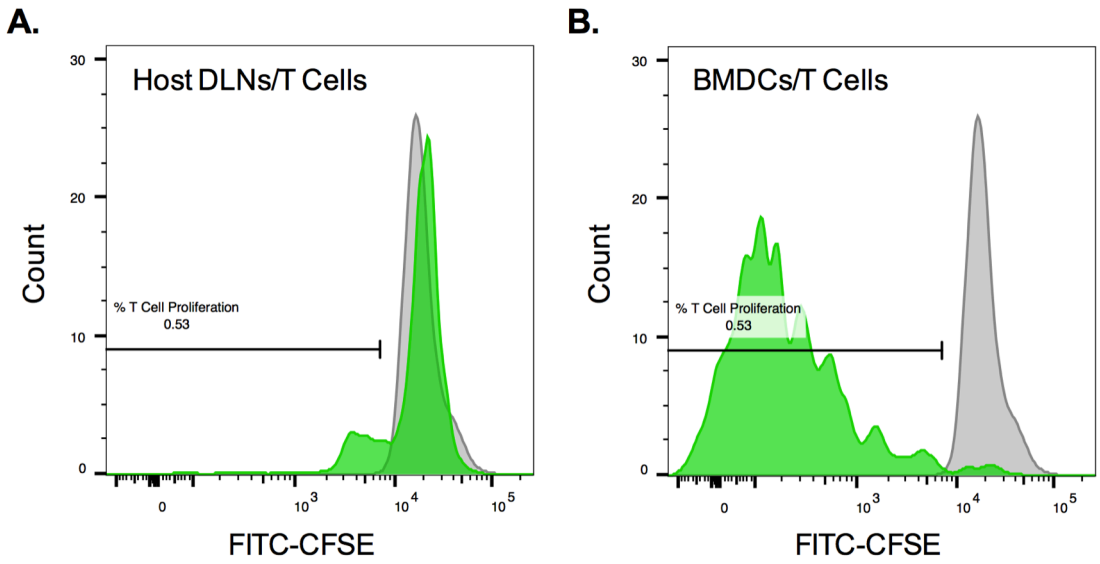

Figure 5 - 14 Histograms of CD4+ T cell proliferation to *ex vivo* presentation of antigen by host cells versus BMDCs post-*ex vivo* OVA delivery. Host cells (A) and BMDCs (B) were pulsed *ex vivo* with soluble OVA and co-cultures were assayed for CD4+ T cell proliferation. Gates were set by comparison to the negative control water treatment group (gray).

5.E. DISCUSSION

As an extension to our proof-of-concept model of transepithelial transport and uptake by mucosal DCs, we sought to establish the functional consequence of forming nanoparticle immune complexes (NP ICs) that encapsulate a protein antigen. Overall, we have developed a general strategy for the reproducible formulation of ovalbumin (OVA) within PLGA NPs, and subsequent adsorption of IgG to particle surfaces (OVA NP ICs). Although we previously have shown that IgG adsorption efficiency was much greater than conjugation efficiency in terms of surface coverage as measured by flow

cytometry (Figure 4-1), we chose to evaluate the differences between IgG conjugation and adsorption to PLGA NP surfaces. IgG loading on PLGA NP surfaces was slightly more efficient by adsorption as compared to conjugation. The most compelling results that encouraged moving forward IgG surface adsorption came from the results of our binding study. These results demonstrated that binding of FITC-Protein A was nearly two-fold higher to adsorbed IgG-PLGA surfaces as compared to conjugated IgG-PLGA surfaces. Other groups have also shown that adsorption of mAbs to PLGA nanoparticles better preserved binding affinity in cell culture studies as compared to conjugation[8]. Given these results, we chose to move forward adsorption of IgG to OVA PLGA NPs (OVA NP ICs).

Several studies have shown successful encapsulation of OVA protein within PLGA nanoparticles. Depending on the exact methodology during particle synthesis, studies have reported the generation of OVA NPs ranging between 300 nm, and 2 μm in diameter with OVA encapsulation efficiencies of 20-75%[5,7,18]. Our results demonstrate that by using a double emulsion synthesis, we generated highly reproducible, monodisperse NPs and OVA NPs near ~250 nm in size. We found that NPs had a surface charge ~-40 mV, and OVA NPs exhibited a slight increase in surface charge ~30 mV. Importantly, we showed that mass recovery of NPs and OVA NPs was high nearing ~40% and that OVA encapsulation efficiency was nearly 100%. Importantly, we were able to load ~98 μg OVA/mg NP, representing ~10% drug loading capacity. Importantly, in agreement with works of others, we observed that release of OVA from NPs was negligible at 4C and neared ~3% of encapsulated protein by 72 hours at 37C°[7]. As such, we felt confident about our ability to store OVA NPs overnight in the fridge, prior to *in vitro* or *in vivo* studies without confounding the data by delivering unencapsulated OVA.

Vaginal dosing of soluble OVA has not been thoroughly explored in terms of 1) draining to lymph nodes or 2) T cell functional readouts of antigen presentation. Overall, our *in vivo* studies were designed to understand these questions. Vaginal dosing of OVA described in the literature has ranged from 40 μg to 400 μg depending on the formulation and inclusion or exclusion of adjuvants[10-12]. We performed a dosing study of

soluble fluorescent OVA to the vaginal mucosa, and dissected the reproductive organs and iliac and inguinal draining lymph nodes for imaging. Our vaginal dosing studies with fluorescent OVA showed a dose dependent reduction in maximum bulk fluorescence measured in the reproductive organs. Interestingly, Xenogen images showed some brighter spots in the uterine horns of mice dosed at 40 μg fluorescent OVA. The highest dose showed a ~24-fold increase in bulk fluorescence over the water treatment group by Xenogen image quantification and ~50-fold increase in fluorescence associated with tissue-derived cells quantified by flow cytometry. Importantly, dosing with 20 μg of fluorescent OVA was significantly detectable over background and showed a reduction in fluorescence by roughly half. Even the lowest dose of fluorescent OVA showed 4 to 5 fold increase in fluorescence over the negative control treatment group. Draining patterns to the iliac and inguinal lymph nodes revealed that fluorescent OVA more readily drained to the iliac lymph nodes as compared to inguinal lymph nodes. While only the 40 μg dose of OVA showed fluorescence over the negative control treatment group in inguinal lymph nodes, the 40 μg and 20 ug doses showed a ~9-fold and ~4-fold increase in bulk fluorescence in the iliac lymph nodes. Importantly, flow cytometry data showed that isolated single cell suspensions from all draining lymph nodes showed mean fluorescence intensity higher than the negative control treatment group even in the lowest dose. Taken together, we chose to move forward vaginal dosing at 40 μg of OVA, as we were confident that this dose resulted in distribution within the reproductive organs and overall draining to lymph nodes.

One of the major goals of our study was to assess functional T cell responses either in cell co-culture studies of murine bone marrow-derived DCs and naive syngeneic OT-I CD8+ T cells isolated from transgenic mouse spleens. TCRs in these mice are specifically restricted to recognize, bind, and proliferate in response to OVA 257-264 presented on $H2K^{b19}$. Importantly, these co-culture assays measure the efficiency of cross-presentation of OVA peptides to T cells.. In all of our studies, we evaluated the delivery of OVA at a 20 μg dose in either soluble form or formulated within NPs or NP ICs. The final OVA concentration in all wells was 100 μg/ml. Finally, in order to assess if any differences seen between groups could be mitigated by the addition of

an adjuvant in cell culture, we also examined the effect of incorporating 10 pg/ml of LPS in co-cultures. Overall, our data showed that soluble OVA treated BMDCs maximally stimulated proliferation of primary CD8+ T cells over particle formulated OVA. Interestingly, we did not see a difference between NP and NP IC treatments of BMDCs in cross-presentation of OVA to T cells. Moreover, the addition of LPS boosted T cell proliferation responses of particle formulated OVA both in the case of NPs and NP ICs. LPS is a known adjuvant that has been used to enhance antigen immunogenicity in co-culture assays[20]. T cell responses to soluble OVA were in line with previously published results of similar co-culture systems, where ~89% T cell proliferation was observed at a lower OVA dose of 10 μg/ml[21]. However, our results were surprising to us in the context of published literature on particle formulated versus soluble antigen. A similar study evaluating PLGA microparticle encapsulation of OVA showed that particle formulation resulted in similar levels of CD8+ T cell proliferation, even at a 1000-fold lower protein concentration[22]. Importantly, it is notable that these assays were conducted with human DC-like cells co-cultured with B3Z T cells. It is likely that the use of primary cells in our co-cultures increases the sensitivity of our system to proliferation in response to OVA presentation. Moreover, our release studies show that at 72-hours, NPs release ~3% of OVA. As such, the bioavailability of soluble OVA versus released OVA from particle formulations, regardless of a fixed initial dose, is significantly different and may contribute to the reduced proliferation in particle formulations that we observed in comparison to soluble OVA. Moving forward, we will seek to establish T cell proliferation in response to a dose range of soluble or NP/NP-IC-formulated OVA.

While our T cell proliferation data did not show advantages of particle-formulated OVA in comparison to soluble OVA, cytokine measurements of co-culture supernatants surprisingly showed that both NPs and NP ICs enhanced secretion of IFN-γ and IL-12. Both IFN-γ and IL-12 are known Th1 cytokines. IFN- γ is commonly measured as a secondary metric to analyze T cell proliferation, and it has been shown that IL-12 can augment IFN-γ production[23,24]. Interestingly, our data show that particle formulation of OVA within NPs and NP ICs increased IFN-γ secretion by 6-fold and IL-12 secretion by 1.7-fold. A recent study demonstrating that OVA formulation in microparticles improved

cross-presentation to CD8 T cells show that IL-2 (a Th1 cytokine) secretion in co-cultures was highest and most prolonged in microparticle-OVA treatment groups[22]. They further show that encapsulation of OVA in microparticles resulted in higher concentrations of cytosolic OVA, an important step in accessing the MHC class I pathway. As such, they conclude that enhanced cytokine production and enhanced cross-presentation is enabled by improving cytosolic access in particle formulations of OVA, which may also have contributed to the enhancement of IFN- γ and Il-12 secretion seen in our nanoparticle treatment groups. The addition of LPS to co-cultures increased IFN-γ secretion seen in the soluble OVA treatment group to the level of secretion seen in particle-formulated OVA treatment groups, but did not further increase particle-formulated OVA treatment groups. This suggests that LPS acted on DCs to improve cross-presentation of soluble protein, but did not further maximize cross-presentation beyond what was already achieved by formulating OVA in nanoparticles. Interestingly, we found that LPS treatments resulted in an increase in IL-12 secretion in all treatment groups. As LPS treatment of BMDCs is known to stimulate IL-12 secretion, which is modular based on the timing of treatment, stage of BMDC development, and other cytokines in co-cultures[25], we hypothesize that the vast increase in IL-12 secretion from LPS treatment is predominantly due to activation of BMDCs. Taken together, our proliferation results and ELISA data demonstrate that nanoparticle formulation of OVA does enhance cross-presentation to CD8+ T cells, as evidenced by the heightened secretion of IFN-γ and IL-12. While we do not see differences in NP ICs as compared to NPs, we hypothesize that evaluating a full dose range of OVA delivery would better elucidate any advantage of NP IC-mediated delivery of OVA. Furthermore, evaluating a wider dose range of OVA may help capture differences in T cell proliferation in our primary cell co-culture assay.

Studies evaluating the functional consequence of vaginal immunization with OVA protein are limited. A recent study looking at 20-40 nm NP mediated delivery of OVA showed that OVA formulation within particles induced secretion of local IgG1 and systemic IgG and IgG2c antibody titers[12]. Another study comparing subcutaneous, oral, intestinal, and intravaginal administration routes, showed that OVA formulated in

ethylene-vinyl acetate copolymer (EVAc) polymer disks and placed in the vaginal lumen led to the second highest (subcutaneous injection was most efficient) OVA-specific IgG production in serum as well as notably heightened serum IgA levels, 6-weeks post administration[10]. Moreover, the authors show heightened vaginal IgG and IgA titers in response to vaginal administration of OVA. One study evaluated the differences in CD4+ T cell priming between nasal and vaginal administration using an adoptive transfer model of transgenic CD4+ T cells into host mice[11]. The results demonstrated that vaginal immunization with OVA and CpG resulted in a 5 and 7-fold expansion of adoptively transferred CD4+ T cells in draining lymph nodes at 57 and 72 hours. Moreover, they found that expanded T cells expressed surface markers that allowed for homing to more distal lymphoid tissues. These results are extremely promising, and we hoped to recapitulate these results in an *ex vivo* analysis of CD4+ T cell proliferation after isolating APCs from host vaginal tissues and draining lymph nodes following *in vivo* delivery of OVA NPs and OVA NP ICs. All groups received 20 μg of OVA protein, and soluble OVA was used as a positive control in our assays. To our surprise, we found that co-cultures of host cells derived from reproductive tracts and draining lymph nodes did not exhibit presentation of OVA to CD4+ T cells in any of the treatment groups. Consistent with the lack of T cell proliferation, our ELISA results supported that vaginal OVA treatment did not promote secretion of Th1 or Th2 cytokines. Notably, even the positive control soluble OVA treatment did not elicit any responses and additional LPS addition in co-cultures did not stimulate proliferation or secretion of cytokines. These results suggest that cells derived from the reproductive organs and draining lymph nodes have reduced capacity to efficiently present antigen, at the dose we delivered. Probing the inherent antigen presentation capacity of reproductive tract and draining lymph node cells was established by isolation of these cells and *ex vivo* treatment with OVA. *Ex vivo* OVA pulsing of reproductive tract- and draining lymph-node derived cells with soluble OVA at 100 μg/ml only marginally promoted proliferation of T cells in co-cultures. However reproductive tract cells remained inactive and unable to promote T cell proliferation. Finally, our results demonstrated that isolating CD11c+ DCs versus using all cells derived from the draining lymph nodes did not enhance CD4+ T

cell proliferation. Taken together these data suggest that the native host cells in the reproductive tract and iliac and inguinal draining lymph nodes are not sufficiently activated to prime T cells after vaginal administration of OVA protein. We hypothesize that this may be due to three possibilities: 1) the delivered dose of OVA *in vivo* and *ex vivo* was not sufficient to promote antigen presentation, 2) *in vivo* antigen presentation in the reproductive tract requires co-delivery of an adjuvant to drive inflammatory cell expansion and antigen presentation, or 3) unique aspects of the reproductive tract or iliac and inguinal lymph node environments promote the development of tolerogenic responses. Our fluorescence dosing study of OVA confirmed that soluble OVA reaches draining lymph nodes within 24 hours. Despite the presence of soluble OVA, *in vivo* results showed no priming of CD4+ T cells. In contrast, *ex vivo* pulsing with soluble OVA showed that these cells did have the capacity to minimally present antigen and that the response could be magnified by the addition of LPS to co-cultures. This leads us to believe that *in vivo* responses could be magnified by co-delivery of an adjuvant. Previous studies that have evaluated humoral and cellular responses after vaginal administration have delivered 25 µg OVA/20 µg CpG and 100-150 µg OVA boosted subcutaneously with 300 µg OVA in CFA[11,12]. This suggests to us that exploring a wider range of vaginal OVA doses may better inform the thresholds of observable antigen presentation that can be evaluated using *in vivo* delivery and *ex vivo* antigen presentation assay models. Our system has been recapitulated elsewhere to demonstrate T cell proliferation *ex vivo* to *in vivo* nasal mucosal delivery of OVA antigen formulated in lipid nanoparticles[26]. Finally, it is interesting to consider whether there are environmental factors unique to the reproductive tract or draining lymph node cells that inherently do not promote inflammatory responses to antigens. Pettini et al. showed T cell proliferation in draining lymph nodes after vaginal administration of OVA and CpG[11]. An interesting future study would be to compare *ex vivo* pulsing of OVA to cells isolated from various lymph nodes that drain different tissues to evaluate if some lymph node organs contain DCs that are more poised to present antigen and prime T cells without co-delivery of adjuvants.

We believe there is significant value in further developing these systems for easily testing vaginal delivery of protein antigens. While adoptive transfer studies remain an alternative option, these studies are more complicated. In contrast, the combination of *in vivo* delivery and *ex vivo* antigen presentation assays allows us to compare treatments in an experimentally more controlled manner with less variables. To further develop our understanding of these systems, future work must focus on establishing a wide dose range with *ex vivo* pulsing of reproductive tract and draining lymph node cells and testing various adjuvant combinations. Defining these variables will establish a framework that will allow for future rigorous comparisons of vaginal immunizations with protein antigen.

5.F. CONCLUSION

Overall, our studies were scoped to provide a generalizable strategy for antigen-loaded, IgG-modified PLGA NPs to generate OVA NP ICs. Importantly we sought to understand the benefits of adsorption versus conjugation and protein release from NPs. We described a vaginal dosing study and showed biodistribution of soluble OVA to draining lymph nodes. Finally, our results showed that while we were unable to observe a benefit of forming NP IC, nanoparticles overall showed enhanced cross presentation of antigen to CD8+ cytolytic T cells as evidenced by heightened secretion of Th1 cytokines. Importantly, our *in vivo* and *ex vivo* co-culture data demonstrate that cells derived from the reproductive tissues and draining lymph nodes have reduced capacity to present antigen as opposed to BMDCs. Our studies lay the groundwork for nanoparticle-based delivery of OVA, and future work will focus further optimization of systems to evaluate vaginal immunization with protein antigens.

5.G. ACKNOWLEDGEMENTS

This work is funded by an NIH Director's New Investigator Award to K.A.W. (1DP2HD075703) and with the support of a UW STD/AIDS Training Fellowship to R.R. (NIHT32AI07140).

5.H. REFERENCES

1. Lu, L. *et al.* A neonatal Fc receptor-targeted mucosal vaccine strategy effectively induces HIV-1 antigen-specific immunity to genital infection. *Journal of virology* **85,** 10542–10553 (2011).
2. Ye, L., Zeng, R., Bai, Y., Roopenian, D. C. & Zhu, X. Efficient mucosal vaccination mediated by the neonatal Fc receptor. *Nature biotechnology* **29,** 158–163 (2011).
3. Karagouni, E. *et al.* Uptake of BSA-FITC Loaded PLGA Nanoparticles by Bone Marrow-Derived Dendritic Cells Induces Maturation But Not IL-12 or IL-10 Production. *Nanoscience and Nanotechnology Letters* **5,** 498–504 (2013).
4. Demento, S. L. *et al.* Role of sustained antigen release from nanoparticle vaccines in shaping the T cell memory phenotype. *Biomaterials* **33,** 4957–4964 (2012).
5. Sarti, F. *et al.* In vivo evidence of oral vaccination with PLGA nanoparticles containing the immunostimulant monophosphoryl lipid A. *Biomaterials* **32,** 4052–4057 (2011).
6. Mukherjee, B., Santra, K., Pattnaik, G. & Ghosh, S. Preparation, characterization and in-vitro evaluation of sustained release protein-loaded nanoparticles based on biodegradable polymers. *International journal of nanomedicine* **3,** 487 (2008).
7. Lee, Y.-R., Lee, Y.-H., Im, S.-A., Kim, K. & Lee, C.-K. Formulation and characterization of antigen-loaded PLGA nanoparticles for efficient cross-priming of the antigen. *Immune network* **11,** 163–168 (2011).
8. Kocbek, P., Obermajer, N., Cegnar, M., Kos, J. & Kristl, J. Targeting cancer cells using PLGA nanoparticles surface modified with monoclonal antibody. *Journal of controlled release* **120,** 18–26 (2007).
9. Kamaly, N., Xiao, Z., Valencia, P. M., Radovic-Moreno, A. F. & Farokhzad, O. C. Targeted polymeric therapeutic nanoparticles: design, development and clinical translation. *Chemical Society Reviews* **41,** 2971–3010 (2012).
10. Kuo-Haller, P., Cu, Y., Blum, J., Appleton, J. A. & Saltzman, W. M. Vaccine delivery by polymeric vehicles in the mouse reproductive tract induces sustained local and systemic immunity. *Molecular pharmaceutics* **7,** 1585–1595 (2010).
11. Pettini, E. *et al.* Vaginal immunization to elicit primary T-cell activation and dissemination. (2013).
12. Howe, S. E. & Konjufca, V. H. Protein-coated nanoparticles are internalized by the epithelial cells of the female reproductive tract and induce systemic and mucosal immune responses. *PloS one* **9,** e114601 (2014).
13. Pridgen, E. M. *et al.* Transepithelial transport of Fc-targeted nanoparticles by the neonatal fc receptor for oral delivery. *Science translational medicine* **5,** 213ra167–213ra167 (2013).
14. Heo, M. B. & Lim, Y. T. Programmed nanoparticles for combined immunomodulation, antigen presentation and tracking of immunotherapeutic cells. *Biomaterials* **35,** 590–600 (2014).
15. Chaowanachan, T., Krogstad, E., Ball, C. & Woodrow, K. A. Drug synergy of tenofovir and nanoparticle-based antiretrovirals for HIV prophylaxis. (2013).
16. Inaba, K. *et al.* Generation of large numbers of dendritic cells from mouse bone

marrow cultures supplemented with granulocyte/macrophage colony-stimulating factor. *The Journal of experimental medicine* **176,** 1693–1702 (1992).
17. Park, J. & Bryers, J. D. Chemokine programming dendritic cell antigen response: part II–programming antigen presentation to T lymphocytes by partially maintaining immature dendritic cell phenotype. *Immunology* **139,** 88–99 (2013).
18. Ma, T., Wang, L., Yang, T., Ma, G. & Wang, S. Homogeneous PLGA-lipid nanoparticle as a promising oral vaccine delivery system for ovalbumin. *asian journal of pharmaceutical sciences* **9,** 129–136 (2014).
19. Hogquist, K. A. *et al.* T cell receptor antagonist peptides induce positive selection. *Cell* **76,** 17–27 (1994).
20. Robson, N. C., Beacock Sharp, H., Donachie, A. M. & Mowat, A. M. Dendritic cell maturation enhances CD8+ T-cell responses to exogenous antigen via a proteasome-independent mechanism of major histocompatibility complex class I loading. *Immunology* **109,** 374–383 (2003).
21. Datta, S. K. *et al.* A subset of Toll-like receptor ligands induces cross-presentation by bone marrow-derived dendritic cells. *The Journal of Immunology* **170,** 4102–4110 (2003).
22. Shen, H. *et al.* Enhanced and prolonged cross-presentation following endosomal escape of exogenous antigens encapsulated in biodegradable nanoparticles. *Immunology* **117,** 78–88 (2006).
23. Dobashi, K. *et al.* Regulation of LPS induced IL-12 production by IFN-γ and IL-4 through intracellular glutathione status in human alveolar macrophages. *Clinical & Experimental Immunology* **124,** 290–296 (2001).
24. Henry, C. J., Ornelles, D. A., Mitchell, L. M., Brzoza-Lewis, K. L. & Hiltbold, E. M. IL-12 produced by dendritic cells augments CD8+ T cell activation through the production of the chemokines CCL1 and CCL17. *The Journal of Immunology* **181,** 8576–8584 (2008).
25. Jiang, H.-R. *et al.* Secretion of interleukin-10 or interleukin-12 by LPS-activated dendritic cells is critically dependent on time of stimulus relative to initiation of purified DC culture. *Journal of leukocyte biology* **72,** 978–985 (2002).
26. Li, A. V. *et al.* Generation of effector memory T cell–based mucosal and systemic immunity with pulmonary nanoparticle vaccination. *Science translational medicine* **5,** 204ra130–204ra130 (2013).

Chapter 6: Conclusions

6.A. SUMMARY AND FUTURE DIRECTIONS

The field of vaginal drug and vaccine delivery has made significant strides over the past decade. Key contributions have advanced our fundamental understanding of the anatomy and biology of the reproductive organs that has allowed us to articulate the major challenges that preclude the development of vaginal, mucosal prophylactic or therapeutic vaccines to curb the spread of sexually transmitted infections. From a bioengineering perspective, a major goal is to develop systems that allow us to explore the structure-function relationship of engineered nanomaterials for applications in immunology. In this dissertation, we aspired to focus our efforts on investigating immunomodulatory strategies and functional and targeted nanoparticle systems that allowed us to shape innate immune responses in the genital mucosa.

A hallmark barrier to eliciting rapid innate immune responses to vaginal vaccines is the fine balance the reproductive organs must maintain between tolerance and immunity. In our first specific aim, we investigated mucosal delivery of agents that recruit or expand dendritic cells. We showed that low doses of GM-CSF expanded CD11b+ dendritic cells in the vaginal tract within 24 hours of administration, without affecting systemic cell populations. CD11b+ vaginal dendritic cells are thought to play a key role in trafficking antigen to draining lymph nodes where they prime CD4+ T cells. Our studies show the ability to magnify this key immune cell population, and further results showed that the expanded CD11b+ dendritic cell population readily phagocytosed nanoparticles. Moreover, our results show no increase in inflammatory cytokine secretion. These results highlight the possibility of further exploring the use of GM-CSF as a non-inflammatory mucosal adjuvant in conjunction with vaginal vaccines.

While the main focus of developing nanoparticle systems for vaginal delivery has been to improve mucus penetration, less has been investigated regarding targeting to the vaginal submucosa. In our second aim, we explored surface functionalization of nanoparticles with human serum IgG to form nanoparticle immune complexes (NP-ICs). We hypothesized that NP-ICs could leverage existing receptor pathways that engage

the Fc region of IgG to promote transepithelial transport and uptake by mucosal antigen presenting cells. We show as proof-of-concept, that fluorescent NP-ICs are efficiently transported across the vaginal epithelium – resulting in increased draining to the iliac and inguinal lymph nodes as well as increased uptake by vaginal antigen presenting cells. Fluorescence imaging suggests that a key factor in transepithelial transport may be crosslinking of Fc receptors at vaginal epithelial surfaces. Overall, our studies show that the generation of antibody-nanoparticle complexes is a strategy to appropriate receptor pathways to promote delivery across the vaginal epithelium.

Antigen delivery to the genital tract is challenging due to the presence of degradative enzymes, systemic vascularization, and limited access to mucosal antigen presenting cells. Nanoparticles have been widely investigated reduce off target effects, route vaccines towards target cells, and provide sustained release of cargo. In our third aim, we sought to validate the use of NP-ICs for delivery of a model immunogen, ovalbumin (OVA). We show that OVA could be efficiently loaded into polymer nanoparticles, surface functionalized with human serum IgG to form OVA-NP-ICs. *Ex vivo* analysis of cross presentation to CD8+ cytolytic T cells showed that BMDCs pulsed with nanoparticle treatments enhanced the secretion of Th1 cytokines – IFN-γ and IL-12. Importantly, our results illustrated the significant challenges that still remain in developing robust *ex vivo* assays to quantify cellular response to *in vivo* vaginal delivery of OVA. We demonstrate that nanoparticle platforms clearly promote Th1 responses to encapsulated antigen; however, further optimization is needed to fully characterize a dose range in which NP-IC platforms may drive enhanced cellular immune responses.

This dissertation has focused on evaluating strategies for enhancing vaginal vaccine delivery. However, a significant portion of our research has also focused on developing hybrid hydrogel core, lipid shell nanoparticles for the delivery of small molecule HIV-1 antiretrovirals (ARVs) as a mucosal microbicide. This project is described in Appendix I, and is geared towards physical and biological characterization of ARV-loaded nanocarriers. In summary, this dissertation is geared towards investigating the ability to expand functional, phagocytic mucosal dendritic cells and the utility of functionalized nanoparticles in routing protein antigens across the vaginal

epithelium to antigen presenting cells and draining lymph nodes. We hope that our work motivates the need for further development and exploration of nanoparticle systems for vaginal drug and vaccine delivery.

6.B. LIST OF PUBLICATIONS

1. **Ramanathan, R.**, & Woodrow, K. (2015). Engineering immunity in the mucosal niche against sexually transmitted infections. *Wiley Interdisciplinary Reviews: Nanomedicine and Nanobiotechnology*,*8(1)*, 107-122
    - Chapter 2

2. **Ramanathan, R.**, Park, J., Hughes, S. M., Lykins, W. R., Bennett, H. R., Hladik, F., & Woodrow, K. A. (2015). Effect of Mucosal Cytokine Administration on Selective Expansion of Vaginal Dendritic Cells to Support Nanoparticle Transport. *American Journal of Reproductive Immunology*,*74*(4), 333-344.
    - Chapter 3

3. **Ramanathan, R.**, Park, J., Read, B., Frizzell, H., Krogstad, E.A., Woodrow, K.A. "Antibody nanoparticle immune complexes for vaginal OVA delivery and cross presentation to CD8+ T cells" *(In preparation)*
    - Chapter 4 and 5

4. **R. Ramanathan**, Y. Jiang, B. Read, S. Golan-Paz, K.A. Woodrow "Biophysical characterization of small molecule-antiviral loaded nanolipogels from HIV-1 chemoprophylaxis and topical mucosal application" *(Submitted)*
    - Appendix I

5. J. Park, **R. Ramanathan**, L. Pham, K.A. Woodrow "Nanoparticle delivery to intravaginal mucosal tissue and target lymphoid organs using chitosan as a mucosal adjuvant" *(In preparation)*

6.C. LIST OF PRESENTATIONS

1. **R. Ramanathan**, J. Park, B.J. Read, K.A. Woodrow "Immunoengineering nanoparticles for mucosal drug and vaccine treatment of sexually transmitted infections" CFAR STD and AIDS Research Symposium 2015, Seattle, WA (Invited oral presentation)

2. E. Krogstad, **R. Ramanathan**, C. Nhan, K. Thoreson, K.A. Woodrow "Nanoparticle-releasing Nanofiber Composites for Enhanced *In Vivo* Vaginal Retention" Biomedical Engineering Society, Seattle, WA

3. J. Park, **R. Ramanathan**, L. Pham, K.A. Woodrow "Nanoparticle delivery to intravaginal mucosal tissue and target lymphoid organs using chitosan as a mucosal adjuvant" Controlled Release Society 2014

4. **R. Ramanathan**, J. Park, K.A. Woodrow “Modulating innate immune responses in the genital mucosa to facilitate transport and biodistribution of nanoparticle vaccines” NIH High Risk-High Reward Research Symposium 2013 (Poster, presented by K.A. Woodrow)

5. **R. Ramanathan**, J. Park, W. Lykins, H. Bennett, K. Woodrow “Chemokine and growth factor-mediated expansion of vaginal antigen presenting cells.” Biomedical Engineering Society, Seattle, WA (Invited oral presentation)

6. **R. Ramanathan**, K. Woodrow “Biomaterials for HIV-1 Chemoprophylaxis” Controlled Release Society 2013 (Poster)

7. **R. Ramanathan**, R. Mahadevan, M. Iadanza, T. Chaowanachan, K. Woodrow "Biophysical characterization of hydrogel-core, lipid-shell nanolipogels for HIV chemoprophylaxis." International Microbicides Conference, Sydney, Australia, April 2012. (Poster, presented by K.A. Woodrow)

Appendix I. Biophysical characterization of small molecule-antiviral loaded nanolipogels for HIV-1 chemoprophylaxis and topical mucosal application

AI.A. Abstract

Nanocarriers are versatile vehicles for drug delivery, and emerging as platforms to formulate and deliver multiple classes of antiretroviral (ARV) drugs in a single system. Here we describe the fabrication of hydrogel-core and lipid-shell nanoparticles (nanolipogels) for the controlled loading and topical, vaginal delivery of maraviroc (MVC) and tenofovir disoproxil fumarate (TDF), two ARV drugs with different mechanisms of action that are used in the treatment of HIV. The nanolipogel platform was used to successfully formulate MVC and TDF, which produced ARV drug-loaded nanolipogels that were characterized for their physical properties and antiviral activity against HIV-1 BaL in cell culture. We also show that administration of these drug carriers topically to the vaginal mucosa in a murine model leads to antiviral activity against HIV-1 BaL in cervicovaginal lavages. Our results suggest that nanolipogel carriers are promising for the encapsulation and delivery of hydrophilic small molecule ARV drugs, and may expand the nanocarrier systems being investigated for HIV prevention or treatment.

AI.B. Introduction

Nanoparticles have been widely investigated as carrier systems to deliver small molecule drugs and biologics to improve cell or tissue targeting, reduce side effects, control release, and promote intracellular uptake of agents that have sites of action within cells[1,2]. Hydrophobic small molecule encapsulation within nanocarriers has been employed with notable success in numerous clinical applications, most commonly for cancer therapy[2]. Recently, similar nanocarriers that encapsulate and deliver antiretroviral (ARV) drugs have been investigated for application in HIV prevention and therapy[3-7]. Strategies used for topical prevention of sexually transmitted infections have demonstrated that local delivery of ARV drugs to the vaginal mucosa may sustain higher drug concentrations in the genital tract and reduce systemic exposure[8]. Local delivery may also limit off-target effects that result from systemic delivery. However, there are

few vaginal dosage forms that have been tested for co-delivery of water-soluble small molecule ARV drugs. Previous groups have shown that formulating drugs within nanoparticles is one strategy being explored for drug delivery to the vaginal mucosa, as a strategy to prolong drug retention in the reproductive organs and reduce systemic delivery of ARV drugs[9]. To date, only a few nanocarriers have been investigated as microbicides, and these have been limited to the delivery of single ARV drugs in most cases. Expanding the number of nanocarriers that are amenable to vaginal mucosal delivery may expand the number of single and combination agents that can be used for topical HIV prevention

Generally, the most widely investigated nanoparticle systems that have been evaluated for ARV drug delivery include liposomes and polymer nanoparticles. A key advantage to liposomes is the ability to formulate hydrophobic and hydrophilic drugs within the lipid shell and aqueous core[10]. Liposomes have been used to formulate hydrophilic and hydrophobic ARV agents such as indinavir and AZT within the aqueous core or lipid bilayer at ~3-30% drug encapsulation efficiency[4,11,12]. As an alternative to liposomes, polymeric nanocarriers have also been investigated for formulating ARV drugs. Formulation of hydrophobic ARV drugs such as efavirenz, saquinavir, and dapivirine in polymer-based nanocarriers have shown promising results with high encapsulation efficiencies nearing 100%[5,9]. In contrast, studies evaluating hydrophilic ARV drug delivery (AZT and tenofovir) in poly(lactic-co-glycolic acid) (PLGA), poly(isobutylcyanoacrylate), and chitosan nanoparticles showed that these systems exhibited encapsulation efficiencies 5 - 10%[13-15]. These studies highlight the capacity of different nanomaterials to formulate a range of physicochemically diverse ARV drugs, and motivate the need for further characterization of nanoparticle systems for ARV drug formulation and delivery.

Nanolipogels are an emerging platform being investigated as an alternative to the more widely used liposomes or polymer nanoparticles. These dual structure nanoparticles have a distinct lipid bilayer encompassing a polymer core and have been synthesized by UV-induced gelation of a hydrogel network within liposomes using various processes[16,17]. In general, the approaches promote gelation within a liposome

reactor to generate nanogel particulates, which were subsequently isolated[16-18]. Nanolipogels have been utilized previously for the encapsulation of several types of agents, including dyes, small hydrophilic cancer drugs, and small and large proteins in various biomedical applications[19-24]. Nanolipogels have been used to incorporate physicochemically diverse agents within the lipid bilayer and the aqueous core, including a small hydrophobic TGF-β inhibitor and IL-2 protein, for a tumor immunotherapy application[19]. In addition, active loading can be used to drive drugs that are weak bases into the acidic hydrogel core of nanolipogels, where they become entrapped and are less likely to partition across a neutrally charged lipid membrane[24]. This has been shown to result high encapsulation efficiency and provide controlled release of the encapsulated drug. These reasons make nanolipogels an interesting platform to investigate for physical and biological formulation attributes that facilitate ARV drug delivery as topical microbicides for HIV chemoprophylaxis.

Here, we investigate the use of nanolipogels for formulation and mucosal delivery of the hydrophilic ARV drugs maraviroc (MVC) and tenofovir disoproxil fumarate (TDF) using nanolipogels. MVC and TDF are two HIV antivirals with distinct mechanisms of action against HIV viral replication. MVC is a small molecule agonist, which specifically inhibits CCR5-dependent viral entry of HIV-1[25]. In contrast, TDF is a nucleoside reverse transcriptase inhibitor and a prodrug of tenofovir. Once internalized, TDF is converted to tenofovir diphosphate, which is the active form of the drug capable of inhibiting reverse transcription[26]. MVC and tenofovir are hydrophilic drugs that have been tested in a range of clinical trials as topical microbicides[8,27-30]. Both drugs have been formulated into semi-solid dosage forms for vaginal drug delivery (e.g., rings and gels) for the purposes of HIV pre-exposure prophylaxis. However, recent research has shown that encapsulation of ARV drugs, such as dapivirine in nanocarriers, improves local retention of drug in the reproductive organs resulting in decreased systemic biodistribution of drug[9]. To this end, we evaluated the utility of nanolipogels for encapsulation and delivery of MVC and TDF.

We observed that nanolipogels exhibited high levels of ARV drug encapsulation and this study demonstrates the biological utility of these vehicles for use in HIV

chemoprophylaxis. Specifically, we highlight the potential of ARV drug-loaded nanolipogels to inhibit cell-free and cell-cell HIV-1 infection of epithelial cells. Finally, we demonstrate the *in vivo* application of MVC- and TDF-nanolipogels as a topical vaginal microbicide. The implications of our results support nanolipogels as a system for delivery of hydrophilic ARV drugs for HIV-1 prevention and treatment and worthy of further investigation in future studies.

AI.C. Materials and methods

AI.C.1. Materials

Egg phosphaditylcholine (EPC) was obtained from Avanti Polar Lipids (Alabaster, AL, USA). Acrylamide (AAm), N,N'-methylenebis(acrylamide) (MBA), 2,2-diethoxyacetophenone (DEAP), and cholesterol were obtained through Sigma Aldrich (St. Louis, MO, USA). MVC was synthesized, purified, and donated by the Suydam Lab at Seattle University. TDF was obtained through the NIH AIDS Research and Reference Reagent Program (http://www.aidsreagent.org/). Water used in buffer solution was purified using a Milli-Q purification system (Millipore Corporation, Billerica, MA, USA). TZM-bL cells, PM-1 cells, and HIV-1 BaL isolate were also obtained through the NIH AIDS Research and Reference Reagent Program. Medroxyprogesterone acetate was purchased through the University of Washington pharmacy (Greenstone LLC, Peapack, NJ, USA).

AI.C.2. Synthesis and preparation of nanolipogels

Nanolipogels were synthesized by modifying previously established methods for photopolymerization of a hydrogel core within a lipid vesicle reactor[16,17]. EPC and cholesterol were dissolved in chloroform at 20 mg/ml and 10 mg/ml. EPC and cholesterol at a mass ratio of 3:1 were transferred to a round-bottom flask, which was attached to a rotary evaporator (Buchi, Flawil, Switzerland) rotating at 120 rpm over a 35°C water bath until all solvent was removed. AAm, MBA, and DEAP were dissolved in 50 mM Tris-HCL buffer and used to rehydrate the lipid film to 5 mg lipids/film, forming multilamellar vesicles (MLVs). ARV drugs were dissolved in DI water and were incorporated into the rehydration buffer at 10% (w/w) of the total material mass. MVC and TDF were loaded separately. MLVs were extruded with a hand-held needle extruder

(Avanti Polar Lipids, Alabaster, AL) involving 21 passes with syringes through a 200 nm polycarbonate membrane. This produced unilamellar vesicles (ULVs) ~200 nm in diameter. Ascorbic acid was added to a final concentration of 150 mg/ml, at a 200 fold excess of the photoinitiator, to prevent external polymerization during subsequent UV exposure[31]. Particles were vortexed well and exposed to UV light 1-inch below a Blak-Ray ® B-100AP/R High Intensity UV lamp (100 Watts, 365 nm, UVP, Upland, CA) for 15 min on ice. The resulting nanolipogels were purified from unencapsulated materials using a PD-10 column (GE Healthcare, Little Chalfont, UK).

AI.C.3. Nanolipogel size distribution, bilayer dissolution, and mass recovery

Hydrodynamic size and polydispersity (PDI) of nanolipogels was determined by dilution in 10 mM NaCl and quantification by dynamic light scattering (DLS) with a Malvern Zetasizer (Malvern Instruments, Malvern, UK). Dissolution of lipid bilayers and characterization of the nanogel core was performed by incubation of nanolipogels in 1% Triton X-100 for 10 min at room temperature. The efficiency of nanolipogel mass recovery was quantified by freezing and overnight lyophilization of an aliquot of the PD-10 purified samples, and measuring the lyophilized mass using an analytical balance.

AI.C.4. Cryogenic transmission electron microscopy of nanolipogels

Cryogenic transmission electron microscopy (cryo-TEM) samples were prepared by the vitrification-plunging method. Briefly, a 10-µl drop of the sample was applied on a Lacey Carbon grid (TED Pella, Inc., Redding, CA). The drop was blotted and immediately plunged into liquid ethane. Cryo-TEM samples were stored in liquid nitrogen until imaging. Samples were transferred to the microscope using the Gatan 626 cryo-holder (Gatan, Inc., Pleasanton, CA) and cryo-transfer station. During microscope imaging, the samples were kept at a temperature below -178°C. Cryo-TEM samples were imaged by the Tecnai G2 F20 transmission electron microscope (FEI Co., Hillsboro, OR) at 200kV with a field emission gun, in a low-dose mode to minimize electron-beam radiation damage. A 4K CCD camera (4k Eagle Camera, FEI) was used to record the images.

AI.C.5. Quantification of drug encapsulation and release kinetics

Drug quantification of MVC and TDF was performed using a Prominence LC20AD UV-HPLC (Shimadzu) on a C18 column (Phenomenex, Torrance, CA) and chromatograms

were analyzed using the LCSolutions software. Samples for HPLC were prepared by incubation of ARV drug-loaded nanolipogels with 25% isopropyl alcohol (IPA) (v/v) to rupture the lipid bilayer. Methods for MVC detection were adapted as described[32], and consisted of a 15-min isocratic flow method at 1.0 ml min^{-1} in 26%/74% acetonitrile (ACN)/50 mM KH_2PO_4 adjusted to pH 3.2 with formic acid. The injection volume was 20-µl and the oven temperature was maintained at 44°C. MVC was detected at 193 nm at a retention time of 8-9 min. MVC was quantified using standards made in Milli-Q water. TDF was detected using a 15-min isocratic flow method at 1.0 ml min^{-1} in 28%/72% H_2O with 0.045% trifluoracetic acid/CAN with 0.036% TFA. The injection volume was 10-µl and the oven temperature was maintained at 30°C. TDF was detected at 259 nm at a retention time ~12-min. Drug loading was calculated using drug concentrations, as measured by HPLC and particle material recovery, as measured using the analytical balance. Drug and encapsulation efficiency were calculated using the following equations were used to calculate drug loading and encapsulation efficiency:

$$Drug\ Loading = 100\ x\ \frac{Mass\ of\ drug\ (mg)}{Mass\ of\ particles\ (mg)}$$

$$Encapsulation\ efficiency = \ 100\ x\ \frac{Drug\ loading}{Theoretical\ drug\ loading}$$

Drug release from nanolipogels was determined by placing suspensions in membrane-capped dialysis tubes with a 1-kDA molecular weight cutoff (GE USA). The tube was inverted into 5 ml of DI water (MVC) or 10 mM NaCl, pH 4 (TDF) in a 50 ml Falcon tube, which was placed on an orbital shaker rotating at 120 rpm at 37°C. At various timepoints over 24 hours, release buffer was collected and analyzed for drug content by HPLC.

AI.C.6. Cell viability

TZM-bL cells were cultured in 96 well plates in the absence or presence of various concentrations of blank and drug-loaded nanolipogels ranging from 0.0625 – 2 mg/ml. After three days in culture, cell viability was assessed using a CellTiter-Blue® Cell Viability Assay (Promega, Fitchburg, WI) following the manufacturer's recommended protocol. Cells were incubated for 4h with 20µl/well of CellTiter-Blue®Reagent and

fluorescence was recorded at 560/590nm using a TECAN plate reader (Männedorf, Switzerland).

AI.C.7 Evaluation of ARV drug-loaded nanolipogels against cell-free HIV-1 infection

The antiviral activity of MVC, TDF, and ARV drug-loaded nanolipogels were assessed based on a reduction in luciferase reporter gene expression after infection of TZM-bL cells with HIV-1 BaL. Briefly, TZM-bL cells were seeded at a concentration of $1x10^4$ per well in 96-well microplates. The next day, TZM-bL cells were incubated with various concentrations of free ARV drugs or ARV drug-loaded nanolipogels, alone and in combination, at 37^0C for 1h prior to virus exposure. Cell-free HIV-1 BaL (200 $TCID_{50}$) was added to the cultures and incubated for an additional 48-hours. Untreated cells were used as control representing 100% infection. The Promega™ Luciferase Assay System (Promega, Fitchburg, WI) was used to determine luciferase expression. Antiviral activity was expressed as an IC_{50} value, which is the sample concentration giving 50% of relative luminescence units (RLUs) compared to the virus control after subtraction of background RLUs. Quantification of IC_{50} values was performed using GraphPad Prism.

AI.C.8. Evaluation of ARV drug-loaded nanolipogels against cell-cell HIV-1 transmission

For cell-cell transmission assays, TZM-bL cells were seeded at a concentration of $1x10^4$ per well in 96-well microplates. The next day, TZM-bL cells were incubated with various concentrations of free ARV drugs or ARV drug-loaded nanolipogels, alone and in combination, at 37^0C for 1h to exposure to chronically infected PM-1 cells. Chronically infected PM-1 cells were generated by culturing cells for three days in the presence of HIV-1 BaL. PM-1 cells were washed twice with PBS to remove cell-free HIV-1 BaL before they were added to the TZM-bL cell culture at $5x10^3$ cells/well. After a 1-hour incubation, PM-1 cells were removed by washing wells twice with PBS. TZM-bL cells were then incubated in the presence of the same ARV drug treatment for an additional 48-hours. Cells were lysed and the luciferase activity of the cell lysate was measured using the luciferase assay system (Promega, Fitchburg, WI). Antiviral activity was expressed as an IC_{50} value as described above.

AI.C.9 In vivo administration and determination of antiviral activity in cervicovaginal lavages (CVLs)

Female C57BL/6J mice (8-12 weeks) were purchased from Jackson Laboratories (Bar Harbor, Maine). Four days prior to topical administration of drug-loaded nanolipogels, mice were subcutaneously injected with 100-µl of medroxyprogesterone acetate (Depo-Provera®) formulated at 20 mg/ml in Dulbecco's Phosphate-Buffered Saline (DPBS). Progesterone treatment of female mice to induce diestrus reduces variability resulting from biological and physiological differences at various stages of the estrus cycle. Mice were anesthetized in an induction chamber and taped around the abdomen with Fisherbrand tape (Fisher Scientific, Pittsburgh, PA) to prevent self-grooming after vaginal administration. Vaginal tracts were flushed out three times with 80-µl of endotoxin-free water and two Calginate swabs were used to remove the mucus. MVC-nanolipogels in combination with TDF-nanolipogels were premixed and delivered at 5 µg/drug in a total volume of 25-µl. Unformulated MVC and TDF were delivered in combination at the same drug concentrations. 25 µl of sterile PBS was administered to mice as a control group. Post-administration, mice were inverted for 10-min in the induction chamber to enhance vaginal retention of administered materials. Mice were caged individually to prevent grooming between animals. 24-hours after vaginal administration, mice were euthanized by cervical dislocation. CVLs were collected post-mortem with 4-50 µl lavages in PBS or cDMEM. HPLC was performed on PBS lavages to detect MVC and TDF using methods described in *Section 2.5*. cDMEM lavages were combined and used in TZM-bL antiviral assays against cell-free HIV-1 BaL, as described previously. All animal studies and protocols were approved and monitored by the University of Washington Institutional Animal Care and Use Committee.

AI.D. Results

AI.D.1 Synthetic strategy and physical characterization of nanolipogels

We report here significant improvements to existing methods for fabricating nanolipogels with controlled size and low polydispersity. We demonstrate that our optimized approach reproducibly fabricates nanolipogels loaded with MVC or TDF. Hydrogel constituents and ARV drugs were combined within liposome, followed by UV

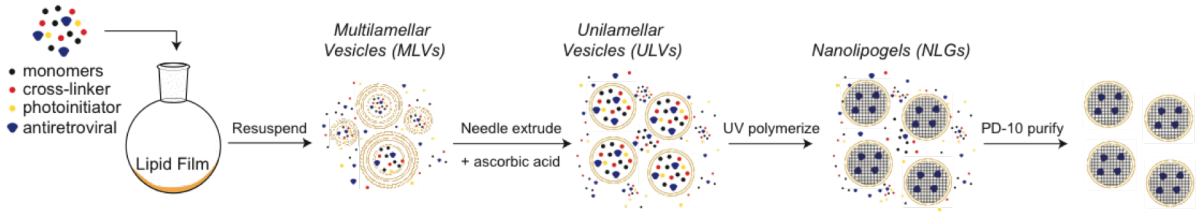

Figure AI - 1 Synthetic strategy Nanlipogels are formed by resuspension of a lipid film with polymer constituents, photoinitiator, and drug. The resulting multilamellar vesicles (MLVs) are needle extruded to form unilamellar vesicles (ULVs), Ascorbic acid is added to prevent external polymerization, and ULVs are placed 1-inch under a UV-light source for 15 min to form nanolipogels (NLGs). NLGs are purified through a PD-10 column to remove unencapsulated materials.

exposure to induce crosslinking and formation of a hydrogel core (Figure AI-1). The resulting particles were purified to remove unencapsulated materials and yield ARV drug-loaded nanolipogels. Although previous approaches to fabricate nanolipogels report on bath sonication to produce homogenous particle populations[16], we found that these methods resulted in particles with a high polydispersity (PDI > 0.6, data not s hown). Instead, we used needle extrusion to produce uniform particles with a hydrodynamic diameter ~200 nm and a narrow PDI <0.1 (Table AI-1). Incorporation of either MVC or TDF resulted in drug-loaded nanolipogels of similar size and PDI to the blank (drug-free) particles. We found that dilution, as reported by others[16], and ultracentrifugation to purify the nanolipogels from residual polymerizable excipients and unencapsulated ARV drug were ineffective. In contrast, we added ascorbic acid prior to UV exposure to effectively quench external polymerization, and then used a desalting column as a final purification step to isolate nanolipogels from any remaining unencapsulated small molecule excipients.

Table AI - 1 MVC- and TDF-nanolipogel particle characterization Size and polydispersity of drug-loaded NLGs were measured by dynamic light scattering. All values are represented as mean ± s.d. from three independently synthesized nanolipogel batches.

	Unpolymerized ULVs			Polymerized NLGs		
Samples	**Blank ULVs**	**MVC ULVs**	**TDF ULVs**	**Blank NLGs**	**MVC NLGs**	**TDF NLGs**
Size (d, nm)	171.8	196.1 ± 5.5	218.5 ± 23.9	141.3	163.5 ± 6.3	164.7 ± 5.8
PDI	0.093	0.2 ± 0.1	0.3 ± 0.02	0.094	0.1 ± 0.01	0.1 ± 0.02
% Particle mass recovery*	-			-	7.8 ± 6.4	15.4 ± 1.9
% Encapsulation efficiency**	-			-	36.7 ± 11.5	16.2 ± 5.6
% Theoretical drug loading	-			-	10	5
% Drug loading **	-			-	3.7 ± 1.2	0.8 ± 0.3

*Measured by lyophilization of nanolipogel samples and massing with an analytical balance
**Measured by reverse phase UV-HPLC after rupturing the lipid bilayer by incubating particles with 25% IPA. All values represented as mean ± SD from three independently synthesized batches.

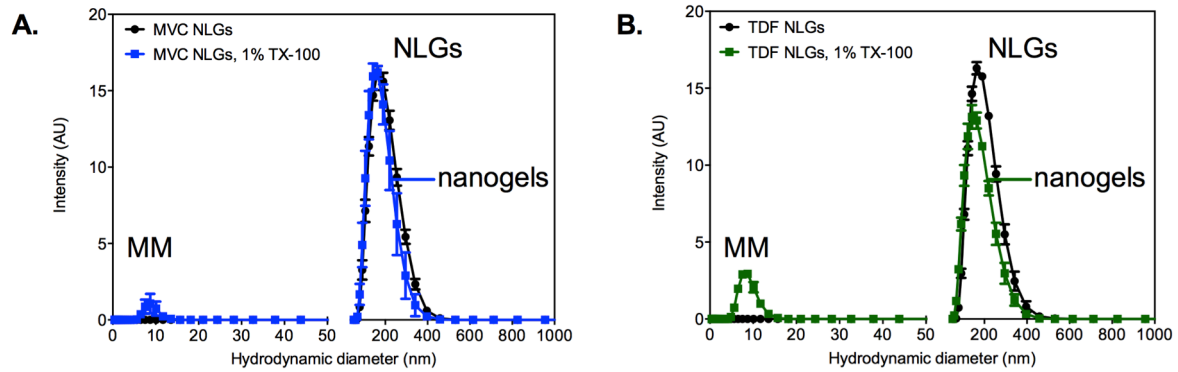

Figure AI - 2 Hydrogel core characterization by detergent removal of lipid bilayer Presence of hydrogel-core, lipid-shell particles was characterized by dynamic light scattering. Nanolipogels (NLGs) were incubated with 1% TX-100 for 10 min at room temperature to facilitate removal of the lipid bilayer, creating a mixed micelle (MM) population and a nanogel population. All values are represented as mean ± SEM from three independently synthesized nanolipogel batches.

DLS was used to evaluate the presence of the hydrogel core and the size distribution of particles at different stages of the nanolipogel synthesis. Lipid bilayers can be stripped using detergents such as Triton X-100 to expose the hydrogel core[16,17], which is a common technique to isolate the nanogel core from the lipid-shell. After incubation of MVC- or TDF-nanolipogels with 1% Triton X-100 for 10 min at room temperature, we observed a mixed micelle population (~10 nm) and a separate nanogel peak (~200 nm) by DLS (Figure AI-2). These results support the existence of a hydrogel-core interior surrounded by a lipid vesicle. The hydrodynamic diameter of unpolymerized MVC ULVs and TDF ULVs were 196 nm and 218 nm (Table AI-1). Following polymerization and purification with a desalting column, the resulting MVC-nanolipogels and TDF-nanolipogels were ~200 nm with a low PDI ~0.1.

We investigated lyophilization as a storage condition for our ARV drug-loaded nanolipogels. However, we found that resuspension of lyophilized nanolipogels produced significantly aggregated particles of 400-600 nm diameter with a high PDI of

Table AI - 2 Nanolipogel stability in a sucrose cryoprotectant

	Polymerized NLGs		
Samples	**Blank NLGs**	**MVC NLGs**	**TDF NLGs**
Size, post-lyophilization in 3% sucrose (d, nm)	157.8	305.6 ± 37.4	206.7 ± 22.9
PDI, post-lyophilization in 3% sucrose	0.118	0.4 ± 0.04	0.2 ± 0.01

0.4 (MVC-nanolipogels) and 0.3 (TDF-nanolipogels) (data not shown). Lyophilization of the nanolipogels in the presence of a 3% (w/v) sucrose better preserved the original size and PDI of nanolipogels after resuspension. Use of sucrose as a cryprotectant helped preserve particle size for both MVC-nanolipogels (d = 306 nm, PDI = 0.4) and TDF nanolipogels (d = 207 nm, PDI = 0.2) (Table AI-2).

AI.D.2. Cryo-TEM imaging of nanolipogels

Cryo-TEM was used to directly visualize the morphology and core-shell architecture of our nanolipogel carriers. Nanolipogels were identified by cryo-TEM as filled vesicles, with a dense and polymerized core, surrounded by a bilayer structure, indicative of a lipid-shell (Figure AI-3A, white arrows). In contrast, liposomes were visualized as vesicles with empty or hollow cores (Figure AI-3C, black arrows). The presence of a vesicle core filled with a polymer network was further probed by continued electron beam exposure, which causes radiation damage to polymers that can be visualized on electron micrographs[33]. We observed white striations in our electron micrographs of nanolipogels that was consistent with radiolysis of organic polymers (Figure AI-3B). These images support that our synthetic strategy results in the formation of nanolipogels with a dense polymer core and lipid bilayer shell architecture.

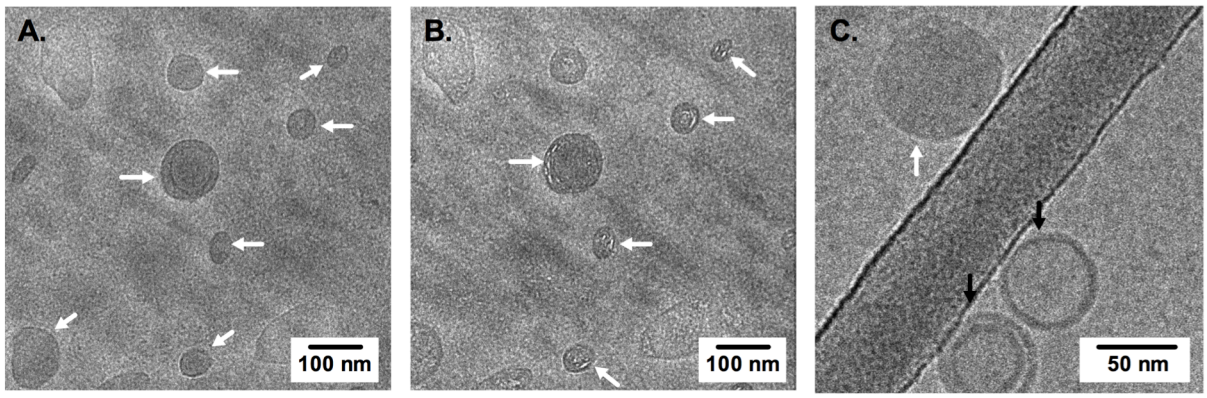

Figure AI - 3 Cryoelectron microscopy micrographs of nanolipogels. Nanolipogels are indicated by white arrows (A), radiation damage from continued electron beam exposure to polymer cores are indicated in white arrows (B), and co-existence of nanolipogels (white arrows) with empty liposomes (black arrows) was observed (C).

AI.D.3. Material recovery and ARV drug encapsulation and release

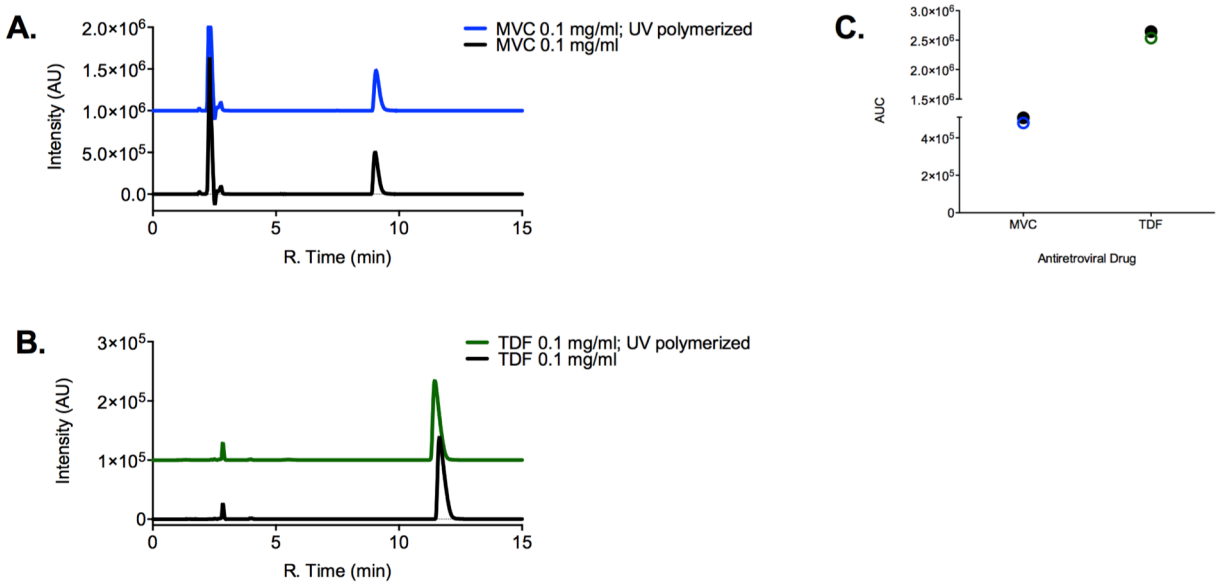

Figure AI - 4 HPLC chromatograms of maraviroc and TDF RP-HPLC was used to obtain drug peak chromatograms taken before and after UV polymerization of a 0.1 mg/ml solution of maraviroc (absorbance 193 nm) and TDF (absorbance 197 nm). Drug solutions were UV polymerized for 15 min to replicate UV-exposure during NLG synthesis. Full chromatograms are displayed with a y-axis offset to visualize UV polymerized drugs (a). Quantification of area under the curve (AUC) of the drug peak revealed a >94% recovery after UV polymerization.

MVC and TDF were incorporated into nanolipogels at 10% and 5% (w/w), respectively (Table AI-1). We used HPLC to quantify the actual drug loading of MVC and TDF from the nanolipogels recovered after synthesis. HPLC of UV exposed but unformulated MVC and TDF showed no change in chromatograms compared to non-UV exposed drugs (Figure AI-4), indicating that the UV polymerization does not alter the drug. Drug quantification of MVC-nanolipogels and TDF-nanolipogels as not confounded by any vehicle excipient or IPA solvent peaks (Figure AI-5). The total mass recovery of MVC-nanolipogels and TDF-nanolipogels was 7.8% and 15.4%. HPLC drug quantification indicated that the drug loading of MVC in nanolipogels was 3.7% (w/w), which corresponds to an encapsulation efficiency of 36.7%. TDF drug load ing in nanolipogels was measured to be 0.8% (w/w) for an encapsulation efficiency of 16.2%. These results show that both MVC and TDF were successfully incorporated into nanolipogel vehicles, although TDF showed much lower loading.

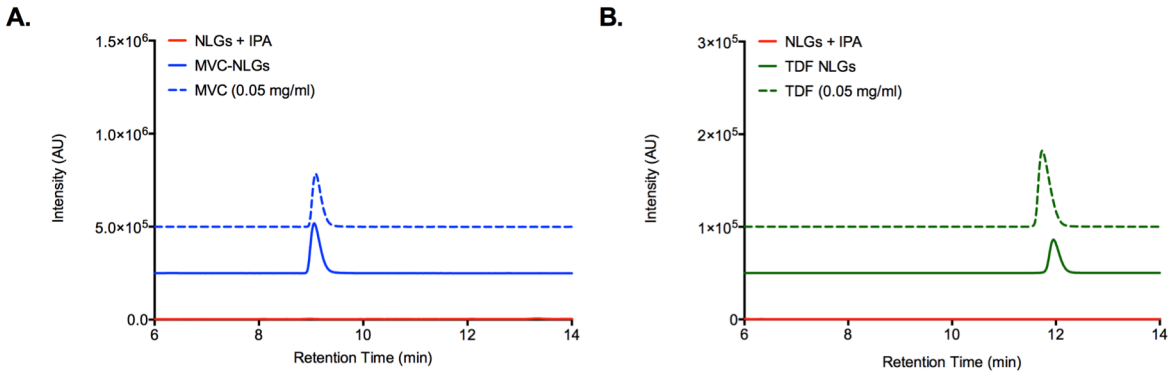

Figure AI - 5 HPLC chromatograms of drug-loaded nanolipogels RP-HPLC was used to obtain drug peak chromatograms of a 0.05 mg/ml solution of drug, drugs formulated in nanolipogels and spiked with IPA, and blank nanolipogels spiked with IPA. Intensity, plotted in absorbance units (MVC, 193 nm; TDF, 197 nm), is shown as a function of retention time.

MVC and TDF drug release from nanolipogels was measured over 72-hours at 37°C. We found that MVC and TDF release curves were pseudo-linear within between 6-8 hours for both drugs, followed by plateau region that persisted out to 72-hours (Figure AI-6). We did not observe burst release of drugs from particles, indicating that they were not surface associated but rather completely formulated either within the hydrogel core or lipid bilayer of the nanolipogels. We observed a higher overall cumulative percentage release for MVC compared to TDF. We further tested the impact of cholesterol content on drug release from nanolipogels, and found that incorporation of higher levels of cholesterol in the lipid membrane slows release of drugs from nanolipogels (Figure AI-7).

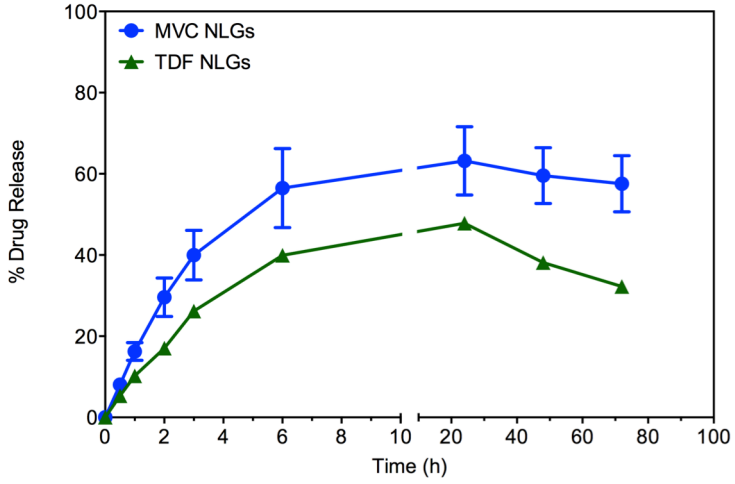

Figure AI - 6 Maraviroc and TDF drug release from nanolipogels. Maraviroc and TDF release from nanolipogels was measured using 1,000 MWCO dialysis tubes inverted into a 50-mL conical containing a sink volume of 5 mL DI water (MVC) and 10 mM NaCl, pH 4 (TDF). Released drug was quantified by reverse phase UV-HPLC. All values are represented as mean ± SEM from three independently synthesized nanolipogel batches.

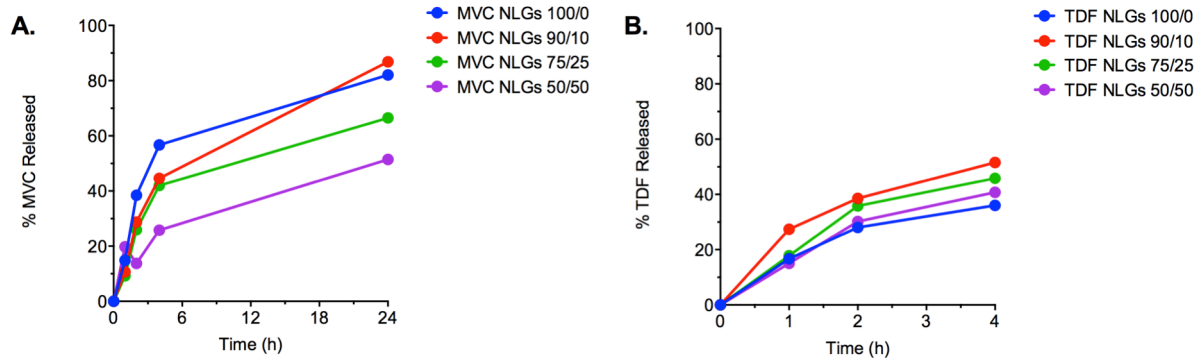

Figure AI - 7 Impact of particle composition on drug release Maraviroc and TDF was formulated in nanolipogels at 10% (w/w) lipid mass with lipid/cholesterol ratios of 90/10, 75/25, and 50/50. Drug release from nanolipogels was measured using 1,000 MWCO dialysis tubes inverted into a 50-mL conical containing a sink volume of 5 mL DI water (MVC) and 10 mM NaCl, pH 4 (TDF). Released drug was quantified by reverse phase UV-HPLC.

AI.D.4. Cell viability and in vitro anti-HIV activity

To understand the potential biological applications for MVC- and TDF-nanolipogels as microbicides, we mea sured their toxicity and anti-HIV activity in cell culture. Cell viability was tested in TZM-bL epithelial cells and CEMx174 T lymphocytes. Our results showed that drug-free (empty) nanolipogels exhibited little to no cytotoxicity in both cell types at low nanolipogel concentrations (Figure AI-8). Blank nanolipogels did exhibit toxicity at the highest concentration (2 mg/mL nanolipogels) in TZM-bL epithelial cells. Once loaded with MVC or TDF, we observed an even further reduction in cell viability at high particle and drug concentrations.

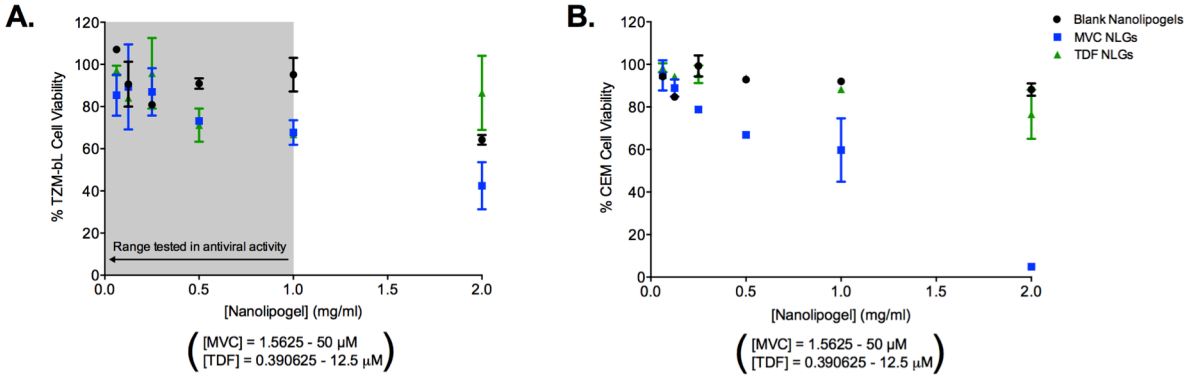

Figure AI - 8 Cell viability of TZM-bL and CEMX174 cells TZM-bL (epithelial cell line) and CEMx174 (T cell line) were exposed to blank and drug-loaded nanolipogels, and cytotoxicity was assessed using CellTiter-Blue® Cell Viability Assay (Promega). Fluorescence was recorded at 560/590 nm. The corresponding MVC and TDF concentrations used in the assay are indicated on the graph. The highest ARV concentrations used in subsequent antiviral assessment are indicated by the shaded area. All values represented as mean± SEM from duplicates.

Our cell cytoxicity results were used to set the concentration range to perform the antiviral studies that measure HIV-1 BaL infection of TZM-bL epithelial cells. We chose ARV-loaded nanolipogels concentrations that exhibited high TZM-bL cell viability such that the measured antiviral activity would be minimally confounded by cytotoxic effects. MVC- and TDF-nanolipogels potently inhibited HIV-1 BaL infection of TZM-bL cells in a dose-dependent manner. In cell-free infection models, MVC nanolipogels displayed an IC_{50} value of 9.6 nM, which is comparable to the IC_{50} value of unformulated MVC (10.8 nM). TDF nanolipogels displayed an IC_{50} value of 7.5 nM, similar to that of unformulated TDF (5.4 nM) (Figure AI-9B). Our results demonstrate that transmission of virus from chronically infected PM-1 cells to TZM-bL cells was much more efficient than cell-free virus infection. As such, both drugs showed a higher IC_{50} value as compared to the IC_{50} value in cell-free HIV-1 BaL infection (Figure AI-9G). As a result of the increased efficiency of infection by cell-cell HIV-1 transmission, MVC nanolipogels displayed an approximately seven-fold increase in the IC_{50} value (76.9 nM) as compared to TDF-nanolipogels (10.7 nM) (Figure AI-9D-E). Finally, treatment of TZM-bL cells with MVC nanolipogels and TDF nanolipogels at a molar combination of 1:1 showed minimal dose reduction compared to single ARV drug-loaded nanolipogel treatment groups, and were not significantly different from free drug at a molar combination of 1:1 (Figure AI-9C, F). Notably, combination treatment in the cell-cell transmission assay reduced the IC_{50} value by nearly half as compared to treatment with MVC nanolipogels alone. We hypothesize that this reduction is due to the presence of TDF nanolipogels, which exhibit more potent activity than MVC nanolipogels.

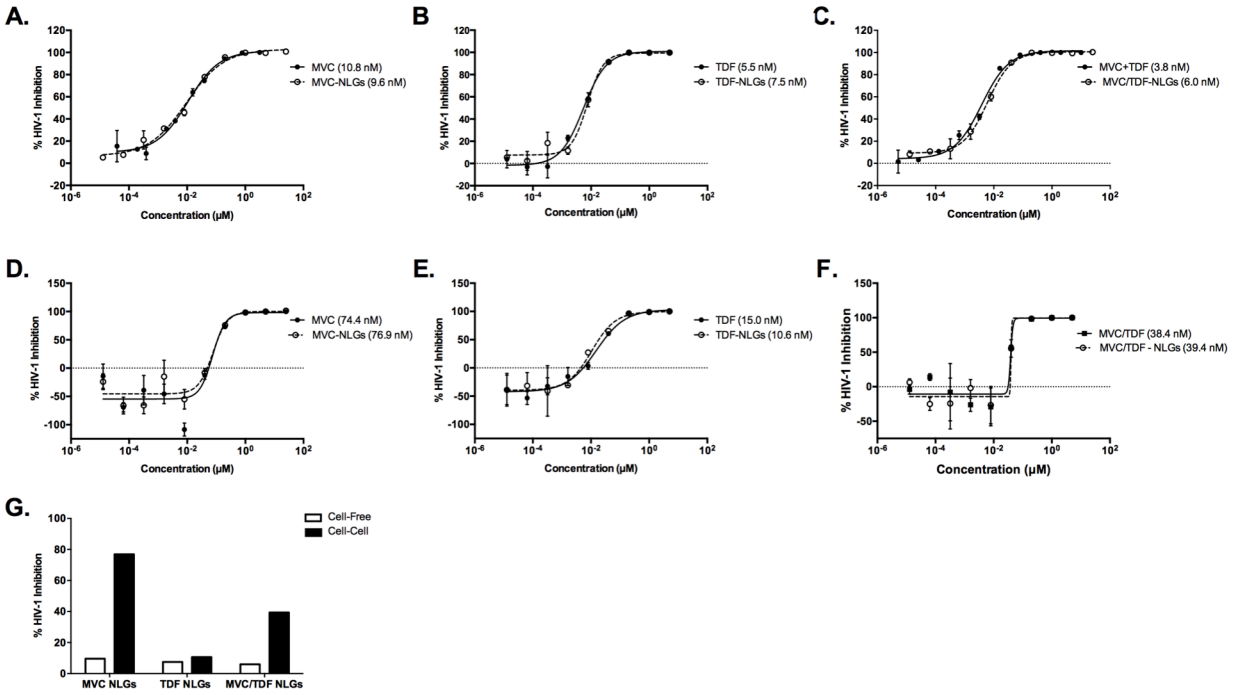

Figure AI - 9 Antiviral activity of MVC NLGs, TDF NLGs, and combination treatment against cell-free and cell-associated HIV-1 BaL in TZM-bL cells Antiviral activity of drug-loaded single nanolipogel and combinations was assessed based on a reduction in luciferase reporter gene expression after infection of TZM-bL cells with cell free HIV-1 BaL (A-C) and cell associated HIV-1 BaL (D-F). Antiviral activity was expressed as an IC50 value, which was the sample concentration giving 50% of relative luminescence units (RLUs) compared with those of virus control after subtraction of background RLUs. All values represented as mean ± SEM from duplicates. IC50 values of all NLG treatment groups in cell-free and cell-associated antiviral assays are summarized (G).

AI.D.5. In vivo retention of antiviral activity in CVL fluids

To understand the *in vivo* application of these materials as topical, mucosal microbicides, we evaluated retained antiviral activity in CVLs after intravaginal delivery of ARV drug-loaded nanolipogels in an established female mouse model. Standard progestin-induced diestrous was employed to reduce mouse-to-mouse variability and eliminate cycle-dependent biological variability. MVC and TDF nanolipogels were administered together intravaginally and CVLs were collected 24-hours post-administration. We were unable to measure MVC or TDF in the CVLs analyzed by HPLC. However, we found that combination administration of both drugs resulted in retained antiviral activity in CVLs against HIV-1 BaL (Figure AI-10). At a dilution of 32-fold, CVLs still provided >60% viral inhibition *in vitro*, which indicated local retention of drug. Using the previously determined IC_{50} values for MVC and TDF in these assays (Figure AI-9A,B), we were able to quantify the amount of drug retained in CVLs at 24-

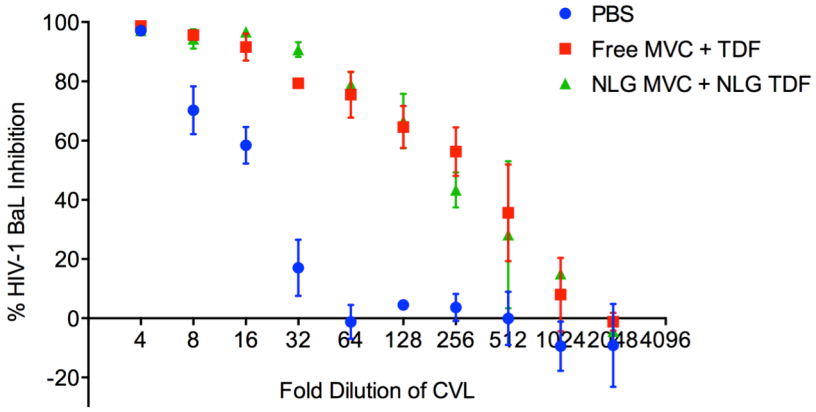

Figure AI - 10 Antiviral activity in cervicovaginal lavage fluids (CVLs) MVC-NLGs and TDF-NLGs were intravaginally administered at 5 mg/drug in a C57BL/6J murine model. 24h-post administration, mice were euthanized and cervicovaginal lavage was collected with 200 ml cDMEM. The antiviral activity in CVL samples was determined using a titer reduction assay with TZM-bl cells. Briefly, serial dilutions of CVLs were made and tested for antiviral activity against cell-free HIV infection. Inhibition of infection was determined by luciferase quantification of cell lysates.

hours. By using the fold-dilution of CVLs, which was performed and comparing concentrations which yield 50% viral inhibition, we determined that ~1.1% of the total drug dose was retained at 24-hours post-vaginal administration. These results are promising and suggest that nanolipogels have potential for use in topical, vaginal delivery of drugs against sexually transmitted infections (STIs).

AI.E. Discussion

In this report, we demonstrate the successful synthesis and biophysical characterization of ARV drug-loaded nanolipogels for HIV-1 chemoprophylaxis. Our synthetic technique for fabricating nanolipogels was adapted to achieve uniform particle size and removal of unencapsulated material. Previous methods to synthesize nanolipogels using bath sonication typically resulted in a polydisperse particle population ranging in size from 30-300 nm in diameter[16]. Size polydispersity can lead to variability in drug loading and prohibit accurate prediction of drug release, intracellular uptake, and carrier dosing for *in vivo* applications. To reduce the polydispersity of nanolipogels resulting from bath sonication, we employed needle extrusion through a uniform pore size membrane to produce a homogenous population of particles ~200 nm in hydrodynamic diameter and a low PDI < 0.1, which did not change significantly post-polymerization and purification (Table AI-1). Previous approaches have diluted unpolymerized nanolipogel suspensions in order to prevent external polymerization[16,34]. However, dilution may create concentration gradients across the lipid bilayer, causing hydrogel components to diffuse

out of particles[31]. Additionally, dilution of particles does not remove unencapsulated drug, which may confound release studies and dosing for anti-HIV-1 assays. Our results showed that the addition of ascorbic acid post-particle formation, prior to UV exposure, worked well to prevent external polymerization, and was easily removed along with unencapsulated drug using a simple desalting column. Overall, our nanolipogel fabrication strategy to synthesize ARV drug-loaded nanolipogels was highly reproducible and resulted in particles with controlled size and low polydispersity.

In agreement with the work of others, we found that nanolipogels incubated with detergent allowed for removal of the lipid bilayer and revealed a nanogel core near the size of the original nanolipogel population (Figure AI-2)[16]. Electron microscopy further validated the formation of hydrogel-core and lipid-shell nanolipogels with spherical morphology. However, it is notable that we did observe formation of some liposomes. To our knowledge, previous research on nanolipogel synthesis and drug encapsulation has not described or measured the percentage of liposomes that may coexist with nanolipogels following the different synthesis schemes. The formation of these liposomes may be mitigated by longer polymerization times than are published in the literature, tuning the monomer-crosslinker-photoinitiator ratio, or choosing a different lipid composition that is more restrictive to drug diffusion out of the vesicle core prior to polymerization. Further investigation into these parameters and their impact on efficient polymerization of the hydrogel-core may improve the efficiency of nanolipogel synthesis.

Our results demonstrate that nanolipogels may be used to formulate anti-HIV small molecule anti-HIV drugs that are highly water soluble and difficult to formulate in more common nanocarrier platforms. Both MVC and TDF were encapsulated at relatively high efficiencies for hydrophilic small molecules at 37% and 16%. The higher encapsulation of MVC may have to do with the ionizable group on the drug, which becomes protonated at low pH. The polymer core of nanolipogels has previously been determined to be pH 3[24]. At a pKa of 7.3[25], the ionizable amine group of MVC may be protonated, and is less likely to diffuse out of the acidic hydrogel core and traverse the lipid bilayer. This would reduce leakage of small molecules and thereby entrap a greater amount of drug. The hydrogel network may also create a barrier for drug diffusion by

decreasing water penetration into the core. While drug loading of MVC and TDF in nanolipogels was sufficient for biological studies, further optimization may be done to enhance drug loading. For example, groups have used strategies such as active loading of pH-sensitive drugs into the nanolipogel core[24]. While active loading may be used for certain classes of drugs with ionizable side groups such as MVC, it may not be useful for small molecules that are not pH-sensitive. Drug loading may also be modulated by further optimization of the lipid bilayer composition, varying the density of the hydrogel core, or increasing the initial drug to material ratio.

In addition to high efficiency of drug encapsulation in nanolipogels, our results also demonstrate that MVC and TDF do not burst release from nanolipogel vehicles. Previous papers that have evaluated the kinetics of hydrophilic drug release from both lipid nanoparticles, report burst release profiles in which most of the drug is released within the first hour[13,35]. Other papers evaluating drug release kinetics from polymeric particles show biphasic release – including an initial burst release phase, which may be due to surface-associated drug[36]. Our results highlight the advantage of nanolipogels as a vehicle to provide release on the scale of 6-8 hours of both drugs. Recent research evaluated the advantages of nanolipogel platforms in direct comparison to liposomes for the loading and release of small molecule anti-cancer drugs[24]. Wang et al. demonstrated that release is more sustained from nanolipogels, and that this was likely due to a combination of the acidic core in conjunction with slower diffusion out of a crosslinked core. Our results support the hypothesis by Wang et al., that the acidic, hydrogel network slows diffusion and partitioning of both drugs out of the core and across the lipid bilayer. We further demonstrate that the inclusion of cholesterol may be used as one strategy to dampen release of both drugs from the nanolipogel core.

Cellular cytotoxicity of nanolipogel vehicles is minimal in both cell types that were tested, indicating their utility as a safe material for use in ARV drug delivery (Figure AI-8). Interestingly, we found that while both TZM-bL epithelial cell and T cells were robust and displayed high viability in response to exposure to ARV drug-free nanolipogels, ARV drug-loaded nanolipogels did induce cellular cytotoxicity at high concentrations greater than 10 μM. Moreover, at high concentrations of MVC (~50 μM), CEMx174 T

cells were especially sensitive to cell death. Importantly, these results demonstrate that cellular toxicity originated from reactions to high concentrations of ARV drugs, not components or excipients of the nanolipogel vehicles. Furthermore, at the highest drug concentrations (25 μM) tested in our antiviral studies in TZM-bL cells, ARV drug-loaded nanolipogels exhibit minimal cytotoxicity. As such the antiviral activity and IC_{50} value quantification in subsequent biological assays was due to drug-dependent inhibition, and not general cellular cytotoxicity.

The antiviral activity of MVC- and TDF-loaded nanolipogels demonstrate that both drugs retain their antiviral bioactivity and are successful at inhibition of HIV-1 infection. Both MVC and TDF retained IC_{50} values that were near that of unformulated free drugs, both in the case of cell-free HIV-1 infection and PM-1 cell-cell HIV-1 transmission. Interestingly, we found that cell-cell HIV-1 transmission was more efficient than cell-free HIV-1 infection of TZM-bL cells. This was evident by the increase in IC_{50} values for both MVC and TDF, indicating that in both cases, more drug was required to achieve the same level of viral inhibition. This was especially the case with MVC, where there was a near seven-fold loss of activity versus a two to three-fold loss of activity in TDF treatment groups. These differences may be attributed to the difference in mechanisms of action for both drugs. MVC is an entry inhibitor of HIV-1 and may experience an on- off-rate of binding CCR5 in cell culture, and thus would not be capable of constantly inhibiting viral entry. On the other hand TDF is a reverse transcriptase inhibitor with an intracellular site of action. Once internalized, TDF remains intracellular until it is metabolized to the active drug tenofovir, which has a long half-life of ~95-hours[26]. As such, the latter drug is present at more constant levels at its site of action. The differences between these drugs is more noticeable in cell-cell transmission, as this assay captures the effect of heightened and increasing production of HIV-1 virus over time by chronically infected PM-1 cells. Further, while it is impossible to state that no infection in the cell-cell transmission assay is due to cell-free virus, it is likely that the most probable route of infection during the one-hour incubation of TZM-bL cells with infected PM-1 cells is primarily through cell-associated transmission[37]. Cell-associated transmission of HIV-1 likely occurs through the formation of a cell-cell virological

synapse that enables interactions between gp120 on budding virus from PM-1 cells and receptors on target cells[38]. In this scenario, gp-120 most likely interacts with CD4, which is engineered to be displayed on the TZM-bL cell line[39]. As such a CCR5 agonist entry inhibitor such as MVC would display reduced inhibitory activity, since the primary mode of infection is via CD4. Overall, our results demonstrate key biological characteristics of the ARV drug-loaded nanolipogel systems. First, the nanolipogel synthetic procedure does not alter the bioactivity of either drug post-formulation. Further, combination treatment of TZM-bL cells resulted in potent antiviral activity against cell-free and cell-cell transmission of virus.

Finally, we are interested in evaluating the application ARV drug-loaded nanolipogels as a topical, vaginal microbicide. We were unable to detect MVC or TDF in CVLs 24-hours post-administration by HPLC. However, we expect that this was due to the fact that any drug remaining in CVLs was below the level of detection using our HPLC methods. As reported by das Neves et al., who vaginally delivered dapivirine loaded polymer nanoparticles in a mouse model, only ~1% of administered drug was detected in CVLs 24-hours post-administration[9]. This low level of drug recovery in CVLs may be detectable with further optimization of HPLC methods for the detection of MVC and TDF in future works. However, we were surprised to find that CVLs from ARV drug-loaded nanolipogel treated mice did show antiviral activity against cell-free HIV-1 BaL infection in TZM-bL cells that was above background (Figure AI-10). Even at a dilution of 32-fold, CVLs still provided >60% viral inhibition, comparable to the activity of both ARV drugs delivered together in mice. This indicates that the delivered ARV drugs were still present at protective concentrations, 24-hours post-vaginal administration in mice. While these *in vivo* studies have laid the ground work for the use of nanolipogels for topical microbicide applications, future studies must be focused on improving dosing and local retention through the use of a semi-solid or solid dosage platform and on evaluating the time-dependent antiviral activity in CVLs, with direct comparisons between free and formulated ARV drugs. Furthermore, improvements on vehicle design such as PEGylation to improve mucus penetration, may be incorporated into the nanolipogel system to improve their application for vaginal drug delivery[40,41].

AI.F. CONCLUSION

Nanolipogels show promise for further *in vitro* and *in vivo* studies involving delivery of this important class of pharmaceutical compounds. Furthermore, investigation of lipid formulation and vehicle design may result in improving drug loading and encapsulation efficiencies. We have found that the nanolipogel systems are robust carrier for loading and modulated release of two classes of antiretroviral drugs. Our ARV drug-loaded nanolipogels show potent antiviral activity *in vitro*, and retain antiviral activity in CVLs after topical, vaginal delivery. These systems have the potential to expand the dosage forms available for water-soluble ARV drugs as topical microbicides. Applications to delivery of other small molecule hydrophilic drugs could benefit from these materials, which bridge efficient delivery and therapeutic efficacy. Future work will examine the ability to co-deliver hydrophobic and hydrophilic ARV drugs simultaneously in nanolipogels. We expect that nanolipogels will serve as a promising platform for combination ARV drug delivery for prevention and treatment of HIV.

AI.G. ACKNOWLEDGEMENTS

This research is supported by funding to K.A.W. from (AI094412), the NIH New Innovator Award (DP2HD075703) and with the support of a UW STD/AIDS Training Fellowship to R.R. (NIHT32AI07140).

AI.H. REFERENCES

1. Singh, R. & Lillard, J. W. Nanoparticle-based targeted drug delivery. *Experimental and molecular pathology* **86,** 215–223 (2009).
2. Slingerland, M., Guchelaar, H.-J. & Gelderblom, H. Liposomal drug formulations in cancer therapy: 15 years along the road. *Drug discovery today* **17,** 160–166 (2012).
3. Ojewole, E., Mackraj, I., Naidoo, P. & Govender, T. Exploring the use of novel drug delivery systems for antiretroviral drugs. *European Journal of Pharmaceutics and Biopharmaceutics* **70,** 697–710 (2008).
4. Gagné, J.-F., Désormeaux, A., Perron, S., Tremblay, M. J. & Bergeron, M. G. Targeted delivery of indinavir to HIV-1 primary reservoirs with immunoliposomes. *Biochimica et Biophysica Acta (BBA)-Biomembranes* **1558,** 198–210 (2002).
5. Chaowanachan, T., Krogstad, E., Ball, C. & Woodrow, K. A. Drug synergy of tenofovir and nanoparticle-based antiretrovirals for HIV prophylaxis. (2013).
6. Mainardes, R. M., Gremião, M. P. D., Brunetti, I. L., Da Fonseca, L. M. & Khalil, N. M. Zidovudine-loaded PLA and PLA–PEG blend nanoparticles: Influence of polymer type on phagocytic uptake by polymorphonuclear cells. *Journal of*

pharmaceutical sciences **98,** 257–267 (2009).
7. Zhang, T., Sturgis, T. F. & Youan, B.-B. C. pH-responsive nanoparticles releasing tenofovir intended for the prevention of HIV transmission. *European Journal of Pharmaceutics and Biopharmaceutics* **79,** 526–536 (2011).
8. Karim, Q. A. *et al.* Effectiveness and safety of tenofovir gel, an antiretroviral microbicide, for the prevention of HIV infection in women. *science* **329,** 1168–1174 (2010).
9. Neves, das, J. *et al.* Biodistribution and pharmacokinetics of dapivirine-loaded nanoparticles after vaginal delivery in mice. *Pharmaceutical research* **31,** 1834–1845 (2014).
10. Immordino, M. L., Dosio, F. & Cattel, L. Stealth liposomes: review of the basic science, rationale, and clinical applications, existing and potential. *International journal of nanomedicine* **1,** 297 (2006).
11. Phillips, N. C., Skamene, E. & Tsoukas, C. Liposomal encapsulation of 3'-azido-3'-deoxythymidine (AZT) results in decreased bone marrow toxicity and enhanced activity against murine AIDS-induced immunosuppression. *JAIDS Journal of Acquired Immune Deficiency Syndromes* **4,** 959–966 (1991).
12. Xu, X., Khan, M. A. & Burgess, D. J. A quality by design (QbD) case study on liposomes containing hydrophilic API: I. Formulation, processing design and risk assessment. *International journal of pharmaceutics* **419,** 52–59 (2011).
13. Hillaireau, H. *et al.* Encapsulation of antiviral nucleotide analogues azidothymidine-triphosphate and cidofovir in poly (iso-butylcyanoacrylate) nanocapsules. *International journal of pharmaceutics* **324,** 37–42 (2006).
14. Mandal, T. K., Lopez-Anaya, A., Onyebueke, E. & Shekleton, M. Preparation of biodegradable microcapsules containing zidovudine (AZT) using solvent evaporation technique. *Journal of microencapsulation* **13,** 257–267 (1996).
15. Meng, J., Sturgis, T. F. & Youan, B.-B. C. Engineering tenofovir loaded chitosan nanoparticles to maximize microbicide mucoadhesion. *European Journal of Pharmaceutical Sciences* **44,** 57–67 (2011).
16. Kazakov, S., Kaholek, M., Teraoka, I. & Levon, K. UV-induced gelation on nanometer scale using liposome reactor. *Macromolecules* **35,** 1911–1920 (2002).
17. Patton, J. N. & Palmer, A. F. Photopolymerization of bovine hemoglobin entrapped nanoscale hydrogel particles within liposomal reactors for use as an artificial blood substitute. *Biomacromolecules* **6,** 414–424 (2005).
18. Patton, J. N. & Palmer, A. F. Engineering temperature-sensitive hydrogel nanoparticles entrapping hemoglobin as a novel type of oxygen carrier. *Biomacromolecules* **6,** 2204–2212 (2005).
19. Park, J. *et al.* Combination delivery of TGF-β inhibitor and IL-2 by nanoscale liposomal polymeric gels enhances tumour immunotherapy. *Nature materials* **11,** 895–905 (2012).
20. Kiser, P. F., Wilson, G. & Needham, D. A synthetic mimic of the secretory granule for drug delivery. *Nature* **394,** 459–462 (1998).
21. Murphy, E. A. *et al.* Targeted nanogels: a versatile platform for drug delivery to tumors. *Molecular cancer therapeutics* **10,** 972–982 (2011).

22. Umamaheshwari, R. B. & Jain, N. K. Receptor-mediated targeting of lipobeads bearing acetohydroxamic acid for eradication of Helicobacter pylori. *Journal of controlled release* **99,** 27–40 (2004).
23. Jin, T., Pennefather, P. & Lee, P. I. Lipobeads: a hydrogen anchored lipid vesicle system. *FEBS letters* **397,** 70–74 (1996).
24. Wang, Y., Tu, S., Pinchuk, A. N. & Xiong, M. P. Active drug encapsulation and release kinetics from hydrogel-in-liposome nanoparticles. *Journal of colloid and interface science* **406,** 247–255 (2013).
25. MacArthur, R. D. & Novak, R. M. Maraviroc: the first of a new class of antiretroviral agents. *Clinical Infectious Diseases* **47,** 236–241 (2008).
26. Delaney, W. E. *et al.* Intracellular metabolism and in vitro activity of tenofovir against hepatitis B virus. *Antimicrobial agents and chemotherapy* **50,** 2471–2477 (2006).
27. Chen, B. A. *et al.* Phase 1 Safety, Pharmacokinetics, and Pharmacodynamics of Dapivirine and Maraviroc Vaginal Rings: a Double-Blind Randomized Trial. (2014).
28. Sepúlveda-Crespo, D. *et al.* Triple combination of carbosilane dendrimers, tenofovir and maraviroc as potential microbicide to prevent HIV-1 sexual transmission. *Nanomedicine* **10,** 899–914 (2015).
29. Malcolm, R. K. *et al.* Pharmacokinetics and efficacy of a vaginally administered maraviroc gel in rhesus macaques. *Journal of Antimicrobial Chemotherapy* **68,** 678–683 (2013).
30. Marrazzo, J. M. *et al.* Tenofovir-based preexposure prophylaxis for HIV infection among African women. *New England Journal of Medicine* **372,** 509–518 (2015).
31. Schillemans, J. P., Flesch, F. M., Hennink, W. E. & van Nostrum, C. F. Synthesis of bilayer-coated nanogels by selective cross-linking of monomers inside liposomes. *Macromolecules* **39,** 5885–5890 (2006).
32. D'Avolio, A. *et al.* A validated high-performance liquid chromatography-ultraviolet method for quantification of the CCR5 inhibitor maraviroc in plasma of HIV-infected patients. *Therapeutic drug monitoring* **32,** 86–92 (2010).
33. Talmon, Y. The Study of Latex IPNs by Cryo-TEM Using Radiation-Damage Effects. *Technomic Publishing Company, Advances in Interpenetrating Polymer Networks.* **2,** 141–156 (1990).
34. Van Thienen, T. G. *et al.* On the synthesis and characterization of biodegradable dextran nanogels with tunable degradation properties. *Macromolecules* **38,** 8503–8511 (2005).
35. Dembri, A., Montisci, M.-J., Gantier, J. C., Chacun, H. & Ponchel, G. Targeting of 3′-azido 3′-deoxythymidine (AZT)-loaded poly (isohexylcyanoacrylate) nanospheres to the gastrointestinal mucosa and associated lymphoid tissues. *Pharmaceutical research* **18,** 467–473 (2001).
36. Christoper, G. P., Raghavan, C. V., Siddharth, K., Kumar, M. S. S. & Prasad, R. H. Formulation and optimization of coated PLGA–Zidovudine nanoparticles using factorial design and in vitro in vivo evaluations to determine brain targeting efficiency. *Saudi Pharmaceutical Journal* **22,** 133–140 (2014).
37. Buffa, V. *et al.* Cyanovirin-N potently inhibits human immunodeficiency virus type

1 infection in cellular and cervical explant models. *Journal of General Virology* **90,** 234–243 (2009).
38. Abela, I. A. *et al.* Cell-cell transmission enables HIV-1 to evade inhibition by potent CD4bs directed antibodies. *PLoS Pathog* **8,** e1002634–e1002634 (2012).
39. Platt, E. J., Wehrly, K., Kuhmann, S. E., Chesebro, B. & Kabat, D. Effects of CCR5 and CD4 cell surface concentrations on infections by macrophagetropic isolates of human immunodeficiency virus type 1. *Journal of virology* **72,** 2855–2864 (1998).
40. Ensign, L. M. *et al.* Mucus-penetrating nanoparticles for vaginal drug delivery protect against herpes simplex virus. *Science translational medicine* **4,** 138ra79–138ra79 (2012).
41. Cu, Y. & Saltzman, W. M. Controlled surface modification with poly (ethylene) glycol enhances diffusion of PLGA nanoparticles in human cervical mucus. *Molecular pharmaceutics* **6,** 173–181 (2008).